RESONANT TRANSMISSION THROUGH NEGATIVE PERMITTIVITY MATERIALS

A Thesis Submitted to the

College of Graduate Studies and Research

in Partial Fulfillment of the Requirements

for the degree of Master of Science

in the Plasma Physics Laboratory of Physics and Engineering Physics

University of Saskatchewan

Saskatoon

By

Koloman Varady

PERMISSION TO USE

In presenting this thesis in partial fulfilment of the requirements for a Postgraduate degree from the University of Saskatchewan, I agree that the Libraries of this University may make it freely available for inspection. I further agree that permission for copying of this thesis in any manner, in whole or in part, for scholarly purposes may be granted by the professor or professors who supervised my thesis work or, in their absence, by the Head of the Department or the Dean of the College in which my thesis work was done. It is understood that any copying or publication or use of this thesis or parts thereof for financial gain shall not be allowed without my written permission. It is also understood that due recognition shall be given to me and to the University of Saskatchewan in any scholarly use which may be made of any material in my thesis.

Requests for permission to copy or to make other use of material in this thesis in whole or part should be addressed to:

Head of the Department of Physics and Engineering Physics
116 Science Place
University of Saskatchewan
Saskatoon, Saskatchewan
Canada
S7N 5E2

ABSTRACT

At the heart of the field of photonics is the control of the reflection and transmission of light. Plasmonics looks at this problem of control of electromagnetic radiation in the context of surface plasmon polaritons (SPP). SPPs are propagating electromagnetic modes localized at the interfaces between media with positive and negative permittivities. Their excitation can accompany the enhancement of transmission, reflection, or absorption of EM radiation. There are a number of ways to excite SPPs and this work looks at several geometries and analyzes the transmission and reflection characteristics using a numerical approach based on the finite element method.

The first method of excitation is by incident evanescent wave that was totally internally reflected from an earlier interface. It is shown that an evanescent wave can excite SPPs and create resonant transmisison. It is also found that high values of dissipation limit transmission and instead create resonant absorption. The second method involves the modulation of the negative permittivity of the plasma slab itself. Numerical results are compared to analytical ones and are in good agreement because harmonics of the solution above the first are negligible. An investigation of transmission through a plasma slab with a single thin diffraction grating placed nearby follows. Analytical and numerical calculations show that a single thin grating is sufficient to create transmission resonance. It is found that for large values of diffraction grating modulation parameter, higher harmonics, usually not accounted for in analytical solutions, results in discrepancies between analytical and numerical results. The next geometry considered is of a plasma layer with only part of it having modulated permittivity. The presence of modulation of only part of the plasma layer is shown to create transmission and reflection resonances. By tailoring parameters of the system, it is shown how the resonant frequencies can be shifted. The final geometry considers a copper grating beside a plasma and transmission of a radio frequency wave. Even though the copper used here in this simulation is very absorbing, there are ranges of frequencies when transmission or reflection are enhanced.

ACKNOWLEDGEMENTS

I am very happy to thank everyone who has helped me during my stay at the University of Saskatchewan.

I would first like to start by thanking my supervisor, Professor Andrei Smolyakov. It was he who gave me the opportunity to enter the exciting field that is plasmonics. It was also with his guidance and support that made this work possible.

Professors Xiao and Hirose also deserve my thanks for the help they've offered when I've found myself knocking on their doors. I'd like to further thank colleagues Andre Pant, Dallas Trembach, Damian Rohraff, Winston Frias, Sayf Gamudi, and all my other friends in the Plasma Physics Laboratory for helpful and useful discussions in and out of the office.

And finally, I, of course, owe much to the support and encouragement of my amazing family, my parents, Koloman Varady and Helena Varady, and my brother, Martin Varady.

Dedicated to my family.

CONTENTS

Permission to Use i

Abstract ii

Acknowledgements iii

Contents v

List of Figures vii

1 Introduction 1
- 1.1 Background and Motivation . . . 1
- 1.2 Maxwell's Equations . . . 4
- 1.3 Classical Electron Model of Permittivity . . . 5
- 1.4 The Wave Equation . . . 6
- 1.5 Surface Waves at a Single Interface Boundary . . . 7
- 1.6 Negative Refraction and Energy Flow in Surface Modes . . . 10
- 1.7 Insulator-Metal-Insulator System . . . 13
- 1.8 Excitation of Surface Plasmon Polaritons . . . 15

2 Finite Element Method 18
- 2.1 Numerical Methods . . . 18
- 2.2 Finite Element Method . . . 18
- 2.3 Formulation of Finite Element Method Equations . . . 19
- 2.4 Boundary Conditions . . . 22
  - 2.4.1 Continuity Condition . . . 22
  - 2.4.2 Matched Boundary Condition . . . 23
  - 2.4.3 Periodic Boundary Condition . . . 24
- 2.5 Perfectly Matched Layers . . . 25
- 2.6 COMSOL Multiphysics . . . 29

3 Resonant Amplification of Evanescent Waves and Reflectionless Absorption 30
- 3.1 Summary . . . 36

4 Resonant Transmission Through a Film with Modulated Permittivity 40
- 4.1 Summary . . . 48

5 Resonant Amplification of Evanescent Waves with a Diffraction Grating 49
- 5.1 Analytical Model . . . 50
  - 5.1.1 Vacuum Region 1 . . . 53
  - 5.1.2 Vacuum Region 2 . . . 53

5.1.3 Plasma Region 54
5.1.4 Vacuum Region 3 55
5.1.5 Surface Wave Resonance 55
5.2 Numerical Results 58
5.3 Summary 74

6 Plasma Layer as a Diffraction Grating **75**
6.1 Summary 78

7 Enhanced Transmission with Metal Grid **79**

8 Summary **83**

A Transmission Matrices **92**

LIST OF FIGURES

1.1 Profile of the magnetic field in a surface wave; $\epsilon_1 > 0$ for $x < 0$ and $\epsilon_2 < 0$ for $x > 0$. 8
1.2 The solid line shows the dispersion relation of SPPs for an interface between air and a material with a Drude like response. The dashed line shows the dispersion relation for free space, $k = \omega/c$ 10
1.3 Direction of phase velocities during the reflection and refraction of an incident plane wave with a medium with *(a)* positive group velocity and *(b)* negative group velocity 12
1.4 The single eigenmode of Figure 1.1 splits into two eigenmodes, an even solution and an odd solution. 15
1.5 (a) Kretschmann configuration (b) Otto configuration. Also illustrated are possible lightpaths. 16
1.6 Geometry of a two layer plasma system. Here $0 < \epsilon_1 < 1$ and $\epsilon_2 < 0$. . . 17

2.1 Examples of two dimensional elements 19
2.2 Wave incident on an object as well as the reflected and transmitted wave. . 23
2.3 Use of PML layers to truncate the computational domain along the x-axis 25

3.1 Geometry of a two layer plasma system. Here $0 < \epsilon_1 < 1$ and $\epsilon_2 < 0$. . . 31
3.2 Transmission coefficient for $\gamma = 0$ and $\epsilon_1 = 0.3428$, $\omega/\omega_{p2} = 0.5019$, $d_1 = 64.702$ cm, $d_2 = 7.4769$ cm 32
3.3 Transmission coefficient for $\gamma = 0.1\omega$ and $\epsilon_1 = 0.3428$, $\omega/\omega_{p2} = 0.5019$, $d_1 = 64.702$ cm, $d_2 = 7.4769$ cm 32
3.4 Reflection (solid line) and absorption (dashed line) coefficient for $\gamma = 0.1\omega$ and $\epsilon_1 = 0.3428$, $\omega/\omega_{p2} = 0.5019$, $d_1 = 64.702$ cm, $d_2 = 7.4769$ cm 33
3.5 Transmission coefficient for $\gamma = 0.2\omega$ and $\epsilon_1 = 0.3428$, $\omega/\omega_{p2} = 0.5019$, $d_1 = 64.702$ cm, $d_2 = 7.4769$ cm 33
3.6 Reflection (solid line) and absorption (dashed line) coefficients for $\gamma = 0.2\omega$ and $\epsilon_1 = 0.3428$, $\omega/\omega_{p2} = 0.5019$, $d_1 = 64.702$ cm, $d_2 = 7.4769$ cm 34
3.7 Transmission coefficient for $\gamma = \omega$ and $\epsilon_1 = 0.3428$, $\omega/\omega_{p2} = 0.5019$, $d_1 = 64.702$ cm, $d_2 = 7.4769$ cm 34
3.8 Reflection (solid line) and absorption (dashed line) coefficients for $\gamma = \omega$ and $\epsilon_1 = 0.3428$, $\omega/\omega_{p2} = 0.5019$, $d_1 = 64.702$ cm, $d_2 = 7.4769$ cm . . . 35
3.9 Transmission coefficient for $\gamma = 0$ and $\epsilon_1 = 0.5428$, $\omega/\omega_{p2} = 0.5$, $d_1 = 16.68$ cm, $d_2 = 3$ cm 36
3.10 Transmission coefficient for $\gamma = 0.1\omega$ and $\epsilon_1 = 0.5428$, $\omega/\omega_{p2} = 0.5$, $d_1 = 16.68$ cm, $d_2 = 3$ cm 37
3.11 Reflection (solid line) and absorption (dashed line) coefficients for $\gamma = 0.1\omega$ and $\epsilon_1 = 0.5428$, $\omega/\omega_{p2} = 0.5$, $d_1 = 16.68$ cm, $d_2 = 3$ cm 37
3.12 Transmission coefficient for $\gamma = 0.2\omega$ and $\epsilon_1 = 0.5428$, $\omega/\omega_{p2} = 0.5$, $d_1 = 16.68$ cm, $d_2 = 3$ cm 38

3.13 Reflection (solid line) and absorption (dashed line) coefficients for $\gamma = 0.2\omega$ and $\epsilon_1 = 0.5428$, $\omega/\omega_{p2} = 0.5$, $d_1 = 16.68$ cm, $d_2 = 3$ cm 38
3.14 Transmission coefficient for $\gamma = 0.5\omega$ and $\epsilon_1 = 0.5428$, $\omega/\omega_{p2} = 0.5$, $d_1 = 16.68$ cm, $d_2 = 3$ cm 39
3.15 Reflection (solid line) and absorption (dashed line) coefficients for $\gamma = 0.5\omega$ and $\epsilon_1 = 0.5428$, $\omega/\omega_{p2} = 0.5$, $d_1 = 16.68$ cm, $d_2 = 3$ cm 39

4.1 Geometry of a periodically modulated film of thickness d. 41
4.2 Transmittance versus wavelength of incident plane wave for a modulated silver film: $\gamma = 0$ 41
4.3 Transmittance for a modulated silver film: $\gamma = 0.5\,\omega_\tau$ 42
4.4 Transmittance versus wavelength of incident plane wave for a modulated silver film: $\gamma = \omega_\tau$. 42
4.5 Transmittance for a modulated silver film: $\gamma = 1.5\,\omega_\tau$ 43
4.6 Absorption versus wavelength of incident plane wave for a modulated silver film: $\gamma = 0.5\,\omega_\tau$. 43
4.7 Absorption for a modulated silver film: $\gamma = \omega_\tau$ 44
4.8 Absorption versus wavelength of incident plane wave for a modulated silver film: $\gamma = 1.5\,\omega_\tau$ 44
4.9 Profile of the normalized $|H_0|^2$ harmonic of the left transmission peak along the x-axis. The metal layer is located between $x = 0$ and $x = d$. . . 45
4.10 Profile of the normalized $|H_1|^2$ harmonic of the left transmission peak along the x-axis. The metal layer is located between $x = 0$ and $x = d$. . . 46
4.11 Profile of the normalized sum $\sum_{n=2}^{8} |H_n|^2$ harmonics of the left transmission peak along the x-axis. The metal layer is located between $x = 0$ and $x = d$. 46
4.12 Profile of the normalized $|H_0|^2$ harmonic of the right transmission peak along the x-axis. The metal layer is located between $x = 0$ and $x = d$. . . 47
4.13 Profile of the normalized $|H_1|^2$ harmonic of the right transmission peak along the x-axis. The metal layer is located between $x = 0$ and $x = d$. . . 47
4.14 Profile of the normalized sum of the $\sum_{n=2}^{8} |H_n|^2$ harmonics of the right transmission peak along the x-axis. The metal layer is located between $x = 0$ and $x = d$. 48

5.1 Geometry of the problem. A plasma (bounded by the solid lines) with permittivity ϵ_p is situated between two half-spaces of air $\epsilon = 1$ with an infinitely thin diffraction grating a distance a in front of the plasma. . . . 51
5.2 Analytical calculation of the reflection coefficient as a function of q, the periodic wave vector of the diffraction grating, for a metal film. 56
5.3 Numerical calculation of the reflection coefficient as a function of q, the periodic wave vector of the diffraction grating, for a metal film. 58

5.4 Profile of the magnitude of the normalized harmonics $|H_0|^2$ (solid line), $|H_1|^2$ (dashed line), $\sum_{n=2}^{8} |H_n|^2$ (dotted line) for q_1 59
5.5 Profile of the magnitude of the normalized harmonics $|H_0|^2$ (solid line), $|H_1|^2$ (dashed line), $\sum_{n=2}^{8} |H_n|^2$ (dotted line) for q_2 59
5.6 Reflection as a function of the modulated wave vector, q for $\alpha = 2$ and $h_g = 0.025$. The solid line shows the analytical solution and the dashed line shows the numerical solution. 60
5.7 Reflection as a function of the modulated wave vector, q for $\alpha = 2$ and $h_g = 0.05$. The solid line shows the analytical solution and the dashed line shows the numerical solution. 61
5.8 Analytical calculation of reflection coefficient as a function of q, the periodic wave vector of the diffraction grating for $\alpha = 2$ 61
5.9 Numerical calculation of reflection coefficient as a function of q, the periodic wave vector of the diffraction grating for $\alpha = 2$ 62
5.10 Analytical calculation of reflection coefficient as a function of q, the periodic wave vector of the diffraction grating for $\alpha = 4$ 62
5.11 Numerical calculation of reflection coefficient as a function of q, the periodic wave vector of the diffraction grating for $\alpha = 4$ 63
5.12 Analytical calculation of reflection coefficient as a function of q, the periodic wave vector of the diffraction grating for $\alpha = 6$ 63
5.13 Numerical calculation of reflection coefficient as a function of q, the periodic wave vector of the diffraction grating for $\alpha = 6$ 64
5.14 The normalized harmonic $|H_0|^2$ for resonance at $q = q_1$ and $\alpha = 2$. 64
5.15 The normalized harmonic $|H_0|^2$ for resonance at $q = q_1$ and $\alpha = 4$. 65
5.16 The normalized harmonic $|H_0|^2$ for resonance at $q = q_1$ and $\alpha = 6$. 65
5.17 The normalized harmonic $|H_1|^2$ (solid line) and the normalized sum $\sum_{n=2}^{8} |H_n|^2$ (dashed line) for resonance $q = q_1$ for $\alpha = 2$ 66
5.18 The normalized harmonic $|H_1|^2$ (solid line) and the normalized sum $\sum_{n=2}^{8} |H_n|^2$ (dashed line) for resonance $q = q_1$ for $\alpha = 4$ 66
5.19 The normalized harmonic $|H_1|^2$ (solid line) and the normalized sum $\sum_{n=2}^{8} |H_n|^2$ (dashed line) for resonance $q = q_1$ for $\alpha = 6$ 67
5.20 Analytical and numerical results for resonant q as a function of the modulation parameter, α. Solid lines show analytical results and circles show numerical results 68
5.21 The normalized harmonic $|H_0|^2$ for resonance at $q = q_2$ and $\alpha = 2$. 68
5.22 The normalized harmonic $|H_0|^2$ for resonance at $q = q_2$ and $\alpha = 4$. 69
5.23 The normalized harmonic $|H_0|^2$ for resonance at $q = q_2$ and $\alpha = 6$. 69

5.24 The normalized harmonic $|H_1|^2$ (solid line) and the normalized sum $\sum_{n=2}^{8} |H_n|^2$ (dashed line) for resonance $q = q_2$ for $\alpha = 2$ 70
5.25 The normalized harmonic $|H_1|^2$ (solid line) and the normalized sum $\sum_{n=2}^{8} |H_n|^2$ (dashed line) for resonance $q = q_2$ for $\alpha = 4$ 70
5.26 The normalized harmonic $|H_1|^2$ (solid line) and the normalized sum $\sum_{n=2}^{8} |H_n|^2$ (dashed line) for resonance $q = q_2$ for $\alpha = 6$ 71
5.27 The normalized magnitude of the harmonics, $|H_n|^2$ at the diffraction grating at $x = 0$ at $q = q_1$ and $\alpha = 2$. 71
5.28 The normalized magnitude of the harmonics, $|H_n|^2$ at the diffraction grating at $x = 0$ at $q = q_2$ and $\alpha = 2$. 72
5.29 The normalized magnitude of the harmonics, $|H_n|^2$ at the diffraction grating at $x = 0$ at $q = q_1$ and $\alpha = 4$. 72
5.30 The normalized magnitude of the harmonics, $|H_n|^2$ at the diffraction grating at $x = 0$ at $q = q_2$ and $\alpha = 4$. 73
5.31 The normalized magnitude of the harmonics, $|H_n|^2$ at the diffraction grating at $x = 0$ at $q = q_1$ and $\alpha = 6$. 73
5.32 The normalized magnitude of the harmonics, $|H_n|^2$ at the diffraction grating at $x = 0$ at $q = q_2$ and $\alpha = 6$. 74

6.1 Geometry of two layers of plasma, one of which has a periodically modulated permittivity. 76
6.2 Transmission coefficients for two layers of plasma. The dashed line is with $g = 0$ and the solid line is with $g = 0.2$. Other parameters are $f_p = 2.3\,\text{GHz}$, $a = 0.15\,\text{m}$, $\epsilon_m = \epsilon_1$, $d_1 = 0.4\,\text{cm}$, $d_2 = 2\,\text{cm}$ 76
6.3 Transmission with parameters $f_p = 2.3\,\text{GHz}$, $a = 0.15\,\text{m}$, $\epsilon_m = \epsilon_1$, $d_2 = 2\,\text{cm}$, $d_1 = 0.1$ cm (solid line), 0.2 cm (dashed line), 0.4 cm (dotted line) . 77
6.4 Transmission with parameters $f_p = 2.3\,\text{GHz}$, $a = 0.15\,\text{m}$, $d_1 = 2\,\text{cm}$, $d_2 = 0.1\,\text{cm}$, $\epsilon_m = \epsilon_1$ (solid line), $2\epsilon_1$ (dashed line), $3\epsilon_1$ (dotted line), $10\epsilon_1$ (dotted and dashed line) 77

7.1 Geometry of a plasma layer with permittivity $\epsilon_1 = 1 - f_p^2/f^2$ and thickness d_1. To the right of it is a square diffraction grating that alternates permittivity $\epsilon_m = 1 - i\sigma/\omega\epsilon_0$ and the free space permittivity ϵ_0. The grating has periodicity a and thickness d_2. 80
7.2 Transmission through the plasma and diffraction grating configuration for different thicknesses of the diffraction grating, d_2. The dotted line has $d_2 = 0$ cm, the solid line has $d_2 = 0.5$ cm, and the dashed line has $d_2 = 2$ cm 81
7.3 Transmission through the plasma and diffraction grating configuration over a wider range of frequencies. Solid line is with the diffraction grating and dashed line is without the diffraction grating. 81

7.4 Transmission through a thinner plasma and a thinner diffraction grating configuration. Solid line is with the diffraction grating and dashed line is without the diffraction grating. 82

A.1 Reflection and refraction of a TM wave (p wave) 92

CHAPTER 1

INTRODUCTION

1.1 Background and Motivation

Plasmonics, a new but rapidly expanding discipline, studies the physics and technological applications of collective electromagnetic excitations on the surface of negative permittivity materials (like a metal or plasma). Such collective modes (plasmons) generally exist at any interface between two materials with opposite signs of dielectric constants, e.g. air which has positive permittivity, $\epsilon = 1$, and a metal with negative permittivity, $\epsilon < 0$ for frequencies in the optical range. For many applications structures of interest involve nanofilms of noble metals and/or semiconductors on dielectric substrates. Though this research field only found its name less than a decade ago [1], its foundations go back over a century. The history of plasmonics can be traced back to studies of radio wave propagation along a surface. As early as 1899, Sommerfeld found a solution to Maxwell's equations for wave propagation on the surface of a single conducting wire [2]. In 1907, his student, Zenneck, continued that work on surface waves localized at the boundary between a conductor and dielectric. In his studies of radio frequency wave propagation at the air-earth interface, he analytically solved for localized wave solutions that propagated on a flat interface between a half space with finite conductivity, σ, and a half space with permittivity ϵ equal to the permittivity of free space [3]. Plasmonics can also be traced back to experiments by Wood, who in 1935 had observed an anomalous drop in the intensity of light reflected from metallic gratings [4]. Wood's anomaly, as it is called today, is understood to be due the result of surface wave excitation.

The actual application of plasmonic effects can be traced even further back to the staining of glass in ancient Rome (such as the Lycurgus cup). The cup, dated to the 4th

century on stylistic grounds, depicts Lycurgus, a king of the Thracians (around 800 BC) as he becomes entrapped and tormented by Dionysus after lashing out at the Greek god. The cup, when viewed by light that is reflected from the surface, appears green. When it is viewed by light transmitted from inside the cup, it appears red. This curious property is in fact due to gold nanoparticles, typically 5-60 nm, inside the ruby glass [5]. It has been realized that this behaviour occurs due to resonant absorption of light. These so-called Mie resonances [6] are simply the surface wave modes on a conducting sphere.

In a wider sense, plasmonics deals with the propagation of electromagnetic radiation in materials with negative dielectric permittivity and permeability (the so-called metamaterials). Such materials are typically based on metallic sub-wavelength structures immersed in the host dielectric. Surface waves (plasmons) supported by free electrons in the metal and localized at the metal-dielectric interfaces represent a key mode of electromagnetic excitations in such materials. Control of surface plasmons allows for the guiding and manipulation of electromagnetic radiation below the diffraction limit, e.g. the surface waves operating at visible range frequencies (few hundreds THz) can be squeezed into the transverse dimensions below 100 nanometres [7]. This possibility opens up a vast area of applications ranging from terahertz computer chips and the next generation of integrated opto-electronic devices [11] to ultra-sensitive molecular detectors [12, 13] and even an invisibility cloak [14]. The established framework of methods and tools of classical electromagnetic theory (both analytical and computational) and the modern technology of film deposition and nanofabrication create the conditions for dramatic scientific advances and a new class of sub-wavelength integrated opto-electronic components.

There are several key phenomena due to surface waves which are related to our investigation. The anomalously high transmission of electromagnetic radiation has drawn much attention since Ebbesen's pioneering experimental paper [15]. In these experiments, it was found that the observed transmission through an array of sub-wavelength holes in a metal film is an order of magnitude larger than the values expected from standard diffraction theory. The exact nature of this phenomenon is still under debate in the literature but the prevailing view is that it is due to the resonant enhancement of the local electromagnetic field accompanying surface wave excitations. The transmission of light through

optically thick materials is of interest for many applications, in particular, in communication technologies, e.g. as a building block for optical switching [16] and multiplexing [17] devices.

The phenomenon of resonant transmission through opaque materials is closely related to the amplification of evanescent waves. Normally, the information contained in the evanescent part of the wave spectrum is lost due to the fast decays of the evanescent waves. This is an underlying reason for the so-called diffraction limit. The amplification of evanescent waves allows for the retention of the information in the diffraction region thus opening the way to the so-called superlens [18]. Full realization of superlenses requires artificial materials, called metamaterials, with both permittivity, $\epsilon(\omega)$, and permeability, $\mu(\omega)$, being negative [19–21]. A partial superlens, a $''$poor man's$''$ superlens may be possible based on a material that only has negative permittivity (such as silver) and can, at plasmonic resonance, amplify evanescent waves [22, 23].

Plasmon resonance and evanescent wave amplification are accompanied by strong enhancement of the electromagnetic field in a narrow region in space, a confinement of electromagnetic waves [24]. Usually light focused by dielectric lenses cannot be confined to dimensions less than $\lambda/2$. Plasmonics phenomena allows for the confinement of radiation to lengths much smaller than $\lambda/2$. This opens new possibilities for ultrasensitive detectors, more efficient solar cells [25], and surface wave based lasers [26].

Central to these applications are surface plasmon polariton excitations that create anomalous transmission. SPPs cannot be excited on a flat surface by normally incident electromagnetic radiation. As such, it is the goal of this work to investigate different geometry to excite SPPs. We use numerical results from the finite element method (described in Chapter 2) to calculate the transmission characteristics.

The first structure considered is a double layer configuration in Chapter 3. Here SPPs are resonantly excited by an incident evanescent wave which is the result of internal reflection at an earlier interface. Transmission, reflection, and absorption through this structure are calculated for different plasma parameters and comparison is made with analytical results obtained with the transfer matrix method.

In Chapter 4, a metal film layer with sinusoidally modulated permittivity is analyzed

numerically and the results are compared with published analytical results.

Evanescent waves, in this case generated by a diffraction grating, are used again in Chapter 5 to excite SPPs on a plasma layer. Presented is an impedance analytical solution that only considers the contribution of the fundamental and first harmonics to calculate transmission. Accompanying numerical solutions are presented which show the role played by higher harmonics that were neglected in the analytical theory. This analysis shows that for small amplitude of the grating modulations the higher harmonics are small and the numerical and analytical solutions show good matching. For larger amplitudes, the higher harmonics are important and the numerical solution can different substantially from the analytical theory.

In Chapter 6, a plasma with permittivity partially modulated is considered. The effects of changing geometrical parameters, such as permittivity and thickness, on the transmission characteristic are analyzed.

Chapter 7 considers the transmission of incident EM radiation through an unmodulated plasma slab with an adjacent square copper grating. As the copper grating's permittivity is mostly imaginary, it is found that, while total reflection resonances exists, transmission resonances are not as pronounced.

1.2 Maxwell's Equations

For completeness we give Maxwell's macroscopic equations [27] as they are used here. In the absence of external charges and sources,

$$\nabla \cdot \mathbf{D} = 0, \tag{1.1a}$$

$$\nabla \cdot \mathbf{B} = 0, \tag{1.1b}$$

$$\nabla \times \mathbf{E} = -\frac{\partial \mathbf{B}}{\partial t}, \tag{1.1c}$$

$$\nabla \times \mathbf{H} = \frac{\partial \mathbf{D}}{\partial t}. \tag{1.1d}$$

These four equations relate the macroscopic fields $\mathbf{D}$ (the electric displacement), $\mathbf{E}$ (the electric field), $\mathbf{H}$ (the magnetic field), and $\mathbf{B}$ (the magnetic flux density or magnetic induction). If we limit ourselves to linear and isotropic media, then the field $\mathbf{D}$ can be related to

the field $\mathbf{E}$ and the field $\mathbf{B}$ can be related to the field $\mathbf{H}$ using the constitutive relations

$$\mathbf{D} = \epsilon_0 \epsilon \mathbf{E}, \tag{1.2a}$$

$$\mathbf{B} = \mu_0 \mu \mathbf{H}, \tag{1.2b}$$

where ϵ is called the dielectric constant or relative permittivity, ϵ_0 is the permittivity of free space (8.85×10^{-12} C^2/Nm^2), μ is the relative permeability, and μ_0 is the permeability of free space ($4\pi \times 10^{-7}$ N/A^2). In nonmagnetic media, which are dealt with exclusively in this work, $\mu = 1$.

1.3 Classical Electron Model of Permittivity

Over a wide range of frequencies (as high as UV for alkali metals and as high as visible frequencies for noble metals), the optical properties of metals can be explained by a plasma model. The electrons can be modelled as oscillating in response to the applied electric field. Their motion is damped by collisions characterized by the collision frequency γ and γ is on the order of 10^{-14} s at room temperature for a metal. We assume the electrons obey the following equation of motion:

$$m\frac{d^2}{dt^2}\mathbf{x} + m\gamma\frac{d}{dt}\mathbf{x} = -e\mathbf{E}, \tag{1.3}$$

where $\mathbf{x}$ is the relative position of the electron, m is the mass of the electron, $\mathbf{E}$ is the applied electric field, and $-e$ is the electron charge. Because the wavelength of the optical wave is much longer than the atom size, we can take $\mathbf{E}$ to be constant across the atom. We also assume that $\mathbf{E}$ has a harmonic time dependence, that is to say $\mathbf{E} = \mathbf{E}_0 e^{-i\omega t}$, where ω is the frequency of oscillation. The solution for $\mathbf{x}$ then is

$$\mathbf{x} = \frac{e}{m(\omega^2 + i\gamma\omega)}\mathbf{E}(t). \tag{1.4}$$

The macroscopic polarization inside the material due to the displacement of electrons from their positively charged nucleus is simply $\mathbf{P} = -en\mathbf{x}$, where n is the electron density. More explicitly,

$$\mathbf{P} = \frac{-ne^2}{m(\omega^2 + i\gamma\omega)}\mathbf{E}(t). \tag{1.5}$$

Using Eq. (1.5), the electric displacement can be defined as $\mathbf{D} = \epsilon_0\mathbf{E} + \mathbf{P}$, and comparing to the constitutive relations in Eq. (1.2), we find the permittivity, ϵ, can be expressed as

$$\epsilon(\omega) = 1 - \frac{\omega_p^2}{\omega^2 + i\gamma\omega}, \tag{1.6}$$

where $\omega_p^2 = ne^2/\epsilon_0 m$. If γ is non-zero then $\epsilon(\omega)$ is a complex value and is often expressed as $\epsilon(\omega) = \epsilon'(\omega) + i\epsilon''(\omega)$. In this case, the real and imaginary components can be calculated as,

$$\epsilon'(\omega) = 1 - \frac{\omega_p^2\tau^2}{1 + \omega^2\tau^2}, \tag{1.7}$$

$$\epsilon''(\omega) = \frac{\omega_p^2\tau}{\omega(1 + \omega^2\tau^2)}, \tag{1.8}$$

where τ is the relaxation time of the free electrons and $\tau = 1/\gamma$. The electron plasma and the collision frequencies for metals are often expressed in energy units. An example of typical values are those for silver which has $\omega_p = 9.1$ eV and $\gamma = 0.021$ eV.

1.4 The Wave Equation

Maxwell's equations are the general equations of classical EM phenomena. To address wave phenomena it is convenient to cast Maxwell's equations in the form of the wave equation. Combining Maxwell's equations (1.1) and the constitutive relations (1.2) one arrives at the equation

$$\nabla \times (\epsilon^{-1}\nabla \times \mathbf{H}) = -\epsilon_0\mu_0\mu\frac{\partial^2}{\partial t^2}\mathbf{H} \tag{1.9}$$

If we assume that the time evolution for the $\mathbf{E}$ and $\mathbf{H}$ fields is harmonic,

$$\mathbf{E}(x, y, z, t) = \mathbf{E}(x, y, z)e^{-i\omega t} \tag{1.10a}$$

$$\mathbf{H}(x, y, z, t) = \mathbf{H}(x, y, z)e^{-i\omega t} \tag{1.10b}$$

then Eq. (1.9) can be further written as

$$\nabla \times (\epsilon^{-1}\nabla \times \mathbf{H}) - k_0^2\mathbf{H} = 0, \tag{1.11}$$

where $k_0 = \omega/c$ is the free space wave vector. We have assumed that the relative permittivity, $\mu = 1$. In general, ε is a complex permittivity $\varepsilon = \epsilon'(\omega) + i\epsilon''(\omega)$. The imaginary part of $\epsilon(\omega)$ is responsible for dissipative losses. An equivalent wave equation can be written in terms of the electric field

$$\nabla \times (\mu^{-1} \nabla \times \mathbf{E}) = -\epsilon_0 \mu_0 \varepsilon \frac{\partial^2}{\partial t^2} \mathbf{E}, \tag{1.12}$$

or

$$\nabla \times (\nabla \times \mathbf{E}) = \varepsilon k_0^2 \mathbf{E}. \tag{1.13}$$

These equations are equivalent but one or another is more convenient depending on the wave polarization. Contrary to waves in free space, where both electric and magnetic field are transverse to the direction of the propagation, in two-dimensional geometry one can distinguish two polarizations: TE and TM modes. For the field which depends on x-y coordinates, the TM mode is defined $\mathbf{H}(x, y, t) = (0, 0, H_z)$, $\mathbf{E}(x, y, t) = (E_x, E_y, 0)$ and the TE mode is defined $\mathbf{H}(x, y, t) = (H_x, H_y, 0)$, $\mathbf{E}(x, y, t) = (0, 0, E_z)$. Respectively, Eq. (1.11) is more convenient for TM modes and the equation (1.13) for TE modes respectively.

1.5 Surface Waves at a Single Interface Boundary

The simplest geometry that can sustain surface wave oscillations is that of a single interface (taken to be in the x-y plane for simplicity) between a dielectric half-space with a real positive permittivity and another material half-space whose real part of the permittivity is negative [28]. The second condition is easily met by materials which have a plasma-like response $\epsilon = 1 - \omega_p^2/\omega^2$, for $\omega < \omega_p$, where ω_p is the plasma frequency (this relation is true for most metals at visible frequencies).

Assuming solutions in the form of $\mathbf{E}(x, y, z, t) = \mathbf{E}(x) e^{i\beta y} e^{-i\omega t}$ (ie. waves that propagate along the interface, β is the wave vector along the y direction) there are two sets of self-consistent solutions, the familiar TE and TM modes. From Eq. (1.11) one finds that

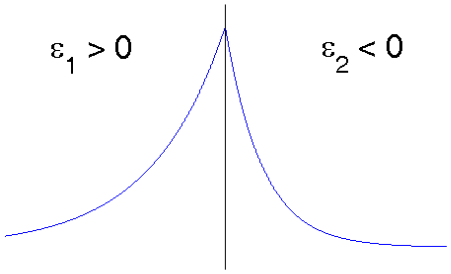

Figure 1.1: Profile of the magnetic field in a surface wave; $\epsilon_1 > 0$ for $x < 0$ and $\epsilon_2 < 0$ for $x > 0$.

TE modes are governed by the system of equations

$$\frac{\partial^2 E_z}{\partial x^2} + (k_0^2\epsilon - \beta^2)E_z = 0 \tag{1.14a}$$

$$H_y = \frac{i}{\omega\mu_0}\frac{\partial E_z}{\partial x} \tag{1.14b}$$

$$H_x = \frac{\beta}{\omega\mu_0}E_z \tag{1.14c}$$

and the TM modes by

$$\frac{\partial^2 H_z}{\partial x^2} + (k_0^2\epsilon - \beta^2)H_z = 0 \tag{1.15a}$$

$$E_y = -\frac{i}{\omega\epsilon_0\epsilon}\frac{\partial H_z}{\partial x} \tag{1.15b}$$

$$E_x = -\frac{\beta}{\omega\epsilon_0\epsilon}H_z. \tag{1.15c}$$

Considering first the TM mode, the electric and magnetic fields are given below. In the half-space $x > 0$ they are

$$H_z(x) = A_2 e^{i\beta y}e^{-k_2 x}, \tag{1.16a}$$

$$E_y(x) = \frac{iA_2k_2}{\omega\epsilon_0\epsilon_2}e^{i\beta y}e^{-k_2 x}, \tag{1.16b}$$

$$E_x(x) = \frac{-A_2\beta}{\omega\epsilon_0\epsilon_2}e^{i\beta y}e^{-k_2 x}, \tag{1.16c}$$

and in the half-space $x < 0$ the fields are

$$H_z(x) = A_1 e^{i\beta y} e^{k_1 x}, \tag{1.17a}$$

$$E_y(x) = \frac{-iA_1 k_1}{\omega \epsilon_0 \epsilon_1} e^{i\beta y} e^{k_1 x}, \tag{1.17b}$$

$$E_x(x) = \frac{-A_1 \beta}{\omega \epsilon_0 \epsilon_1} e^{i\beta y} e^{k_1 x}, \tag{1.17c}$$

where $k_1^2 = \beta^2 - k_0^2 \epsilon_1$ and $k_2^2 = \beta^2 - k_0^2 \epsilon_2$. The boundary condition of continuity of the magnetic field, H_z, at the interface gives

$$A_1 = A_2. \tag{1.18}$$

By using the boundary condition of continuity of E_y or continuity of $\frac{1}{\varepsilon}\frac{\partial H_z}{\partial x}$at the interface, one obtains the dispersion relation for the TM modes

$$\frac{k_2}{k_1} + \frac{\epsilon_2}{\epsilon_1} = 0. \tag{1.19}$$

It is easy to see that ϵ_2 and ϵ_1 should have opposite signs (as it is required that Re[k_2], Re[k_1] > 0 for mode confinement). The resulting dispersion equation for the TM mode can be written in the form

$$\beta = k_0 \sqrt{\frac{\epsilon_1 \epsilon_2}{\epsilon_1 + \epsilon_2}}. \tag{1.20}$$

Similarly, using Eq. (1.14), it can be shown that no surface wave solutions exist for TE polarization for the two half-spaces having opposite signs of permittivity. If, instead of having opposite signs of permittivity, the two half spaces had opposite signs of permeability and $\epsilon = 1$, then the TE mode could excite surface waves and would have the dispersion equation

$$\frac{k_2}{k_1} + \frac{\mu_2}{\mu_1} = 0, \tag{1.21}$$

which is an equation analogous to Eq. (1.19).

Equation (1.19) is illustrated by Figure 1.2 for a single interface between $\epsilon_1 = 1$ and ϵ_2 described by Eq. (1.6) with negligible damping constant γ. At low β, the characteristics of the surface wave are similar to that of an EM field in free space and is weakly confined to the surface. These are also termed Sommerfeld-Zenneck waves. As β gets very large, ω approaches what is called the surface plasmon frequency, $\omega_{sp} = \omega_p/\sqrt{1 + \epsilon_1}$. Inserting

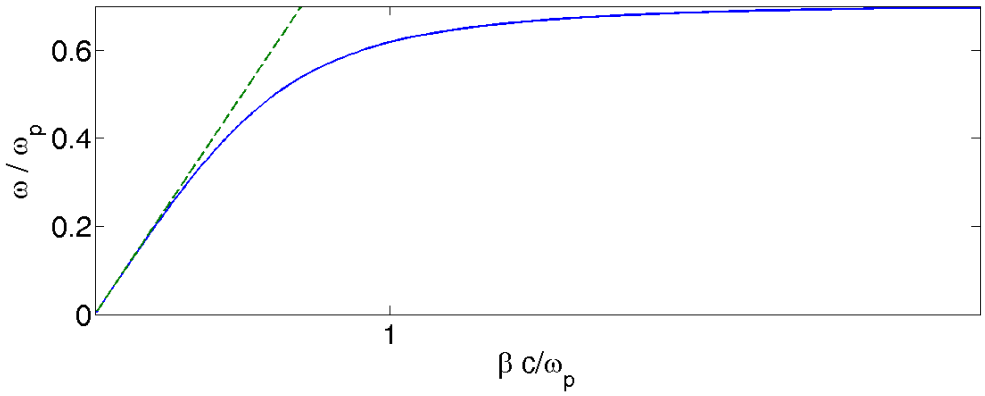

Figure 1.2: The solid line shows the dispersion relation of SPPs for an interface between air and a material with a Drude like response. The dashed line shows the dispersion relation for free space, $k = \omega/c$

Eq, (1.6) into Eq. (1.20) shows that the denominator in Eq. (1.20) approaches 0 as ω approaches ω_{sp}, β goes to infinity and the group velocity, v_g approaches 0. As a result, the surface waves becomes a static mode and no longer propagates along the surface and is known as a surface plasmon. Surface plasmon polaritons are the laterally confined modes that propagate along the surface. They exist at the frequencies below ω_{sp}.

1.6 Negative Refraction and Energy Flow in Surface Modes

Here we briefly describe the negative refraction phenomenon to illustrate that its basic features are related to properties of surface waves. Moreover, the artificially engineered metamaterials, are based on composites which involve metal structures immersed in a host dielectric. It is crucial that the metal structures exhibit surface mode resonances.

Formally, negative refraction can be introduced on a basis of the reflection and refraction laws:

$$\phi = \phi^{'} \tag{1.22a}$$

$$n_1 \sin\phi = n_2 \sin\phi^{''}. \tag{1.22b}$$

What is not often mentioned is that the angle $\pi - \phi^{''}$ also satisfies the Refraction law. Figure 1.3b shows this solution. Usually, the exclusion of the latter solution is considered reasonable as for a wave incident from medium 1 the energy in medium 2 should propagate

away from the interface. The other interpretation of negative refraction is based on the notion that negative refraction occurs in a material with negative refraction index, $n_2 < 0$. Hence changing signs of both $n_2 \rightarrow -n_2$, $\phi'' \rightarrow -\phi''$ provides the negative refaction solution. It was argued that simultaneous negative ε and μ are required to choose the negative sign root in the expression for the refractive index, $n_2 = -\sqrt{\varepsilon_2 \mu_2}$. These formal interpretations based on Snell's law provide limited physics insight into the phenomenon and can be misleading at times.

The physical meaning of negative refraction is better described by using the concept of the phase and group velocity. For simplicity we consider the case of an isotropic medium[1]. In this case the direction of the phase velocity is defined to be along the wave vector

$$\mathbf{v}_p = \frac{\omega}{k}\frac{\mathbf{k}}{k}. \tag{1.23}$$

It is the phase velocity that is normally associated with the direction of the wave propagation. The energy propagates with the group velocity, $\mathbf{S} = U\mathbf{v}_g$, where $\mathbf{S}$ is the energy flux, and U is the time-averaged energy density, $U > 0$ in thermodynamic equilibrium. For an isotropic medium the group velocity is

$$\mathbf{v}_g = \frac{d\omega(\mathbf{k})}{d\mathbf{k}} = \frac{\mathbf{k}}{k}\frac{\partial\omega(k)}{\partial k}. \tag{1.24}$$

Therefore, the group velocity can be parallel or anti-parallel with $\mathbf{k}$ depending on whether $\partial\omega/\partial k$ is positive or negative. Regular refraction occurs for $\partial\omega/\partial k$, when phase and group velocity are in the same direction. This situation is illustrated in Figure 1.3a .

If the energy in medium 2 is to propagate away from the interface and the derivative $\partial\omega/\partial k < 0$, then the solution in Figure 1.3b is the one to keep. In this situation, the refracted wave actually propagates towards the interface, in the direction of the phase velocity, while the energy propagates away from the interface, at the group velocity. As a result, the components of energy propagation along the interface are in opposite directions in the two media.

Therefore negative refraction occurs in the media with negative group velocity, $\partial\omega/\partial k < 0$. Such waves are sometimes called backward waves and often occur in plasmas and flu-

[1]Note that in an anisotropic medium., e.g photonic crystal, negative refraction can also occur through a somewhat different mechanism

ids. A possibility of negative refraction for backward waves was noted a long time ago in the works of Lamb, Schuster and was fully worked out by Mandelstam (for a historical note see [29]).

The following simple example illustrates the double negative condition often cited in the problem of negative refraction, $\varepsilon < 0$ and $\mu < 0$. Consider the dispersion equation of the form

$$\varepsilon\mu\omega^2 = k^2c^2. \tag{1.25}$$

Consider the case of a plasma like medium with $\varepsilon = 1 - \omega_p^2/\omega^2$. In the standard case, with $\mu = 1$ one has the standard dispersion relation for electromagnetic waves in plasma

$$\omega^2 = \omega_p^2 + k^2c^2. \tag{1.26}$$

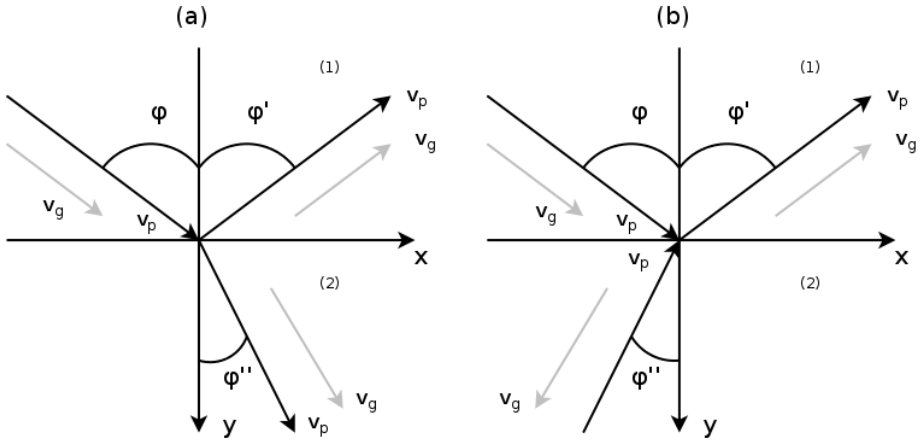

Figure 1.3: Direction of phase velocities during the reflection and refraction of an incident plane wave with a medium with *(a)* positive group velocity and *(b)* negative group velocity

Such waves are propagating only for $\omega > \omega_p$ and are evanescent for $\omega < \omega_p$. Consider now the case $\mu \simeq -1$. Then the dispersion equation becomes

$$\omega^2 = \omega_p^2 - k^2c^2. \tag{1.27}$$

These waves have negative dispersion, $\partial\omega/\partial k < 0$, they are propagating for $\omega < \omega_p$, and both $\varepsilon < 0$ and $\mu < 0$ are negative. As a result negative refraction will occur in such a medium.

It is worth noting that negative values of the dielectric constant, ε, and permeability, μ, are only possible for dispersive materials, $\varepsilon = \varepsilon(\omega)$ and $\mu = \mu(\omega)$. Negative permeability is possible in engineered metamaterials where the magnetic response occurs due to resonances on sub-wavelength metallic structures. In general, these resonances have a surface wave type nature.

We illustrate now that the energy flow in surface wave excitations is consistent with the main feature of negative refraction.

Energy flow is described by Poynting's vector, which is calculated as

$$\mathbf{S} = \mathbf{E} \times \mathbf{H} = \frac{1}{\mu}(\mathbf{E} \times \mathbf{B}). \tag{1.28}$$

We consider the energy flow for the surface wave as described above in Eq. (1.16) and Eq. (1.17). Substituting these expressions we find the energy flow for $x > 0$ as

$$\mathbf{S} = -|A_2|^2 \frac{\beta}{2\omega\epsilon_0\epsilon_2} e^{-2k_2 x}\hat{\mathbf{j}}, \tag{1.29}$$

and

$$\mathbf{S} = -|A_1|^2 \frac{\beta}{2\omega\epsilon_0\epsilon_1} e^{2k_1 x}\hat{\mathbf{j}}, \tag{1.30}$$

for $x < 0$. Because ϵ_1 and ϵ_2 have opposite sign, the flow of energy along the interface on one side of the interface is opposite in direction to the flow of energy on the other side. Again, this is just as is the case at the interface between a positive refraction index material and a negative refraction index material.

1.7 Insulator-Metal-Insulator System

A very important and basic structure is that of a thin metallic layer sandwiched between two semi-infinite dielectrics, also called a insulator/metal/insulator (IMI) heterostructure. For the general TM mode, the fields inside the three media are

$$H_z = Ae^{i\beta y}e^{-k_3 x} \tag{1.31a}$$

$$E_y = \frac{iAk_3}{\omega\epsilon_0\epsilon_3} e^{i\beta y}e^{-k_3 x} \tag{1.31b}$$

$$E_x = \frac{-A\beta}{\omega\epsilon_0\epsilon_3} e^{i\beta y}e^{-k_3 x} \tag{1.31c}$$

for $x > a$,

$$H_z = Be^{i\beta y}e^{k_2 x} \tag{1.32a}$$

$$E_y = \frac{-iBk_2}{\omega\epsilon_0\epsilon_2}e^{i\beta y}e^{k_2 x} \tag{1.32b}$$

$$E_x = \frac{-B\beta}{\omega\epsilon_0\epsilon_2}e^{i\beta y}e^{k_2 x} \tag{1.32c}$$

for $x < -a$, and

$$H_z = Ce^{i\beta y}e^{k_1 x} + De^{i\beta y}e^{-k_1 x} \tag{1.33a}$$

$$E_y = \frac{-iCk_1}{\omega\epsilon_0\epsilon_1}e^{i\beta y}e^{k_1 x} + \frac{iDk_1}{\omega\epsilon_0\epsilon_1}e^{i\beta y}e^{-k_1 x} \tag{1.33b}$$

$$E_x = \frac{C\beta}{\omega\epsilon_0\epsilon_1}e^{i\beta y}e^{k_1 x} + \frac{Dk_1}{\omega\epsilon_0\epsilon_1}e^{i\beta y}e^{-k_1 x} \tag{1.33c}$$

for $-a < x < a$. The wave equation (1.15a) further imposes the condition,

$$k_i^2 = \beta^2 - k_0^2\epsilon_i \tag{1.34}$$

for i = 1, 2, 3. An implicit expression for the dispersion relation can be solved for from the system of equations

$$\exp(-4k_1 a) = \frac{k_1/\epsilon_1 + k_2/\epsilon_2}{k_1/\epsilon_1 - k_2/\epsilon_2}\frac{k_1/\epsilon_1 + k_3/\epsilon_3}{k_1/\epsilon_1 - k_3/\epsilon_3}. \tag{1.35}$$

When $\epsilon_1 = \epsilon_3$, Eq. (1.35) is split and there are now two different eigenmodes that excite surface waves

$$\tanh k_1 a = -\frac{k_2\epsilon_1}{k_1\epsilon_2} \tag{1.36a}$$

$$\tanh k_1 a = -\frac{k_1\epsilon_2}{k_2\epsilon_1}. \tag{1.36b}$$

These two solutions describe modes of odd vector parity (E_x is odd, H_y and E_z are even) and even vector parity (E_x is even, H_y and E_z are odd), respectively. These modes also differ in frequency with the odd mode having a higher frequency than the even mode.

When dissipation is included, the propagation constant, β, becomes complex and as a result the field is damped. The two modes, the odd mode, ω_+, and the even mode, ω_-, respond differently as the thickness of the film is decreased or increased. As the film becomes thinner, the odd mode experiences decreased confinement (and as a result

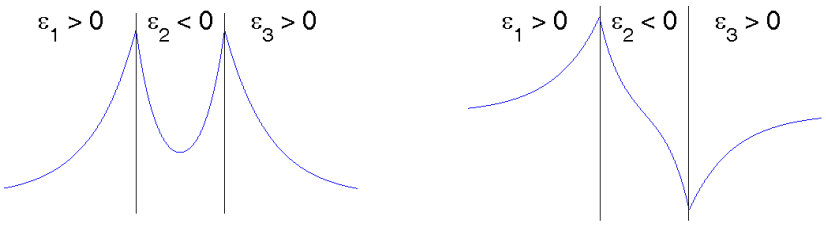

Figure 1.4: The single eigenmode of Figure 1.1 splits into two eigenmodes, an even solution and an odd solution.

increased propagation distance as the film becomes thinner). This mode has come to be known as long-ranging SPPs [30] and is especially of interest in designing plasmon waveguides. The even mode, on the other hand, has its confinement increased as the film is made thinner.

For large wave vector, β, the modes become electrostatic and the frequencies can be expressed as

$$\omega_+ = \frac{\omega_p}{\sqrt{1+\epsilon_2}}\sqrt{1+\frac{2\epsilon_2 e^{-2\beta a}}{1+\epsilon_2}} \tag{1.37a}$$

$$\omega_- = \frac{\omega_p}{\sqrt{1+\epsilon_2}}\sqrt{1-\frac{2\epsilon_2 e^{-2\beta a}}{1+\epsilon_2}}. \tag{1.37b}$$

1.8 Excitation of Surface Plasmon Polaritons

Surface plasmon polaritons (SPP) propagate at a flat interface between metal and a dielectric. For the case when $\epsilon_1 = 1$ and $\epsilon_2 < 0$, we define $n^2 = -\epsilon_2$. Rewriting the expression for the propagation constant, β, of the surface waves as

$$\beta = \frac{k_0 n}{\sqrt{n^2-1}}. \tag{1.38}$$

we can see that the phase velocity of the SPPs along the interface (in the y-direction), $c_p = \omega/\beta = c\sqrt{n^2-1}/n < c$ is less than the speed of light c. On the other hand, the wave in free space propagating in the (x,y) plane, $\omega^2 = \left(k_y^2 + k_x^2\right)c^2$, for $k_x^2 > 0$ has phase velocity along y which is larger than the speed of light, $\omega/k_y = c\left(1+k_x^2/k_y^2\right)^{1/2} > c$. These two waves cannot be matched in frequency and k_y (β). As such, SPPs cannot be

excited by a wave incident from vacuum.

Special configurations have to be arranged to allow for phase matching between the wave vectors k_y of the incident light and β of the surface wave for the excitation of the SPPs [28]. Two conditions are discussed in this paper.

The first condition involves matching ω and β of the SPP with those of an incident evanescent wave, so that $k_x^2 < 0$ and $\omega/k_y = c\left(1 + k_x^2/k_y^2\right)^{1/2} < c$. Several configurations have been employed to that purpose.

For experiments in the optical range, prisms are used to create total internal reflection of the wave in configurations called the Kretschmann [31] or Otto configurations [32] (Figure 1.5). These schemes involves the tunnelling of the the field through the totally internally reflecting barrier to the interface where the SPPs are excited [28]. In the Kretschmann configuration, the field is incident at the prism/metal interface at an angle above the critical angle. It tunnels from the prism through the metal and excites the SPP on the other side of the metal. In the Otto configuration, the field is incident above the critical angle at the prism/air interface. It tunnels through the layer of air to the metal interface to excite SPPs. While the Kretschmann configuration is the most common one, the Otto configuration is used when direct contact with the metal surface is undesirable.

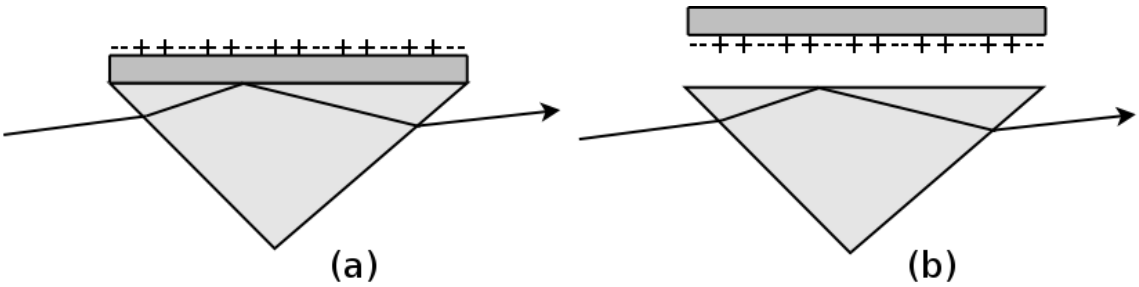

Figure 1.5: (a) Kretschmann configuration (b) Otto configuration. Also illustrated are possible lightpaths.

In our work we will use a transition layer with $0 < \varepsilon < 1$ to create the evanescent wave which can effectively excite the surface wave. This configuration will be utilized in Chapter 3.

The second way of coupling SPPs with incident light is to create periodic modulation of the layer, e.g. permittivity of the opaque layer, $\epsilon = \epsilon_m(1 + g \sin qy)$, with $\epsilon_m < 0$, g

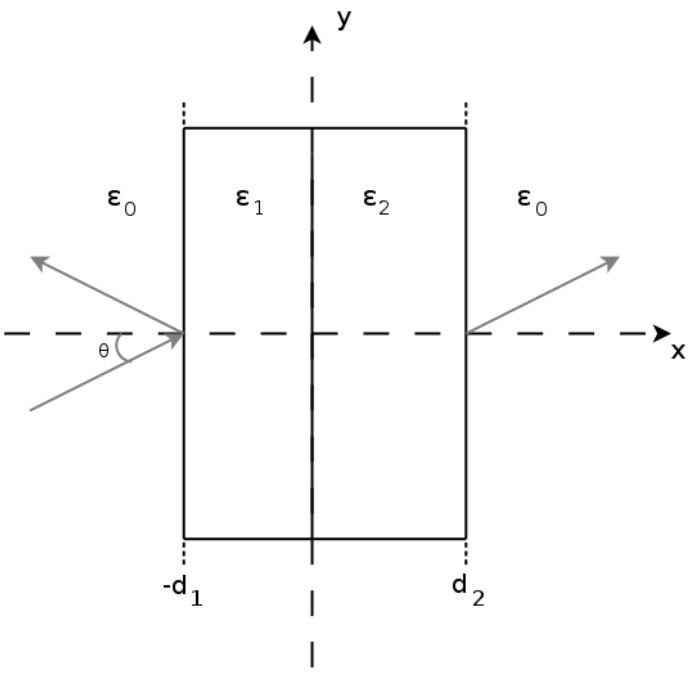

Figure 1.6: Geometry of a two layer plasma system. Here $0 < \epsilon_1 < 1$ and $\epsilon_2 < 0$.

being the modulation strength, and q the wavenumber for the spatial modulation). Then the condition $\beta = k_y \pm mq$, (where k_y is the y-component of the incident wavenumber, $m = 1, 2, 3...$) also allows for the excitation of SPPs at the interface [28]. Chapters following Chapter 3 will utilize this method of coupling. This method allows SPP excitation even for normal incident of the external wave.

CHAPTER 2

FINITE ELEMENT METHOD

2.1 Numerical Methods

There are only a limited number of problems that analytical solutions to Maxwell's, or even most differential, equations are known. In plasmonics, analytical methods, like Mie theory, are limited to planar geometries or objects with simple shapes (such as spheres or cylinders). As such, numerical methods must be employed to look for solutions in most problems. While the finite element method (FEM) is the choice method of this work, there also exist a number of other numerical methods that are in use in plasmonics research. To mention a few, the Green dyadic method and the discrete dipole approximation are used to calculate the scattering from metallic structures embedded in uniform or planarly layered media. The finite-difference frequency methods use piecewise constant expressions to approximate solutions to derivatives. For a more comprehensive review, see [33].

2.2 Finite Element Method

The finite element method is a numerical technique for solving differential equations. Though FEM has its earliest roots in structural mechanics and is found in papers as early as the 1940's [34, 35], today it covers a wide range of areas, including electromagnetism. Though FEM can be applied to a multitude of multidimensional systems, the focus here will be on 2D problems as they are the sort of problems discussed here.

The general 2nd order partial differential equation that is solved is

$$-\frac{\partial}{\partial x}\left[\alpha_x(x,y)\frac{\partial\phi(x,y)}{\partial x}\right]-\frac{\partial}{\partial y}\left[\alpha_y(x,y)\frac{\partial\phi(x,y)}{\partial y}\right]+\beta(x,y)\phi(x,y)=f(x,y), \quad (2.1)$$

where $\phi(x, y)$ is the unknown value, α_x, α_y, and $\beta(x, y)$ are known physical quantities and $f(x, y)$ is the source or excitation function.

For most systems Eq. (2.1) is very difficult to solve. In FEM one approximate solution is not sought for the whole domain, Ω. Instead the domain is divided into smaller subdomains called elements. If the elements are small enough, then the value of $\phi(x, y)$ does not vary in a complicated way over the element and can be approximated by simple trial functions (such as polynomials).

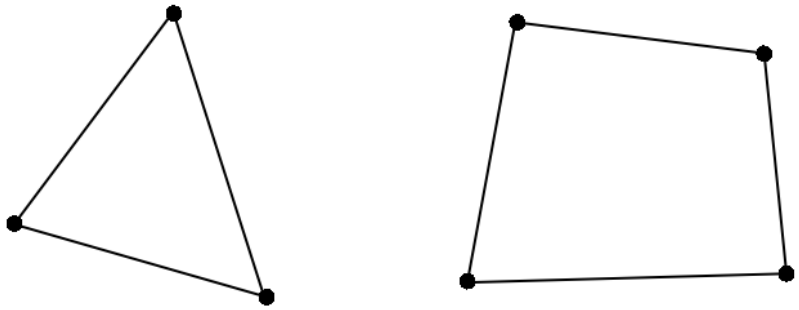

Figure 2.1: Examples of two dimensional elements

The discretization of the domain into elements is the first step in FEM analysis. The elements must not overlap and there must be no gaps between the elements. The shapes of elements are also kept simple to make computations easier. In two dimensional systems, the simple shapes used are triangles or quadrilaterals (Figure 2.1).

2.3 Formulation of Finite Element Method Equations

For each element the value of the approximate function is interpolated from the values at the nodes. For example, for a triangle element e (an element with three nodes), we can derive an expression for the approximate function in the following form:

$$\tilde{\phi^e} = \sum_{i=1}^{3} N_j^e \phi_j^e = \{N^e\}^T \{\phi^e\} = \{\phi^e\}^T \{N^e\}, \tag{2.2}$$

where ϕ_j^e is the value of ϕ at node j on element e and N_j^e are the interpolation functions. The interpolation functions' form varies by shape and order of polynomial used by the element and specifics can be found in any FEM text, such as [36]. An important quality of the interpolation functions is that N_j^e is only non-zero in elements connected with node j.

To form the approximate solution on each element the residual is defined as

$$r = -\frac{\partial}{\partial x}\left(\alpha_x \frac{\partial \phi}{\partial x}\right) - \frac{\partial}{\partial y}\left(\alpha_y \frac{\partial \phi}{\partial y}\right) + \beta\phi - f = 0. \tag{2.3}$$

For the exact solution, $r = 0$ is true everywhere. If an approximate solution, $\tilde{\phi}$, is substituted for the exact solution, ϕ, then r will no longer be 0. The family of weighted residual methods for finding approximate solution seeks to reduce the residual r when finding a satisfactory approximate solution $\tilde{\phi}$. To this end, on each element in the domain they enforce the condition

$$R_i = -\int_{\Omega^e} w_i r d\Omega = 0, \tag{2.4}$$

where R_i is the weighted residual. This condition, rather than seeking $r = 0$ only requires that, after weighted by a function w_i, r should average out to 0 over the area of each element. The Galerkin method [36] is the most widely used of the weighted residual methods and uses the interpolation functions, N_j^e, as the weighing functions, w_i.

The equation for the weighted residual using Galerkin's method is (for convenience, we will designate the approximate solution as ϕ rather than continue with $\tilde{\phi}$)

$$R_i^e = \iint_{\Omega^e} N_i^e \left[-\frac{\partial}{\partial x}\left(\alpha_x \frac{\partial \phi}{\partial x}\right) - \frac{\partial}{\partial y}\left(\alpha_y \frac{\partial \phi}{\partial y}\right) + \beta\phi - f\right] dxdy. \tag{2.5}$$

Using the identity

$$\frac{\partial}{\partial x}\left(\alpha \frac{\partial \phi}{\partial x}\psi\right) = \psi \frac{\partial}{\partial x}\left(\alpha \frac{\partial \phi}{\partial x}\right) + \alpha\left(\frac{\partial \phi}{\partial x}\right)\left(\frac{\partial \psi}{\partial x}\right) \tag{2.6}$$

and the divergence relation

$$\iint_{\Omega}\left(\frac{\partial U}{\partial x} + \frac{\partial V}{\partial y}\right) d\Omega = \oint_{\Gamma} (U\hat{\mathbf{x}} + V\hat{\mathbf{y}}) \cdot \hat{\mathbf{n}} d\Gamma \tag{2.7}$$

Eq. (2.5) becomes

$$\begin{aligned} R_i^e = \iint_{\Omega^e}\left(\alpha_x \frac{\partial N_i^e}{\partial x}\frac{\partial \phi}{\partial x} + \alpha_y \frac{\partial N_i^e}{\partial y}\frac{\partial \phi}{\partial y} + \beta N_i^e \phi\right) dxdy \\ - \iint_{\Omega^e} N_i^e f dxdy - \oint_{\Gamma^e} N_i^e \mathbf{D} \cdot \hat{\mathbf{n}}^e d\Gamma \end{aligned} \tag{2.8}$$

with

$$\mathbf{D} = \left(\alpha_x \frac{\partial \phi}{\partial x}\hat{\mathbf{x}} + \alpha_y \frac{\partial \phi}{\partial y}\hat{\mathbf{y}}\right). \tag{2.9}$$

Substituting the expression for the approximate solution in terms of the nodal values and the interpolation functions, Eq. (2.2), the expression for the weighted residual is

$$R_i^e = \sum_{j=1}^{3} \iint_{\Omega^e} \left(\alpha_x \frac{\partial N_i^e}{\partial x} \frac{\partial N_j^e}{\partial x} + \alpha_y \frac{\partial N_i^e}{\partial y} \frac{\partial N_j^e}{\partial y} + \beta N_i^e N_j^e \right) \phi_j^e dxdy - \iint_{\Omega^e} N_i^e f dxdy - \oint_{\Gamma^e} N_i^e \mathbf{D} \cdot \hat{\mathbf{n}}^e d\Gamma. \tag{2.10}$$

Eq. (2.10) can be also written in matrix form as

$$\{R^e\} = [K^e]\{\phi^e\} - \{b^e\} - \{g^e\} \tag{2.11}$$

where

$$[K^e]_{ij} = \iint_{\Omega^e} \left(\alpha_x \frac{\partial N_i^e}{\partial x} \frac{\partial N_j^e}{\partial x} + \alpha_y \frac{\partial N_i^e}{\partial y} \frac{\partial N_j^e}{\partial y} + \beta N_i^e N_j^e \right) dxdy, \tag{2.12}$$

$$\{b^e\} = \iint_{\Omega^e} N_i^e f dxdy, \tag{2.13}$$

$$\{g^e\} = \oint_{\Gamma^e} N_i^e \mathbf{D} \cdot \hat{\mathbf{n}}^e d\Gamma. \tag{2.14}$$

Since only the elements that are directly connected to the node i contribute to the weighted residual R_i, we may expand Eq. (2.11) using local and global relations and sum over all M elements to arrive at

$$\{R\} = \sum_{e=1}^{M} \{\bar{R}^e\} = \sum_{e=1}^{M} [\bar{K}^e]\{\phi^e\} - \{\bar{b}^e\} - \{\bar{g}^e\} \tag{2.15}$$

where the bar denotes the vector or matrix has been augmented or expanded. The process of summing over the elemental equations to form the final system of equations is called the assembly. Though described separately from the assembly in computer implementation the formulation of the elemental equations happens during the assembly. Further entwined with the elemental formulation and the assembly is the application of boundary conditions which must be applied before solving the problem.

2.4 Boundary Conditions

To solve any differential equation one must also have appropriate boundary conditions. Only by specifying the boundary conditions associated with the domain of the differential equation it is possible to determine the real solution.

If ϕ is the unknown function, then on a boundary of the domain, a boundary condition of the form,

$$\phi|_C = p(x, y), \tag{2.16}$$

where C is the boundary curve, is referred to as a boundary condition of the first kind or a Dirichlet condition. It specifies the field at the boundary. Conditions that specify the value of the derivative normal to the boundary and have the form

$$\left(\alpha_x \frac{\partial \phi}{\partial x} + \alpha_y \frac{\partial \phi}{\partial y}\right)\bigg|_C = q(x, y), \tag{2.17}$$

are referred to as boundary conditions of the second kind or a Neumann condition. Here p and q are known parameters that come about from the known physical properties of the boundary. They could be a boundary source or excitation (such as surface charge or surface current). It is of course possible to make conditions that use both the value of the function as well as its derivative and those are referred to as boundary conditions of the third kind or mixed boundary conditions.

2.4.1 Continuity Condition

The continuity boundary conditions at the interface between two media follow from Maxwell's equations. They are expressed mathematically as

$$\hat{\mathbf{n}} \times (\mathbf{E}_1 - \mathbf{E}_2) = 0, \tag{2.18a}$$

$$\hat{\mathbf{n}} \cdot (\mathbf{D}_1 - \mathbf{D}_2) = \rho_s, \tag{2.18b}$$

$$\hat{\mathbf{n}} \times (\mathbf{H}_1 - \mathbf{H}_2) = \mathbf{J}_s, \tag{2.18c}$$

$$\hat{\mathbf{n}} \cdot (\mathbf{B}_1 - \mathbf{B}_2) = 0, \tag{2.18d}$$

where $\hat{\mathbf{n}}$ is the unit vector normal to the interface pointing from medium 2 into medium 1, ρ_s and $\mathbf{J}_s$ are the surface charge and surface current at the interface. These equations are

known as the field continuity equations. They are also called internal boundary conditions because the boundary described is inside the model between two subdomains that have their own properties.

2.4.2 Matched Boundary Condition

To apply FEM for an infinite domain it is necessary to truncate the model's exterior with an artificial boundary. The matched boundary is an example of such an external boundary condition. It can be used to represent open space if the form of the field is known. The generic geometry is illustrated in Figure 2.2. If a plane wave is incident from the left, then it will interact with the discontinuity illustrated. If the boundaries AB and CD are far enough from the discontinuity, the field at AB can be expressed as the total sum of the incident and reflected waves,

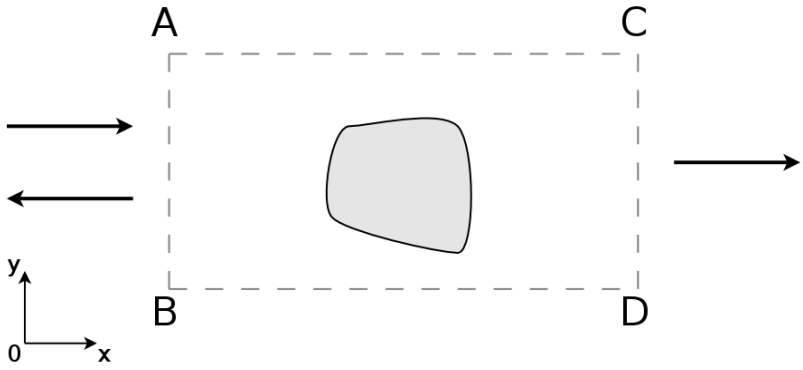

Figure 2.2: Wave incident on an object as well as the reflected and transmitted wave.

$$H_z = H_z^{inc} + H_z^{ref} = H_0 e^{-ik_0 x} + r H_0 e^{ik_0 x}, \tag{2.19}$$

where H_0 is a constant, r is the reflection coefficient, and k_0 is the propagation constant. On boundary CD there is only the transmitted wave

$$H_z = H_z^{trans} = t H_0 e^{-ik_0 x}, \tag{2.20}$$

where t is the transmission coefficient.

After some algebra, the boundary condition at AB can be expressed as

$$\frac{\partial H_z}{\partial x} = -ik_0 H_z - 2ik_0 H_0 e^{-ik_0 x}. \tag{2.21}$$

In this way we have a boundary condition at AB that excludes r and has only one free parameter, H_0, that can be designated in our model. The boundary condition at CD can be expressed as

$$\frac{\partial H_z}{\partial x} = -ik_0 H_z, \tag{2.22}$$

in much the same way. Once the field, H_z, has been found r and t can be calculated from Eq. (2.19) and (2.20):

$$r = \frac{H_z(x_1) - H_0 e^{-ik_0 x_1}}{H_0 e^{ik_0 x_1}}, \tag{2.23}$$

$$t = \frac{H_z(x_2)}{H_0 e^{-ik_0 x_2}}, \tag{2.24}$$

where x_1 denotes the position of boundary AB and x_2 denotes the position of boundary CD. If there are no lossy materials in the model, then

$$|r|^2 + |t|^2 = 1 \tag{2.25}$$

because of the conservation of energy. If there are lossy materials present, the amount of energy dissipated can be calculated as

$$A = 1 - |r|^2 - |t|^2. \tag{2.26}$$

2.4.3 Periodic Boundary Condition

Another way to limit or reduce the size of the simulation is to account for periodicity. If there is periodic structure in the model, a periodic boundary condition can be utilized. An example would be the boundaries AC and BD in Figure 2.2. The periodic boundary condition links two opposite boundaries by either specifying the tangent field components of the solution variable are equal,

$$\mathbf{H}_{dst} = \mathbf{H}_{src}, \tag{2.27}$$

or that the components have opposite sign,

$$\mathbf{H}_{dst} = -\mathbf{H}_{src}, \tag{2.28}$$

or have their values shifted by a phase difference,

$$\mathbf{H}_{dst} = \mathbf{H}_{src} e^{-i\mathbf{k}\cdot(\mathbf{r}_{dst}-\mathbf{r}_{src})}. \tag{2.29}$$

The phase shift is defined by a wave vector **k** and the distance between the source and destination.

2.5 Perfectly Matched Layers

The matched boundary condition allows us to truncate a model that would extend to infinity but it assumes that the form of the fields at the boundary is known. A relatively new and different way to truncate the model is the perfectly matched layer method that was proposed in 1994 by Berenger [37]. Beyond the truncated boundary, it creates a space, as illustrated in Figure 2.3, that is lossy but does not reflect plane waves for all angles of incidence, polarizations, and frequencies. Since Berenger's work, there have been many ways to interpret perfectly matched layers and here we will focus on the interpretation by Chew and Weedon [38].

In the perfectly matched layer space a set of modified Maxwell's equations are solved that stretch the coordinates in the frequency domain. Consider the set of modified source-

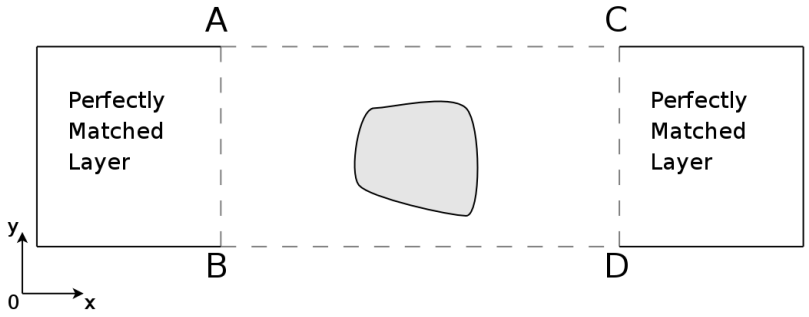

Figure 2.3: Use of PML layers to truncate the computational domain along the x-axis

free Maxwell's equations below:

$$\nabla_s \times \mathbf{E} = -i\omega\mu\mathbf{H}, \tag{2.30}$$

$$\nabla_s \times \mathbf{H} = i\omega\epsilon\mathbf{E}, \tag{2.31}$$

$$\nabla_s \cdot (\epsilon\mathbf{E}) = 0, \tag{2.32}$$

$$\nabla_s \cdot (\mu\mathbf{H}) = 0, \tag{2.33}$$

where ∇_s is defined by

$$\nabla_s = \hat{\mathbf{x}}\frac{1}{s_x}\frac{\partial}{\partial x} + \hat{\mathbf{y}}\frac{1}{s_y}\frac{\partial}{\partial y} + \hat{\mathbf{z}}\frac{1}{s_z}\frac{\partial}{\partial z}. \tag{2.34}$$

∇_s is in a sense the standard ∇ operator in Cartesian coordinate system but whose x, y, and z axes are stretched by a factor s_x, s_y, and s_z, respectively. Also, $s_x = s_x(x)$, $s_y = s_y(y)$, and $s_z = s_z(z)$.

If we substitute a plane wave whose electric and magnetic fields are given by

$$\mathbf{E} = \mathbf{E}_0 e^{-i\mathbf{k}\cdot\mathbf{r}} = \mathbf{E}_0 e^{-i(k_x x + k_y y + k_z z)}, \tag{2.35}$$

$$\mathbf{H} = \mathbf{H}_0 e^{-i\mathbf{k}\cdot\mathbf{r}} = \mathbf{H}_0 e^{-i(k_x x + k_y y + k_z z)}, \tag{2.36}$$

into the system of equations (2.30), then

$$\mathbf{k}_s \times \mathbf{E} = \omega\mu\mathbf{H}, \tag{2.37}$$

$$\mathbf{k}_s \times \mathbf{H} = -\omega\epsilon\mathbf{E}, \tag{2.38}$$

$$\mathbf{k}_s \cdot \mathbf{E} = 0, \tag{2.39}$$

$$\mathbf{k}_s \cdot \mathbf{H} = 0, \tag{2.40}$$

where

$$\mathbf{k}_s = \hat{\mathbf{x}}\frac{k_x}{s_x} + \hat{\mathbf{y}}\frac{k_y}{s_y} + \hat{\mathbf{z}}\frac{k_z}{s_z}. \tag{2.41}$$

Combining the first two equations of (2.37) gives

$$\mathbf{k}_s \times (\mathbf{k}_s \times \mathbf{E}) = \omega\mu\mathbf{k}_s \times \mathbf{H} = -\omega^2\mu\epsilon\mathbf{E}, \tag{2.42}$$

which becomes

$$(\mathbf{k}_s \cdot \mathbf{k}_s)\mathbf{E} = \omega^2\mu\epsilon\mathbf{E}. \tag{2.43}$$

The resultant dispersion relation is

$$\mathbf{k}_s \cdot \mathbf{k}_s = \omega^2 \mu\epsilon = \kappa^2, \tag{2.44}$$

or

$$\left(\frac{k_x}{s_x}\right)^2 + \left(\frac{k_y}{s_y}\right)^2 + \left(\frac{k_z}{s_z}\right)^2 = \kappa^2. \tag{2.45}$$

The solution to Eq. (2.45) is

$$k_x = \kappa s_x \sin\theta\cos\phi, \tag{2.46}$$

$$k_y = \kappa s_y \sin\theta\cos\phi, \tag{2.47}$$

$$k_z = \kappa s_z \cos\theta. \tag{2.48}$$

It is easy to see that if s_i is a complex number, the wave will be attenuated in the i-direction. The wave impedance, however, is unchanged by the stretching factor since

$$\eta = \frac{|E|}{|H|} = \frac{|\mathbf{k}_s|}{\omega\epsilon} = \frac{\omega\mu}{|\mathbf{k}_s|} = \sqrt{\frac{\mu}{\epsilon}}. \tag{2.49}$$

We now consider the reflection of a TM plane-wave from the interface between two half-spaces in the stretched coordinate system (2.30). For a TM plane wave the incident, reflected, and transmitted fields can be written as

$$\mathbf{H}_i = \mathbf{H}_0 e^{-i\mathbf{k}_i\cdot\mathbf{r}}, \tag{2.50}$$

$$\mathbf{H}_r = r^{TM}\mathbf{H}_0 e^{-i\mathbf{k}_r\cdot\mathbf{r}}, \tag{2.51}$$

$$\mathbf{H}_t = t^{TM}\mathbf{H}_0 e^{-i\mathbf{k}_t\cdot\mathbf{r}}, \tag{2.52}$$

where H_0 is a constant vector perpendicular to $\hat{\mathbf{x}}$ and r^{TM} and t^{TM} are the reflection and transmission coefficients for TM polarization, respectively. Using the continuity of the tangential components of the **E** and **H** fields, we can solve for r^{TM}

$$r^{TM} = \frac{k_{1z}s_{2z}\epsilon_2 - k_{2z}s_{1z}\epsilon_1}{k_{1z}s_{2z}\epsilon_2 + k_{2z}s_{1z}\epsilon_1}. \tag{2.53}$$

The subscript 1 denotes the half-space for $z < 0$ and the subscript 2 denotes the half-space for $z > 0$. For a TE wave, the reflection coefficient can be similarly calculated as

$$r^{TE} = \frac{k_{1z}s_{2z}\mu_2 - k_{2z}s_{1z}\mu_1}{k_{1z}s_{2z}\mu_2 + k_{2z}s_{1z}\mu_1}. \tag{2.54}$$

From the matching phase conditions, $k_{1x} = k_{2x}$ and $k_{1y} = k_{2y}$ and equations (2.46), we arrive at

$$\kappa_1 s_{1x} \sin\theta_1 \cos\phi_1 = \kappa_2 s_{2x} \sin\theta_2 \cos\phi_2, \tag{2.55}$$

$$\kappa_1 s_{1x} \sin\theta_1 \sin\phi_1 = \kappa_2 s_{2x} \sin\theta_2 \sin\phi_2. \tag{2.56}$$

If the parameters are chosen such that $\epsilon_1 = \epsilon_2$, $\mu_1 = \mu_2$, $s_{1x} = s_{2x}$, and $s_{1y} = s_{2y}$, then

$$\theta_1 = \theta_2, \tag{2.57}$$

$$\phi_1 = \phi_2, \tag{2.58}$$

must be true and, consequently,

$$r^{TM} = r^{TE} = 0. \tag{2.59}$$

The remarkable fact is that this remains true regardless of the incident angle of the wave, its frequency, or our choice of s_{1z} and s_{2z}. As such, if we make s_{2z} of the form $s_{2z} = s' - is''$, where s' and s'' are constants and real numbers that meet the conditions $s' \geq 1$ (for faster decay of evanescent waves) and $s'' \geq 0$ (for absorption of propagating waves), then $k_{2z} = \kappa_2(s' - is'')\cos\theta$. As a result, the transmitted wave will decay by the exponential factor $\exp(\kappa_2 s'' z \cos\theta)$ in the z-direction.

Of course, the PML layer also cannot extend to infinity and must be truncated as well. Usually it will be truncated with a metal place at a distance L away from the interface. The metal plate creates a reflection of the highly attenuated wave as

$$|r(\theta)| = e^{-2\kappa_2 s'' L \cos\theta}, \tag{2.60}$$

as long as κ_2 is a real value. The PML layer thus must be long enough that $|R(\theta)|$ is small and negligible. In this manner, a metal-backed PML can be used as a reflectionless absorbing layer to simulate a material, such as vacuum, extending to infinity.

The PML layer as derived, however, is only reflectionless in continuum space. In discretized space some reflections will always happen. This unfortunate reflection from a PML is angle dependent and can be very high for angles of incidence approaching $90°$. In this report, PML layers were only used for normal incidence where the reflections can be made very small.

2.6 COMSOL Multiphysics

The FEM software package employed in this paper is COMSOL Multiphysics version 3.5a [39]. COMSOL is a multipurpose FEM program but also comes with modules with predefined equations and variables for a wide range of applications. It allows for the coupling of equations between modules so that different sets of physical equations can be solved simultaneously. COMSOL also offers a large toolbox of preprocessing and postprocessing capabilities as well as allowing for scripting and running simulations with MATLAB.

While the basic application modes cover a number of different applications, such as heat transfer, acoustics, etc., more in depth modules are available to be licensed. Specifically, the RF module, which deals with the characterizations of electromagnetic fields for high-frequency applications, was invaluable in this work. The solved equations and boundary conditions, except for the diffraction grating boundary condition in Chapter 5, were provided by the RF module. Scripts in MATLAB were used to parameterize the simulations as well as perform and assist in much of the post-processing.

CHAPTER 3

RESONANT AMPLIFICATION OF EVANESCENT WAVES AND REFLECTIONLESS ABSORPTION

The simplest geometry that can sustain SPPs, excited by a TM polarized wave, is a single interface between a dielectric with permittivity, $Re[\epsilon_1] > 0$ and a material with $Re[\epsilon_2] < 0$. To excite a SPP with an incident electromagnetic field requires phase matching techniques. One such method to match phases between the EM field and the SPP is to use a field that is evanescent near the interface. To that end, [40] investigates a layer of negative permittivity material in vacuum preceded by a layer of material with $0 < \epsilon < 1$, illustrated in Figure 3.1. Since the field is incident from vacuum, $\epsilon_0 = 1$, and $\epsilon_0 > \varepsilon_1$, the incident wave will be totally internally reflected for incident angles greater than the critical angle, $\theta_c = \sin^{-1}(n_1/n \sin\theta_1)$. When a wave is totally internally reflected, it does still penetrate into the lower permittivity material as an evanescent wave (ie. k_x is imaginary). The evanescent field then has $k_y = \sqrt{\omega^2/c^2 - k_x^2}$ component greater than that of the incident field in vacuum. It is then possible to excite SPPs at the interface between materials with ϵ_1 and ϵ_2 with the evanescent field from the interface with ϵ_0 and ϵ_1.

The negative permittivity in the negative permittivity material is modelled as,

$$\epsilon_2 = 1 - \frac{\omega_{p2}^2}{\omega^2 + i\omega\gamma}, \tag{3.1}$$

for $\omega < \omega_{p2}$ and γ is the absorption parameter.

The case of no absorption was studied analytically in Ref. [40]. The result was confirmed by using the finite element method [39] providing a benchmark test of the numerics. The results of FEM simulations is shown, as a function of the plane wave incidence angle, in Figure 3.2. The wave is almost completely reflected everywhere except at a small

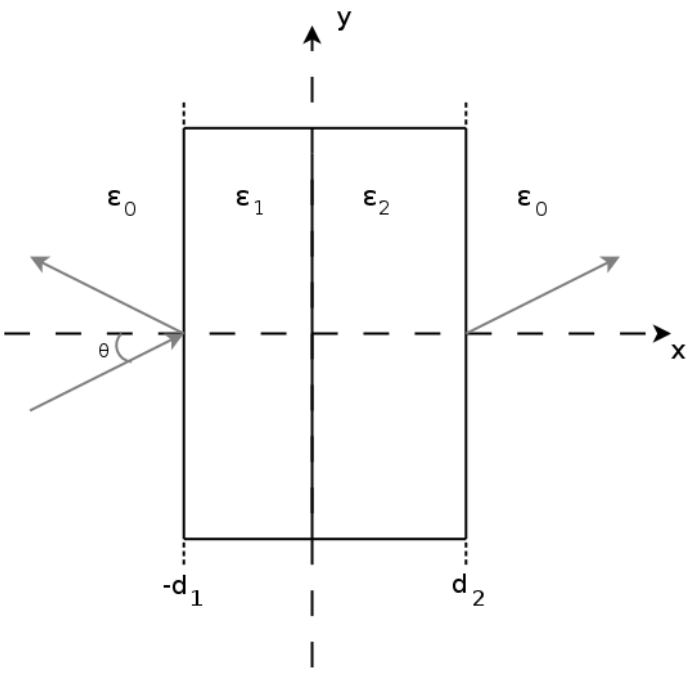

Figure 3.1: Geometry of a two layer plasma system. Here $0 < \epsilon_1 < 1$ and $\epsilon_2 < 0$.

range of angles. The angles at which the wave experiences extraordinary transmission are also greater than the critical angle for total internal reflection and the wave is actually evanescent in the medium with permittivity ϵ_1 as well as the medium with ϵ_2.

Expanding on the $\gamma = 0$ case, further results of transmission and reflection were calculated using the finite element method [39] as well as analytically calculated using the transmission matrix method (see Appendix). These calculations were done for a plasma with finite dissipation. We look to understand how transmission and reflection are changed as different levels of absorption. Absorption is accounted for by introducing the absorption parameter, γ, in the negative permittivity material.

Absorption was calculated using the energy conservation relation $A = 1 - R - T$. Results from the transmission matrix method and the finite element method agreed with each other, proving this to be a benchmark for the numerical method. The parameters for the simulations are $\epsilon_1 = 0.3428$, $\omega/\omega_{p2} = 0.5019$, $d_1 = 27c/\omega_{p2}$, $d_2 = 3.12c/\omega_{p2}$. In our case, $f = 1$ was used and that means that $d_1 = 64.702$ cm and $d_2 = 7.4769$ cm, approximately.

Figure 3.2 displays the numerical result for the $\gamma = 0$ case. Figures 3.3-3.8 show the

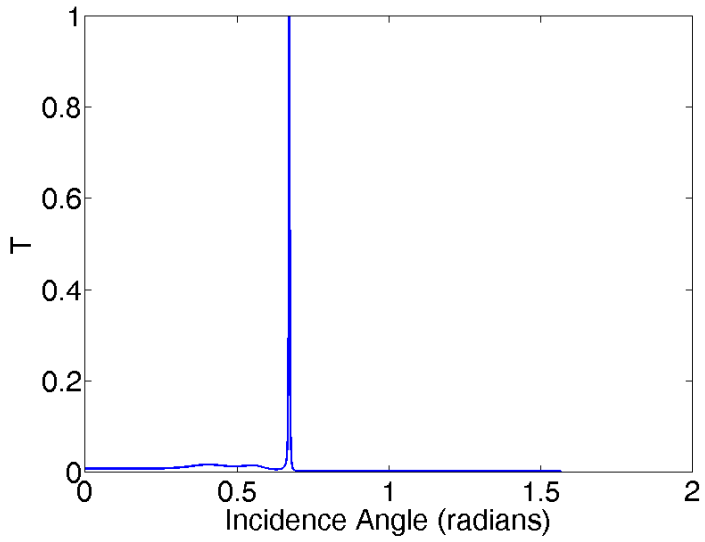

Figure 3.2: Transmission coefficient for $\gamma = 0$ and $\epsilon_1 = 0.3428$, $\omega/\omega_{p2} = 0.5019$, $d_1 = 64.702$ cm, $d_2 = 7.4769$ cm

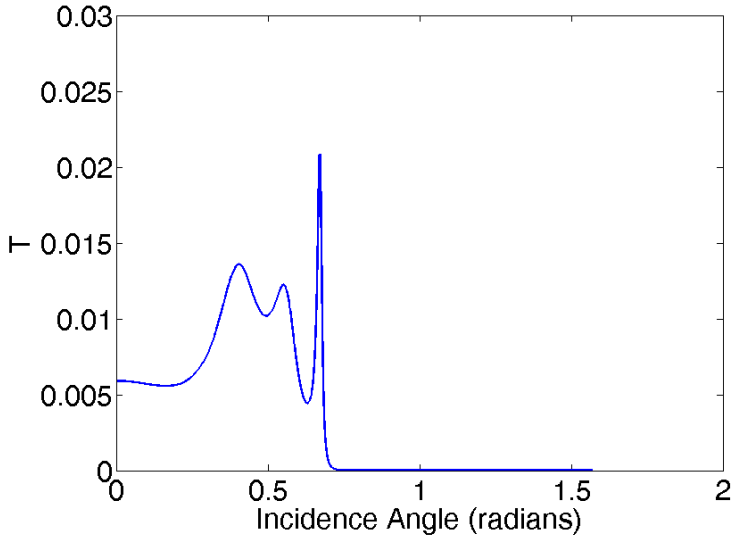

Figure 3.3: Transmission coefficient for $\gamma = 0.1\omega$ and $\epsilon_1 = 0.3428$, $\omega/\omega_{p2} = 0.5019$, $d_1 = 64.702$ cm, $d_2 = 7.4769$ cm

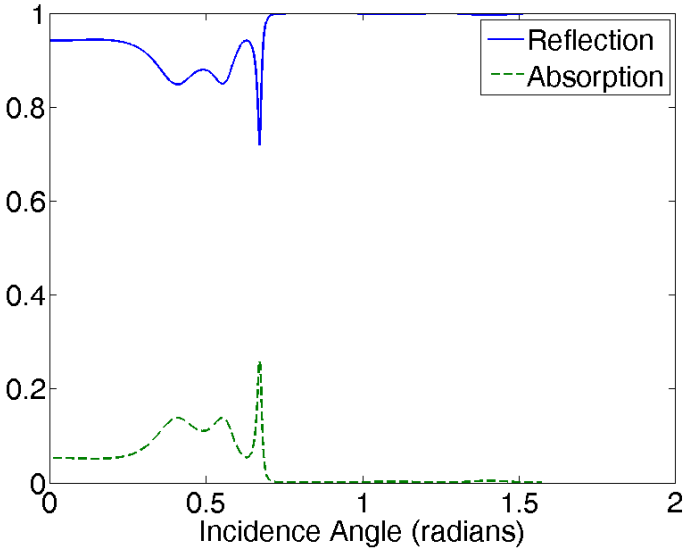

Figure 3.4: Reflection (solid line) and absorption (dashed line) coefficient for $\gamma = 0.1\omega$ and $\epsilon_1 = 0.3428$, $\omega/\omega_{p2} = 0.5019$, $d_1 = 64.702$ cm, $d_2 = 7.4769$ cm

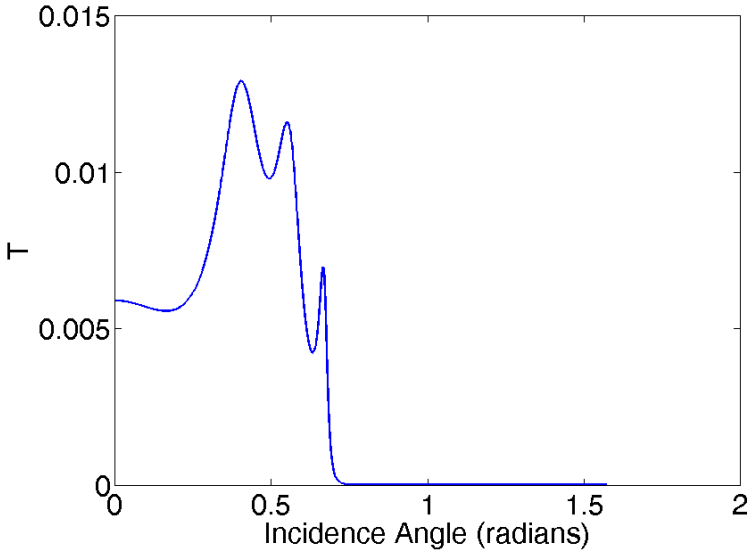

Figure 3.5: Transmission coefficient for $\gamma = 0.2\omega$ and $\epsilon_1 = 0.3428$, $\omega/\omega_{p2} = 0.5019$, $d_1 = 64.702$ cm, $d_2 = 7.4769$ cm

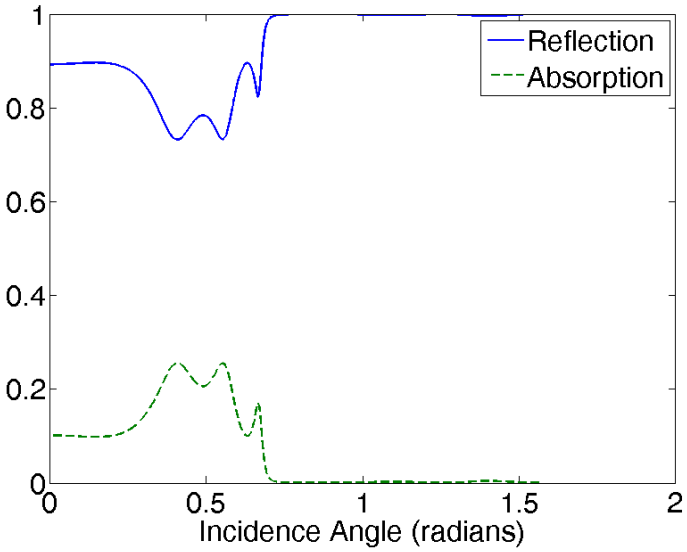

Figure 3.6: Reflection (solid line) and absorption (dashed line) coefficients for $\gamma = 0.2\omega$ and $\epsilon_1 = 0.3428$, $\omega/\omega_{p2} = 0.5019$, $d_1 = 64.702$ cm, $d_2 = 7.4769$ cm

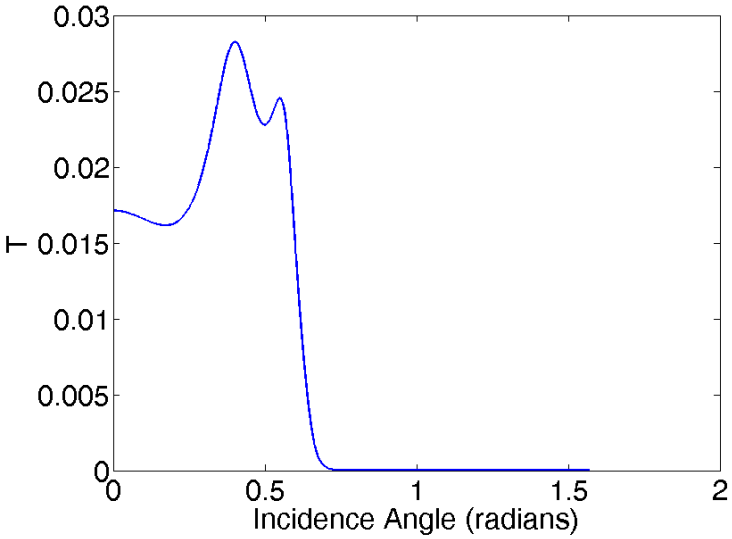

Figure 3.7: Transmission coefficient for $\gamma = \omega$ and $\epsilon_1 = 0.3428$, $\omega/\omega_{p2} = 0.5019$, $d_1 = 64.702$ cm, $d_2 = 7.4769$ cm

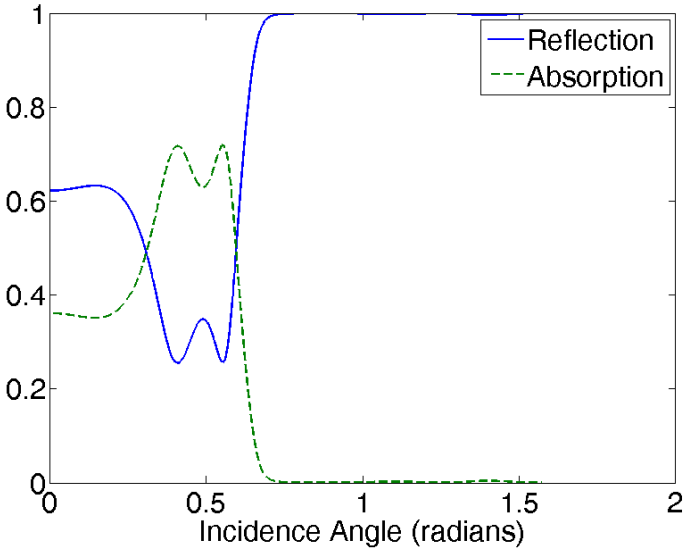

Figure 3.8: Reflection (solid line) and absorption (dashed line) coefficients for $\gamma = \omega$ and $\epsilon_1 = 0.3428$, $\omega/\omega_{p2} = 0.5019$, $d_1 = 64.702$ cm, $d_2 = 7.4769$ cm

absorption, transmission, and reflection plots for successively larger values of the damping constant, γ. Of particular interest is that, though the transmission peak does get smaller and more rounded with $\gamma \neq 0$, other peaks appear, as illustrated in Figure 3.3. As γ is further increased, these peaks also then become even higher than the original peak, as Figures 3.5-3.7 demonstrate. In fact, though the angle of maximum transmission remains mostly unchanged, at a certain value of γ, it changes to a different value that stays unchanged for greater values of the damping constant. When $\gamma = \omega$, the narrow transmission peak at $\gamma = 0$ cannot be found. Transmission, even at its highest, is very small and when reflection does go below 1, it is absorption that absorbs most of the non-reflected energy and very little is transmitted.

The same analysis was repeated for a system where both plasma layers are thinner. The thicknesses were $d_1 = 16.68$ cm and $d_2 = 3$ cm. Figures 3.9-3.14 show the values for absorption, reflection, and transmission, calculated with the numerical method. The permittivities are $\epsilon_1 = 0.5428$ and ϵ_2 is modelled again with Eq. (3.1) with the incident frequency $f = 1$ GHz and $\omega_{p2} = 2\omega$.

This geometry has about 30% transmission when only the ϵ_2 plasma layer is present.

When the ϵ_1 layer is added and ϵ_2 is not absorbing, a resonant transmission peak appears. This peak, however, is wider than in the earlier result in this chapter. As absorption is included in the second layer, modelled as before, it is easy to see that absorption too is resonant at the same frequencies as transmission and reflection were resonant at. As such, while absorption lowers the values of reflection and transmission at every incident angle, it affects transmission most at the resonant frequency.

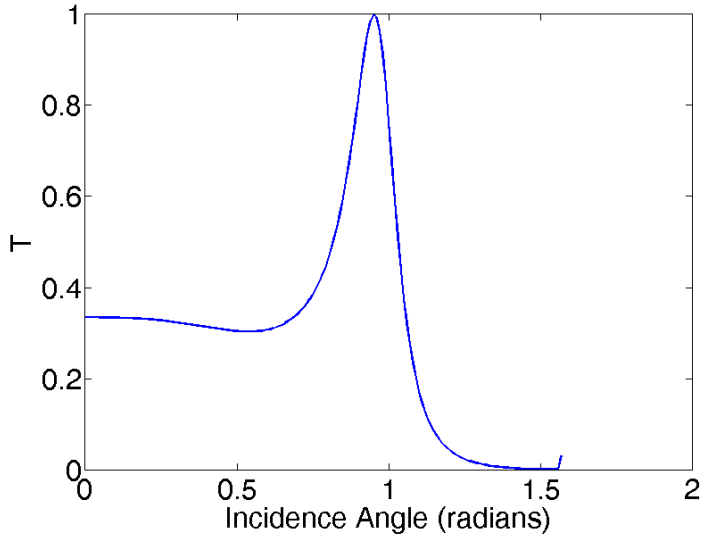

Figure 3.9: Transmission coefficient for $\gamma = 0$ and $\epsilon_1 = 0.5428$, $\omega/\omega_{p2} = 0.5$, $d_1 = 16.68$ cm, $d_2 = 3$ cm

3.1 Summary

In this chapter, we have demonstrated that FEM analysis can agree with analytical results for plasmonic behaviour of both the methods of Ref. [40] and the transmission matrices method of Appendix A. It is shown that for $\gamma = 0$, an evanescent wave can be used to create resonant transmission. This transmission behaviour is modified in the presence of absorption, which greatly limits the transmission. In that case, most of the energy that is not reflected at resonant angles is absorbed.

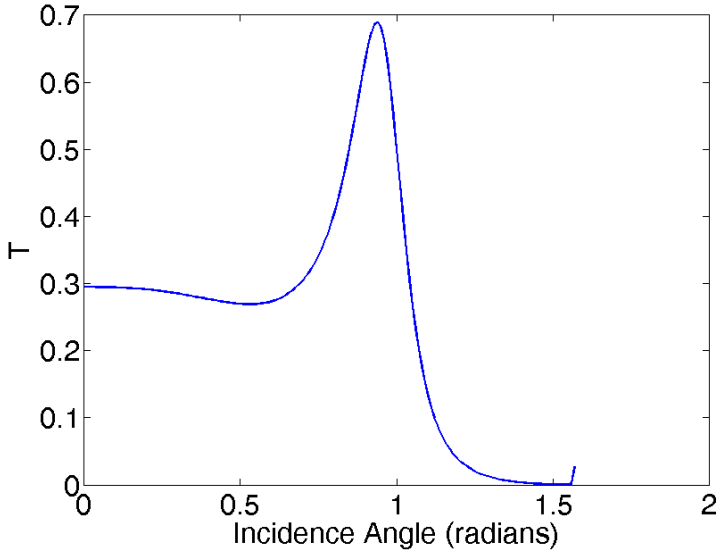

Figure 3.10: Transmission coefficient for $\gamma = 0.1\omega$ and $\epsilon_1 = 0.5428$, $\omega/\omega_{p2} = 0.5$, $d_1 = 16.68$ cm, $d_2 = 3$ cm

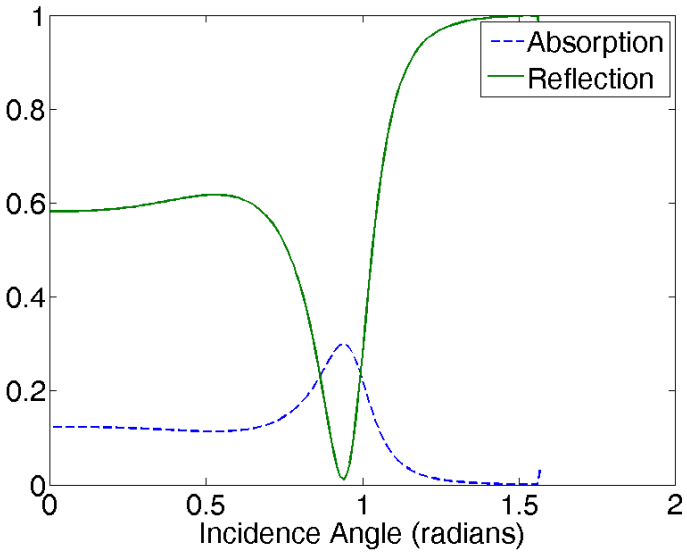

Figure 3.11: Reflection (solid line) and absorption (dashed line) coefficients for $\gamma = 0.1\omega$ and $\epsilon_1 = 0.5428$, $\omega/\omega_{p2} = 0.5$, $d_1 = 16.68$ cm, $d_2 = 3$ cm

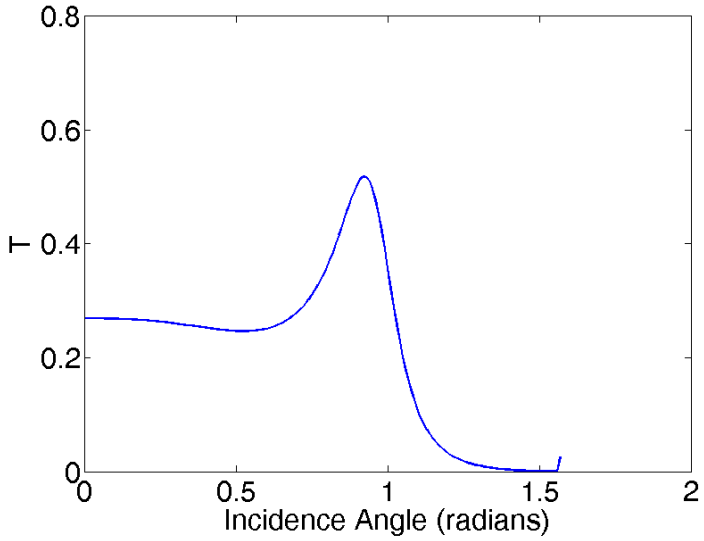

Figure 3.12: Transmission coefficient for $\gamma = 0.2\omega$ and $\epsilon_1 = 0.5428$, $\omega/\omega_{p2} = 0.5$, $d_1 = 16.68$ cm, $d_2 = 3$ cm

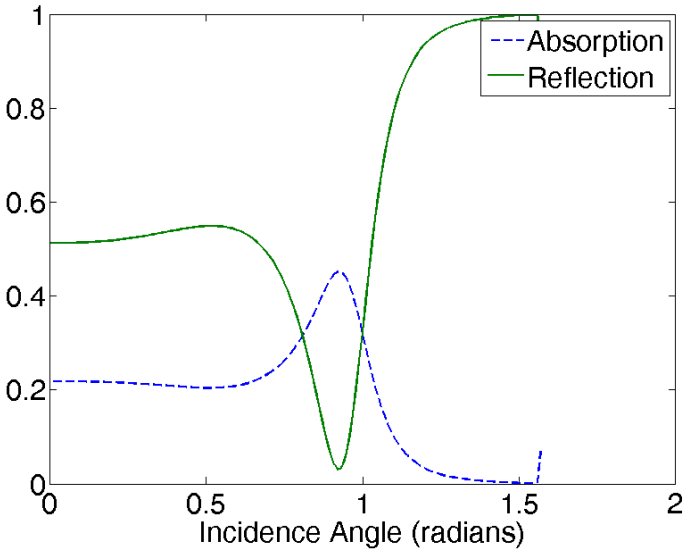

Figure 3.13: Reflection (solid line) and absorption (dashed line) coefficients for $\gamma = 0.2\omega$ and $\epsilon_1 = 0.5428$, $\omega/\omega_{p2} = 0.5$, $d_1 = 16.68$ cm, $d_2 = 3$ cm

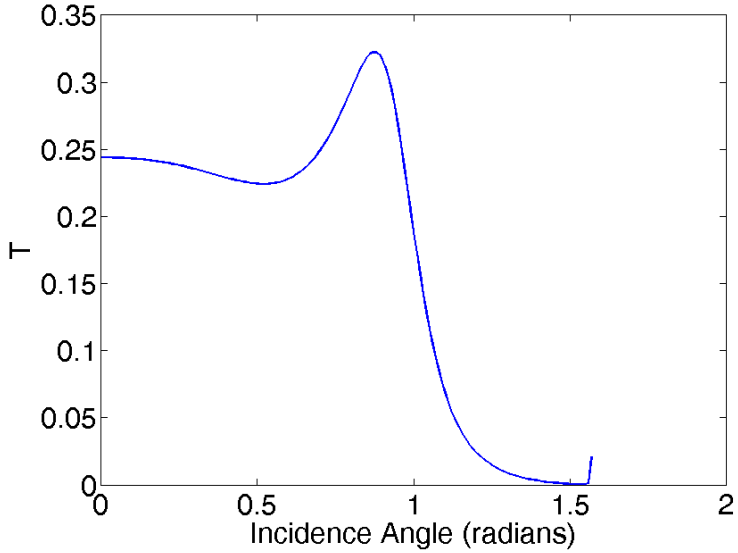

Figure 3.14: Transmission coefficient for $\gamma = 0.5\omega$ and $\epsilon_1 = 0.5428$, $\omega/\omega_{p2} = 0.5$, $d_1 = 16.68$ cm, $d_2 = 3$ cm

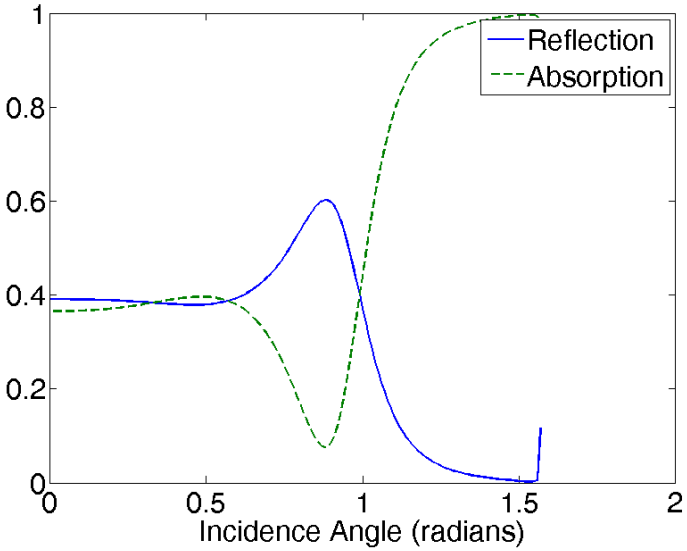

Figure 3.15: Reflection (solid line) and absorption (dashed line) coefficients for $\gamma = 0.5\omega$ and $\epsilon_1 = 0.5428$, $\omega/\omega_{p2} = 0.5$, $d_1 = 16.68$ cm, $d_2 = 3$ cm

CHAPTER 4

RESONANT TRANSMISSION THROUGH A FILM WITH MODULATED PERMITTIVITY

The excitation of SPPs at optical frequencies is of great interest because of the array of possible applications. This includes using the sharp resonances for applications in optical switching [16], enhancement of fluorescent emission [41], imaging [18, 23], as well as sensing [42]. One focus is the study of extraordinary transmission of optical frequencies through thin metal films. Though this work was sparked by transmission through sub-wavelength apertures [15], there is now also work about the transmission of light through a film without apertures.

Resonant transmission through a thin metal film without apertures was studied in Ref. [43] (as well as later in Ref. [44]). The film was assumed to have a modulated permittivity, $\epsilon = \epsilon_m(1 + g \sin qy)$ to create phase matching between the incident electromagnetic wave and the surface mode wave vector. Such a modulation could be imposed in the manufacturing process. It is also possible to induce such modulations with an external source of powerful radiation that can induce surface or bulk modification via, for example, Kerr nonlinearity [45].

In Ref. [43], the absorption and transmission of a normally incident electromagnetic wave was calculated analytically and the results were presented graphically. To model the behaviour of the silver film, a Drude model was utilized with the form,

$$\epsilon_m = \epsilon_b - \frac{\omega_p^2}{\omega(\omega + i\gamma)}. \tag{4.1}$$

The values used were thickness $d = 0.12\,\mu$m, spatial period of modulation $a = 0.5\,\mu$m, modulation parameter $g = 0.2$, interband transition contribution $\epsilon_b = 5$, plasma frequency

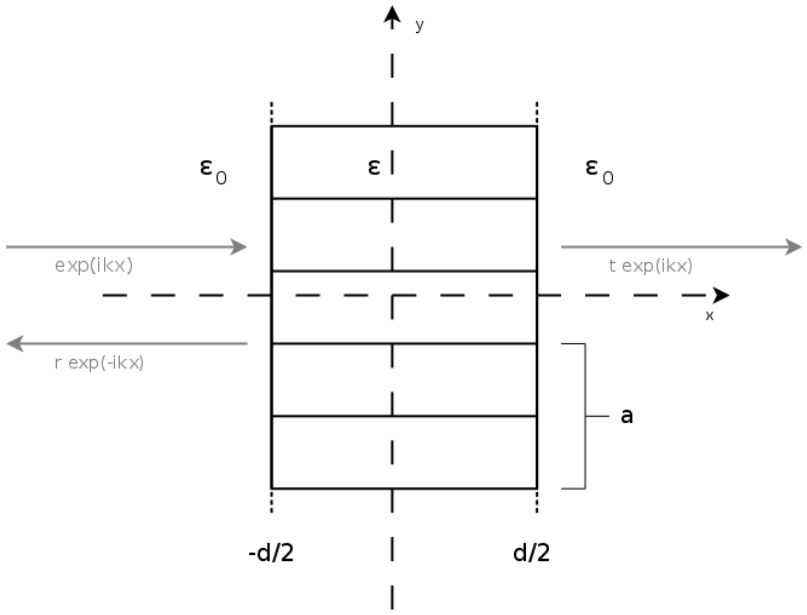

Figure 4.1: Geometry of a periodically modulated film of thickness *d*.

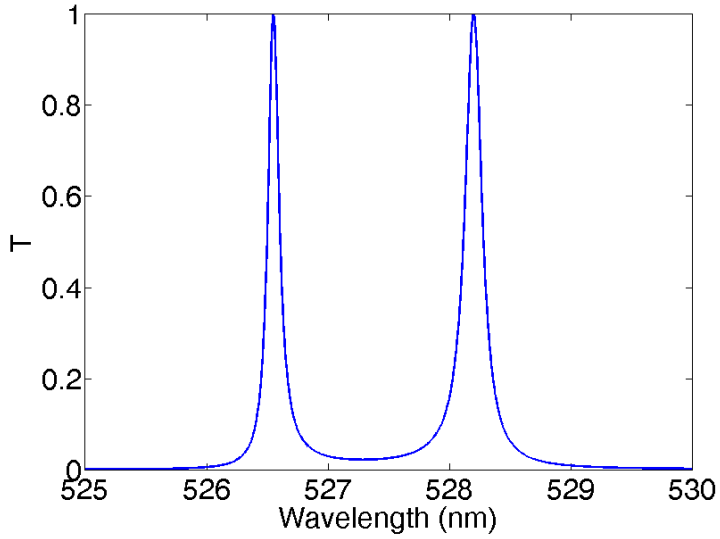

Figure 4.2: Transmittance versus wavelength of incident plane wave for a modulated silver film: $\gamma = 0$

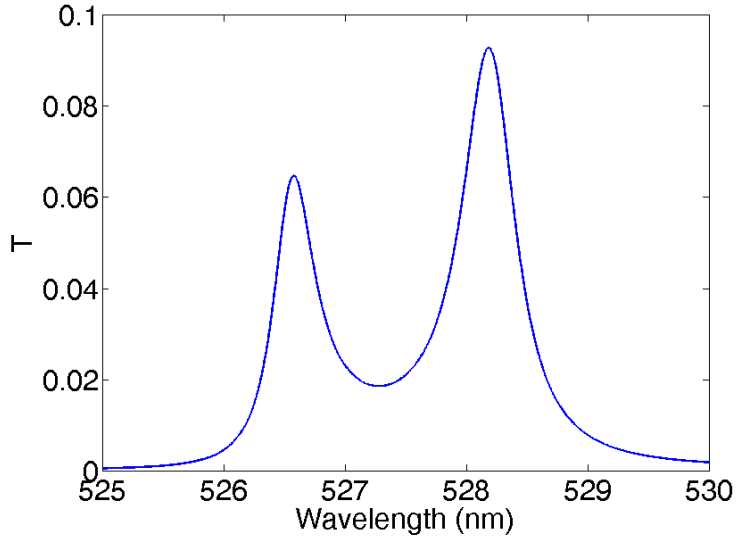

Figure 4.3: Transmittance for a modulated silver film: $\gamma = 0.5\,\omega_\tau$

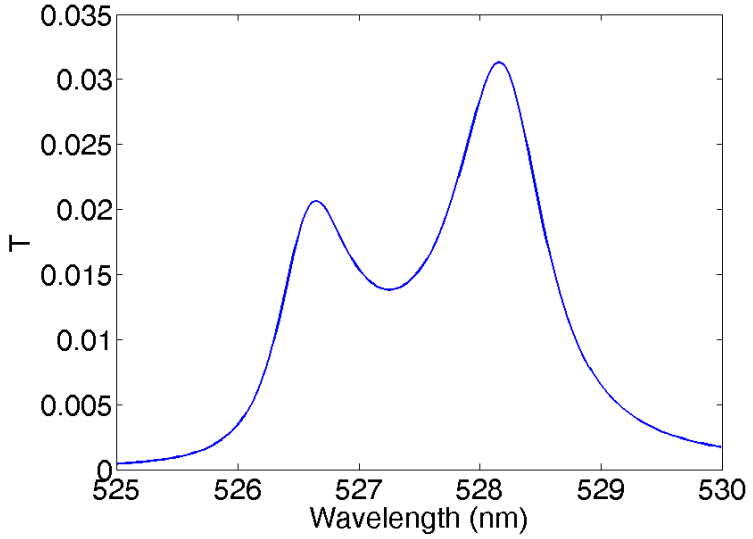

Figure 4.4: Transmittance versus wavelength of incident plane wave for a modulated silver film: $\gamma = \omega_\tau$.

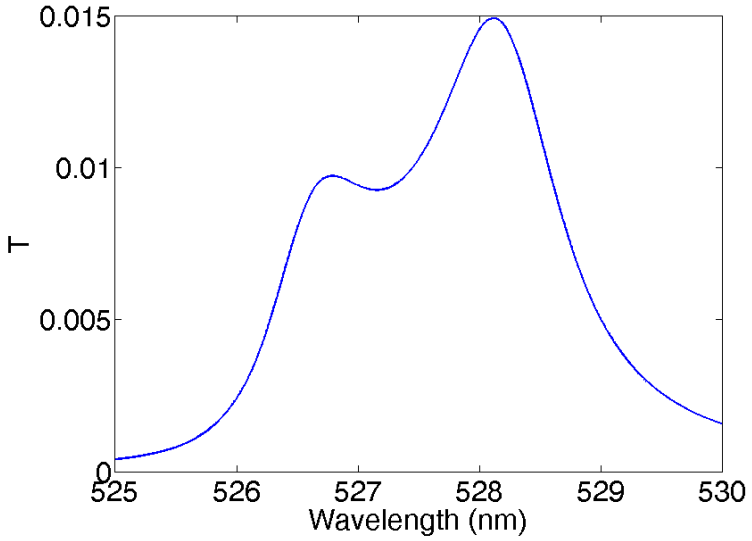

Figure 4.5: Transmittance for a modulated silver film: $\gamma = 1.5\,\omega_\tau$

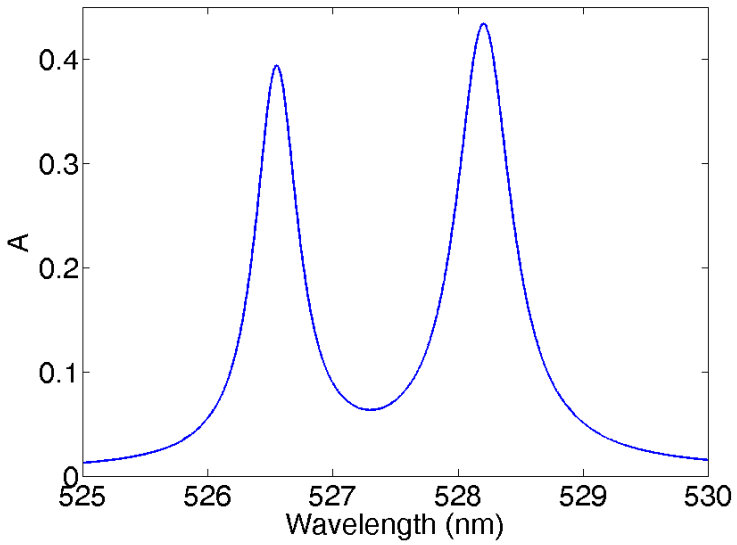

Figure 4.6: Absorption versus wavelength of incident plane wave for a modulated silver film: $\gamma = 0.5\,\omega_\tau$.

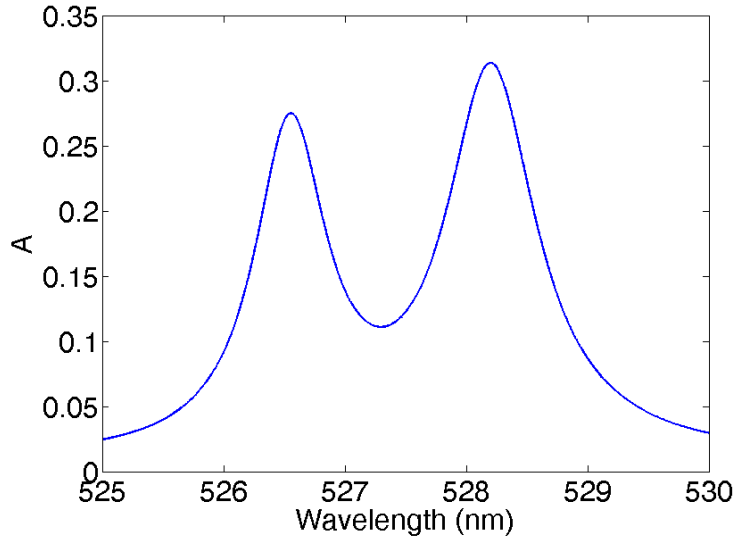

Figure 4.7: Absorption for a modulated silver film: $\gamma = \omega_\tau$

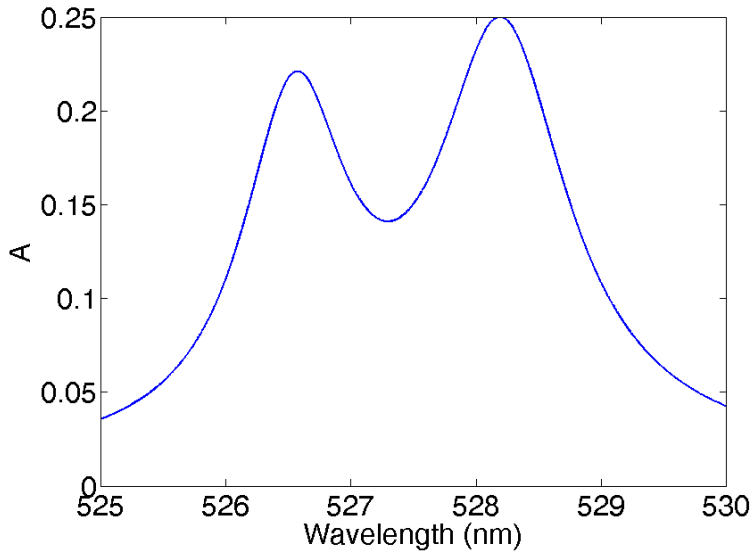

Figure 4.8: Absorption versus wavelength of incident plane wave for a modulated silver film: $\gamma = 1.5\,\omega_\tau$

$\omega_p = 9.1\,\text{eV}$, and damping coefficient $\gamma = \omega_\tau = 0.021\,\text{eV}$, (where ω_τ is the relaxation frequency). Though the transmittance is $< 0.02\,\%$ in the absence of modulation (inside the silver layer, the wave decays as $e^{-\lambda x}$), the transmission becomes strongly enhanced when the modulation is introduced.

We have solved for various parameters of γ in units of ω_τ using finite element analysis. Figures 4.2-4.8 shows the transmission and absorption coefficients as a function of the wavelength of the incident electromagnetic wave. Included as well is the $\gamma = \omega_\tau$ case covered by the analytical analysis of Ref. [43]. We note that though Ref. [43] has come under some criticism for the validity of approximations that was made by the authors [44], for these parameters the results of Ref. [43] agreed with our numerical results. It is important to note that analytical theory of Ref. [43] is based on the truncation of an infinite sequence of side-bands to a single pair of the first side-band (see more details in Chapter 5). Our FEM simulations are free from this assumption and take into account all harmonics. Our results show that the role of higher harmonics, which were neglected in Ref. [43], is insignificant and, as a result, results of the approximate analytical theory are well reproduced by exact numerical simulations.

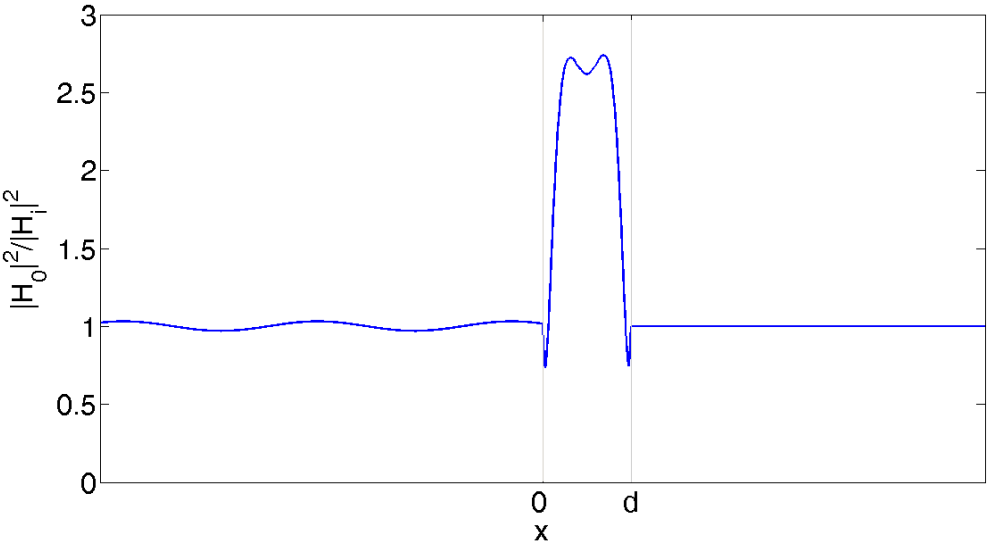

Figure 4.9: Profile of the normalized $|H_0|^2$ harmonic of the left transmission peak along the x-axis. The metal layer is located between $x = 0$ and $x = d$.

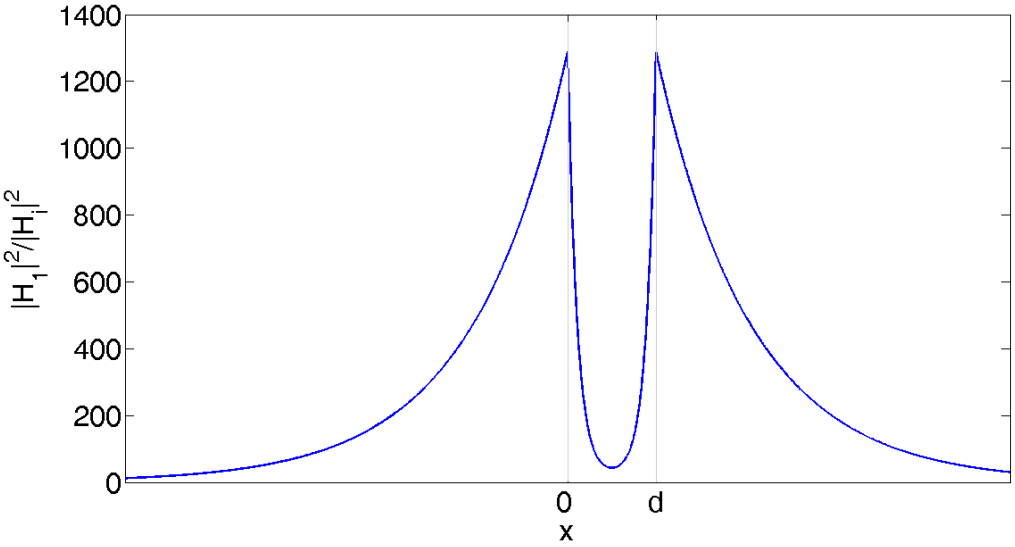

Figure 4.10: Profile of the normalized $|H_1|^2$ harmonic of the left transmission peak along the x-axis. The metal layer is located between $x = 0$ and $x = d$.

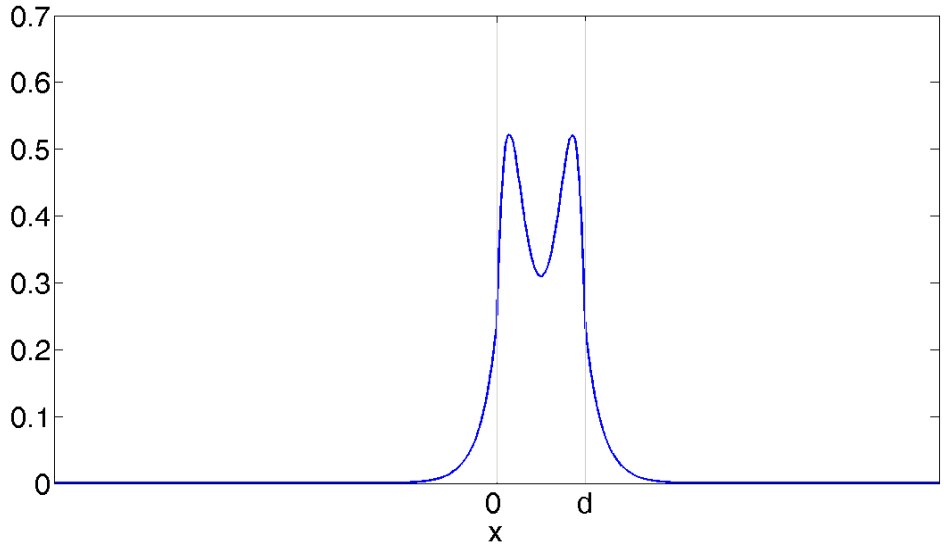

Figure 4.11: Profile of the normalized sum $\sum_{n=2}^{8} |H_n|^2$ harmonics of the left transmission peak along the x-axis. The metal layer is located between $x = 0$ and $x = d$.

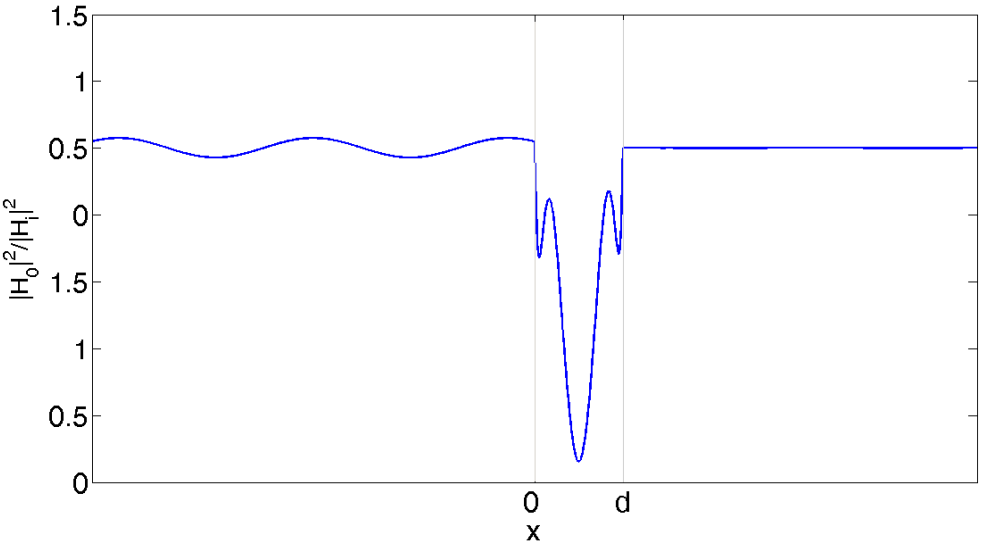

Figure 4.12: Profile of the normalized $|H_0|^2$ harmonic of the right transmission peak along the x-axis. The metal layer is located between $x = 0$ and $x = d$.

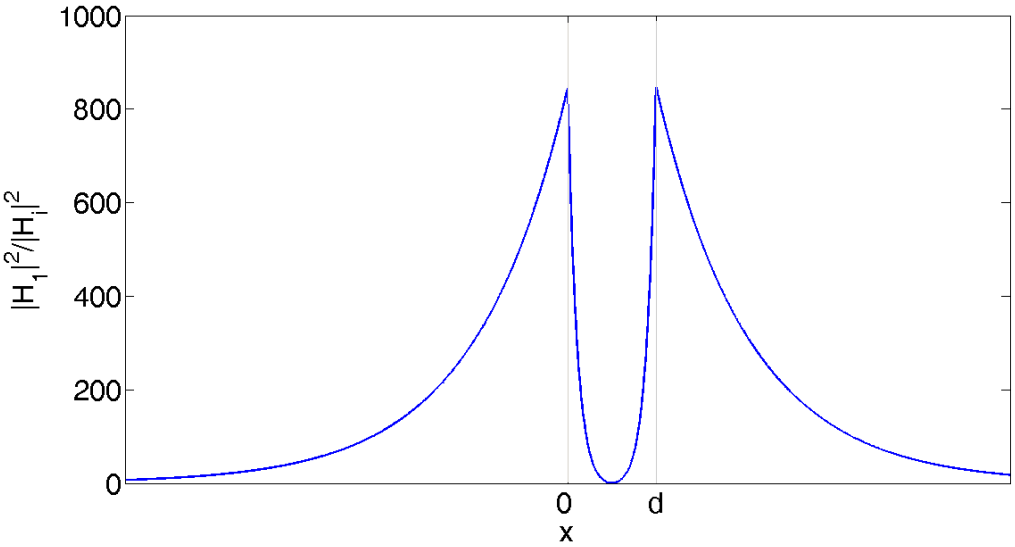

Figure 4.13: Profile of the normalized $|H_1|^2$ harmonic of the right transmission peak along the x-axis. The metal layer is located between $x = 0$ and $x = d$.

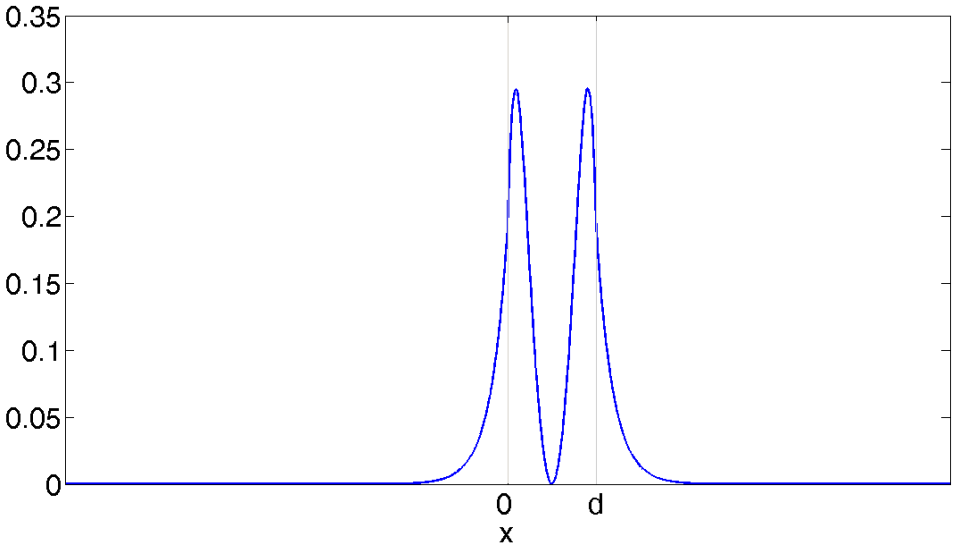

Figure 4.14: Profile of the normalized sum of the $\sum_{n=2}^{8} |H_n|^2$ harmonics of the right transmission peak along the x-axis. The metal layer is located between $x = 0$ and $x = d$.

4.1 Summary

Here we have compared the analytical solution of Ref. [43] with numerical results of the same problem. The analytical solution makes the assumption that the fundamental and first harmonics are sufficient to describe the field. As we have shown, for the sets of parameters used by Ref. [43], this assumption is true and we find that the analytical and numerical solutions agree.

CHAPTER 5

RESONANT AMPLIFICATION OF EVANESCENT WAVES WITH A DIFFRACTION GRATING

As it was noted in Chapter 1, the phenomenon of anomalously large transmission of electromagnetic waves through media with negative dielectric permittivity, such as a dense plasma, has attracted great interest in the last decade [46]. It was observed experimentally that sub-wavelength features in an electrodynamically opaque material can dramatically enhance transmission through the material [15]. Generally, the enhancement of the transmission is thought to be related to the resonant excitation of evanescent waves in the near field of the sub-wavelength structure. Such resonant modes exist both for a single structure, such as a sub-wavelength aperture, as well as for periodic arrays of defects such as holes or slits. The resonances may be related to the excitation of surface electromagnetic modes (polaritons) existing at the interface of two media with opposite signs of dielectric permittivities or with the excitation of cavity or waveguide modes of the individual defect. It is important to note that both types of resonances have been invoked to explain extraordinary transmission in various geometries [47–58]. The resonant modes in general have complicated structure and the exact mechanism can be different depending on the geometry [53, 59].

Most clearly the effects of surface wave [60, 61] excitation present themselves in extraordinary transmission through solid metal films. As it was discussed in Chapter 1, surface waves existing on the boundary of a metal film and vacuum are superluminal and therefore cannot be matched with propagating electromagnetic waves. One way matching between the incident EM wave and the surface charges can be achieved is via the periodic modulation of the film parameters, such as the dielectric constant, or corrugation of the

film thickness. Such modulation shifts the wave vector of the incoming wave to that of the surface wave resulting in resonance. Analytical models of strong enhancement of the transmission through the film with modulated density were presented in Refs. [43, 62–64]. These effects were experimentally observed with prefabricated [65] and photo-induced diffraction grating [62, 63] modulations. The crucial role of surface wave resonances has been established for a number of situations, however, there are still ongoing discussions about the role of other mechanisms [66–68] in extraordinary transmission.

In this chapter, we present a simple analytical model describing the role of surface modes in the transmission of electromagnetic waves through a flat film with negative dielectric permittivity and show the results of finite element simulations for the same geometry.

It was shown in Ref. [69] that extraordinary transmission through a dense film is possible in a configuration where two sub-wavelength diffraction gratings are placed on both sides of the film. Matching of the localized surface mode with the propagating wave in vacuum is achieved via the wave vector shift due to the diffraction grating. The analytical model presented in Ref. [70] demonstrates that extraordinary transmission also exist with a single diffraction grating placed near the dense layer film.

As it was mentioned earlier, a normally incident wave cannot excite a SPP resonance and so we have to find a method to match the phases between the incident and surface waves. The diffraction grating allows the excitation of the surface wave even for a normally incidence wave. Here we present the results of our FEM analysis of the geometry studied by Ref. [70]. The analytical solutions mentioned above consider only the fundamental harmonic and the first side-band harmonics. It is then the intention here not only to verify the accuracy of the analytical solution but also to investigate the role played by the higher harmonics, if any.

5.1 Analytical Model

Consider a TM polarized wave incident on a slab with permittivity ϵ_p (where $\epsilon_p < 0$) preceded by a thin diffraction grating placed a distance a from the negative permittivity

slab (metal or plasma) as shown in Figure 5.1. The geometry is composed of 4 regions. The region of $x < 0$ will be termed region 1, $0 < x < a$ will be termed region 2, and $x > d$ will be region 3. The region of $a < x < d$, where the plasma is situation, will be referred to as region P. The components of the electric field are $\mathbf{E} = (E_x, E_y, 0)$ and of the magnetic field are $\mathbf{H} = (0, 0, H_z)$. In this geometry, Maxwell's equations simplify to

$$\epsilon \frac{\partial}{\partial x}\left(\frac{1}{\epsilon}\frac{\partial H_z}{\partial x}\right) - k_y^2 H_z + \frac{\omega^2}{c^2}\epsilon H_z + \frac{\omega^2}{c^2} h_g(\epsilon_g + \alpha\cos(qy))\delta(x - x_g)H_z = 0. \qquad (5.1)$$

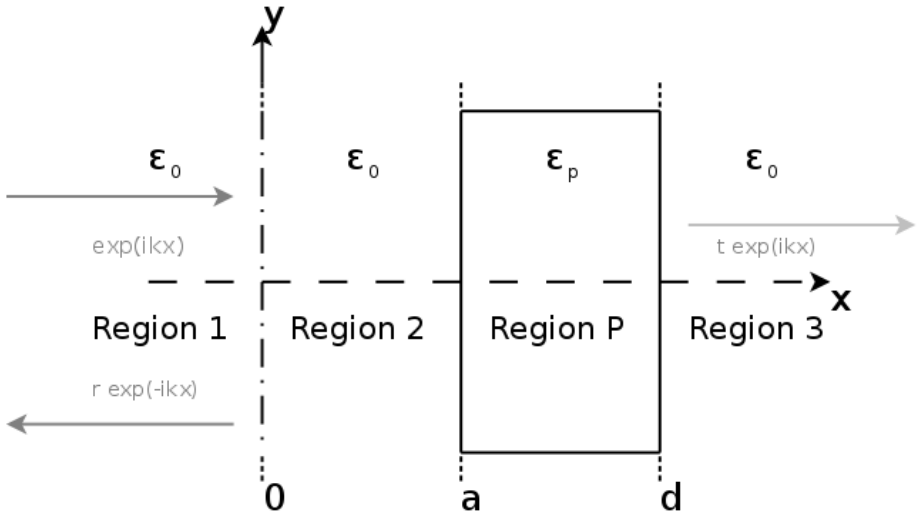

Figure 5.1: Geometry of the problem. A plasma (bounded by the solid lines) with permittivity ϵ_p is situated between two half-spaces of air $\epsilon = 1$ with an infinitely thin diffraction grating a distance a in front of the plasma.

Regions 1, 2, and 3 have vacuum permittivity ϵ_0. Region P has permittivity ϵ and has thickness l ($a + l = d$). For the diffraction grating interface, we will use the model as suggested in Ref. [69]. The diffraction grating is located at $x = 0$ and its wave vector is q, while α is a modulation parameter. From Eq. (5.1) one obtains the following boundary conditions at the diffraction grating

$$[H_z]_-^+ = 0 \qquad and \qquad [\frac{dH_z}{dx}]_-^+ = -\frac{k_\alpha}{2}(e^{iqy} + e^{-iqy})H_z|_{x=0}. \qquad (5.2)$$

It is easy to see that Eq. (5.2) leads to a shift of the k_y wave vector and coupling of side-band harmonics. In the general case, there are multiple harmonics. Considering only the fundamental and the first side-band harmonics, the field can be written out in the form

$$H(x,y,t) = \left[H^0(x)\exp^{ik_y y} + H^+(x)e^{i(k_y+q)y} + H^-(x)e^{i(k_y-q)y}\right] e^{i\omega t}. \tag{5.3}$$

With this, it is possible to find a closed form solution. Higher order harmonics were also neglected in Ref. [43] and [69]. Eq. (5.2) then gives the following boundary conditions,

$$\left[\frac{dH^0}{dx}\right]_{x_g-\delta}^{x_g+\delta} = -k_g H^0|_{x=x_g} - \frac{k_\alpha}{2}(H^+ + H^-)|_{x=x_g}, \tag{5.4}$$

$$\left[\frac{dH^\pm}{dx}\right]_{x_g-\delta}^{x_g+\delta} = -k_g H^\pm|_{x=x_g} - \frac{k_\alpha}{2}H^0|_{x=x_g}, \tag{5.5}$$

where $k_g = \frac{\omega^2}{c^2}\epsilon_g h_g$ and $k_\alpha = \frac{\omega^2}{c^2}\alpha h_g$. At the plasma-vacuum interface the derivative of the magnetic field is discontinuous and the boundary condition is,

$$\left[\frac{1}{\epsilon}\frac{dH_z}{dx}\right] = 0. \tag{5.6}$$

The magnetic field is still continuous at all interfaces, $[H_z] = 0$. A convenient way to write and solve for this is using impedances. Considerable simplifications of the expressions occur because in the impedance formulation two matching conditions reduces to a single one. The wave impedance is defined as,

$$Z = -\frac{E_y}{H_z} = -\frac{i}{\omega\epsilon_0\epsilon_r}\frac{1}{H_z}\frac{\partial H_z}{\partial x}. \tag{5.7}$$

In the general case, to the left of the plasma and grating, there are incident and reflected plane waves and the magnetic field is of the form

$$H_x = A(e^{ikx} + \Gamma e^{-ikx}). \tag{5.8}$$

The current impedance in the region is

$$Z(x) = \kappa\frac{\exp(ikx) - \Gamma\exp(-ikx)}{\exp(ikx) + \Gamma\exp(-ikx)}, \tag{5.9}$$

where κ is the characteristic impedance in this region, $\kappa = \frac{k}{\omega\epsilon_0\epsilon_r}$. Equation (5.9) defines the transformation of the impedances for a finite interval of a length a as,

$$Z(a) = \kappa\frac{Z(0) + \kappa\tanh(ika)}{\kappa + Z(0)\tanh(ika)}, \tag{5.10}$$

$$Z(0) = \kappa\frac{Z(a) - \kappa\tanh(ika)}{\kappa - Z(a)\tanh(ika)}. \tag{5.11}$$

These expressions also work for evanescent waves with the replacement $k \to i\gamma$. In this case, the characteristic impedance, κ, will be imaginary.

5.1.1 Vacuum Region 1

In the left outmost vacuum region, we have the incident and reflected wave,

$$H_1^0 = A_1^0(\exp(ikx) + \Gamma_1^0 \exp(-ikx)), \tag{5.12}$$

where k is the wave vector of the propagating waves in vacuum and $k^2 = k_0^2 - k_y^2 > 0$. The first harmonics are evanescent in a vacuum region. In region 1, they exponentially decay to the left and have the form

$$H_1^{\pm} = A_1^{\pm} \exp(\gamma_v^{\pm} x), \tag{5.13}$$

where $\gamma_v^{\pm 2} = (k_y + q)^2 - k_0^2$, $\gamma_v^{\pm} > 0$. The amplitude of the reflected wave, Γ_1^0, is determined by only the values of the characteristic impedance in the medium and the load impedance at the diffraction grating, where the wave is being reflected from,

$$\Gamma_1^0 = \frac{\kappa_v - Z_1^0}{\kappa_v + Z_1^0}, \tag{5.14}$$

where $\kappa_v \equiv k/\omega/\epsilon_0$ is the characteristic impedance of the vacuum for the principal component. The first harmonics have impedance

$$Z_0^{\pm} = -\frac{i\gamma_v^{\pm}}{\omega\epsilon_0} \equiv -\kappa_v^{\pm}. \tag{5.15}$$

5.1.2 Vacuum Region 2

In the second vacuum region, between the diffraction grating and the plasma layer, the fields of the principle component and side-bands are defined, respectively, as

$$H_2^0 = A_2^0(\exp(ikx) + \Gamma_2^0 \exp(-ikx)), \tag{5.16}$$

and

$$H_2^{\pm} = A_2^{\pm}(\exp(-\gamma_v^{\pm} x) + \Gamma_2^{\pm} \exp(\gamma_v^{\pm} x)). \tag{5.17}$$

At the diffraction grating, Eq. (5.4) and Eq. (5.5) give the boundary condition

$$Z_1^0 = Z_2^0 + \frac{k_\alpha^2}{2\omega^2\epsilon_0^2} \frac{1}{Z_2^+ - Z_1^+}. \tag{5.18}$$

At the right boundary of region 2, where vacuum meets plasma, the impedances are continuous,

$$Z_2^{\pm}(a) = Z_p^{\pm}(0), \tag{5.19}$$

$$Z_2^{0}(a) = Z_p^{0}(0). \tag{5.20}$$

The relations between the impedances of the principle component and the sidebands at the left and right of region two are

$$Z_2^0(a) = \kappa_v^0 \frac{Z_2^0(0) + i\kappa_v^0 \tan(ka)}{\kappa_v^0 + iZ_2^0(0)\tan(ka)}, \tag{5.21}$$

$$Z_2^+(a) = \kappa_v^+ \frac{Z_2^+(0) - i\kappa_v^+ \tanh(\gamma_v^+ a)}{\kappa_v^+ - iZ_2^+(0)\tanh(\gamma_v^+ a)}. \tag{5.22}$$

5.1.3 Plasma Region

Inside the plasma, the principle components and side-band components are evanescent,

$$H_p^0 = A_p^0(\exp(-\gamma_p x) + \Gamma_p^0 \exp(\gamma_p x)), \tag{5.23}$$

$$H_p^{\pm} = A_p^{\pm}(\exp(-\gamma_p^{\pm} x) + \Gamma_p^{\pm} \exp(\gamma_p^{\pm} x)), \tag{5.24}$$

where $\gamma_p^2 = k_y^2 - k_0^2\epsilon_p > 0$, $\gamma_p^{\pm 2} = (k_y^2 + q)^2 - k_0^2\epsilon_p > 0$. The relations between the impedances of the principle component and the sidebands at the left and right of the plasma region are

$$Z_p^0(0) = \kappa_p^0 \frac{Z_p^0(l) + \kappa_p^0 \tanh(\gamma_p l)}{\kappa_p^0 + Z_p^0(l)\tanh(\gamma_p l)}, \tag{5.25}$$

$$Z_p^+(0) = \kappa_p^+ \frac{Z_p^+(l) + \kappa_p^+ \tanh(\gamma_p^+ l)}{\kappa_p^+ + Z_p^+(l)\tanh(\gamma_p^+ l)}, \tag{5.26}$$

where $\kappa_p^{\pm} = i\gamma_p^{\pm}/\omega\epsilon_0\epsilon_p$, $\kappa_p^0 = i\gamma_p/\omega\epsilon_0\epsilon_p$ are characteristic impedances in the plasma region. At the right of the plasma boundary, the impedance is matched to the impedances in vacuum region 3 through

$$Z_p^0(l) = Z_3^0, \tag{5.27}$$

$$Z_p^{\pm}(l) = Z_3^{\pm}. \tag{5.28}$$

5.1.4 Vacuum Region 3

In the last vacuum region, there is only a transmitted propagating wave and the side-bands decay exponentially as $z \to \infty$,

$$H_3^0 = A_p^0 \exp(ikz), \tag{5.29}$$

$$H_3^{\pm} = A_p^{\pm} \exp(-\gamma_v^{\pm} z). \tag{5.30}$$

The impedances in this region are simply the characteristic impedance of vacuum,

$$Z_3^0 = \frac{k}{\omega\epsilon_0} = \kappa_v, \tag{5.31}$$

$$Z_3^{\pm} = \frac{i\gamma_v^{\pm}}{\omega\epsilon_0} = \kappa_v^{\pm}. \tag{5.32}$$

Starting with the impedance of vacuum, Eq. (5.31) and (5.32), it is possible to work backwards through the geometry, calculating the impedances in each region using Eq. (5.25)-(5.28) and (5.19)-(5.22) with the boundary condition (5.18). The transmission coefficient $T = 1 - |\Gamma_1^0|^2$ is determined from Eq. (5.14).

5.1.5 Surface Wave Resonance

For a sufficiently thick negative permittivity material, $\gamma_p l \geq 1$, the transmittivity of a single film is low and most of the radiation is reflected. The transmission can be strongly enhanced by adjusting the parameters of the diffraction grating and the distance between the grating and the film. Such an example of strong enhancement of the transmission is shown in Figure 5.2 for the following parameters: thickness of the film, $l = 20$ nm, the wavelength of the incident radiation, $\lambda = 630$ nm, and the dielectric permittivity of the film, $\varepsilon_p = -9$. The parameters of the diffraction grating were chosen as follows: $\alpha = 5.7366$, $\varepsilon_g = 0$ and it was placed a distance $a = 71.89$ nm from the film. The

transmission coefficient is plotted as a function of the wave vector of the grating. It was found that there are two resonant values: $q_1 = 10^7$ 1/m and $q_2 = 1.52 \cdot 10^7$ 1/m.

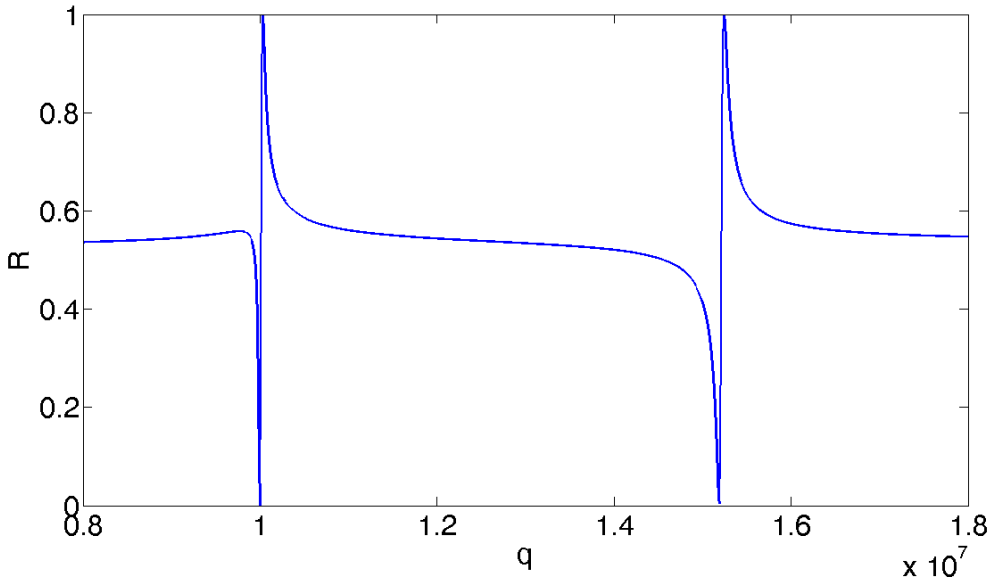

Figure 5.2: Analytical calculation of the reflection coefficient as a function of q, the periodic wave vector of the diffraction grating, for a metal film.

It can be shown analytically that the resonances in the transmission coefficient correspond to surface wave excitation. Let us consider the conditions for absolute transmission when $\Gamma_1^0 = 0$ and $Z_1^0 = \kappa_v$. The impedances of the decaying sidebands in the vacuum region 1 are $Z_1^+ = Z_1^- = -\kappa_v^+$. Then the matching condition at the diffraction grating (5.2) takes the form

$$\kappa_v = Z_2^0(0) + \frac{k_\alpha^2}{2\omega^2\varepsilon_0^2}\frac{1}{Z_2^+(0) + \kappa_v^+}. \tag{5.33}$$

One can see that $Z_2^+(0)$ and κ_v^+ are imaginary and $Z_2^0(0)$ is generally complex. The role of the last term in (5.33) is to cancel the imaginary part of the $Z_2^0(0)$:

$$i\mathbf{Im}\left(Z_2^0(0)\right) + \frac{k_\alpha^2}{2\omega^2\varepsilon_0^2}\frac{1}{Z_2^+(0) + \kappa_v^+} = 0. \tag{5.34}$$

The second condition is that the real part of $Z_2^0(0)$ matches to κ_v :

$$\mathbf{Re}\left(Z_2^0(0)\right) = \kappa_v. \tag{5.35}$$

Eq. (5.35) and Eq. (5.34) have to be satisfied simultaneously to provide absolute transmission, $T = 1$.

After some algebra, Eq. (5.35) takes the form

$$\left[1 + \beta^2\right] \left[L_p^2 + \beta^2 L_v^2 L_p^2 + 2\beta L_v L_p \right] = 0, \tag{5.36}$$

or equivalently

$$(1 + \beta L_v L_p)^2 = 1 - L_p^2, \tag{5.37}$$

where $L_v \equiv \tan(ka)$, $L_p = \tanh(\gamma_p l)$, and $\kappa_p/\kappa_v = i\beta$ (β is a real number). Eq. (5.37) has two roots so that for a given value of the film permittivity, ε_p, and fixed L_p one finds two values of L_v which defines the distance between the plasma slab and the diffraction grating. For large thickness of the plasma slab, $L_p \to 0$ and Eq. (5.37) gives $L_v \simeq -1/\beta$. Note that the condition Eq. (5.37) does not depend on the diffraction grating parameters.

For small α, the resonance condition Eq. (5.34) becomes

$$Z_2^+(0) + \kappa_v^+ = 0.. \tag{5.38}$$

After some algebra, it takes the form

$$\left[1 + L_v^+\right] \left[2\kappa_v^+ k_p^+ + k_v^{+2} L_p^+ + k_p^{+2} L_p^+\right] = 0, \tag{5.39}$$

and the resonant condition is

$$2\frac{\kappa_p^+}{\kappa_v^+} + \left(\frac{\kappa_p^+}{\kappa_v^+}\right)^2 L_p^+ + L_p^+ = 0 \tag{5.40}$$

where $L_p^+ = \tanh\left(\gamma_p^+ l\right)$, $L_v^+ \equiv \tanh(\gamma_v^+ a)$. It is easy to see that this is the exact dispersion equation for the surface wave on a metal layer with a finite thickness l. There are two roots corresponding to the symmetric and antisymmetric bonding of the surface waves localized on the opposite boundaries of the film.

For large thickness $L_p^+ \to 1$ and (5.40) becomes

$$\kappa_v^+ + \kappa_p^+ = 0, \tag{5.41}$$

giving the dispersion equation for a surface mode at the interface of vacuum and semi-infinite layer with $\varepsilon_p < 0$. Two roots of (5.40) merge at

$$q^2 = k_0^2 \frac{\varepsilon_p}{\varepsilon_p + 1}. \tag{5.42}$$

5.2 Numerical Results

The first numerical results we'd like to consider are for an optical frequency plane wave incident on a metal film with parameters the same as the result in Figure 5.2. The wavelength of the plane wave is $\lambda = 630$ nm, the permittivity of the metal is $\epsilon_p = -9$, the metal's thickness is $l = 20$ nm, and the distance between the metal and the diffraction grating is $a = 71.89$ nm, Other parameters were set to $\alpha = 5.7366$, $\varepsilon_g = 0$, and $h_g = 10^{-8}$. The numerical and analytical results agree with each other. The reason for this is shown in Figures 5.4 and 5.5. These two figures show the contributions to the field by the fundamental, first, and the total contribution of the second through eight harmonics. As is evident, most of the field contribution is from the fundamental and first harmonics while the higher harmonics are relatively quite small. This may be because of the small value of the product $h_g \cdot \alpha$ that is the amplitude of the nonlinear term in Eq. (5.1).

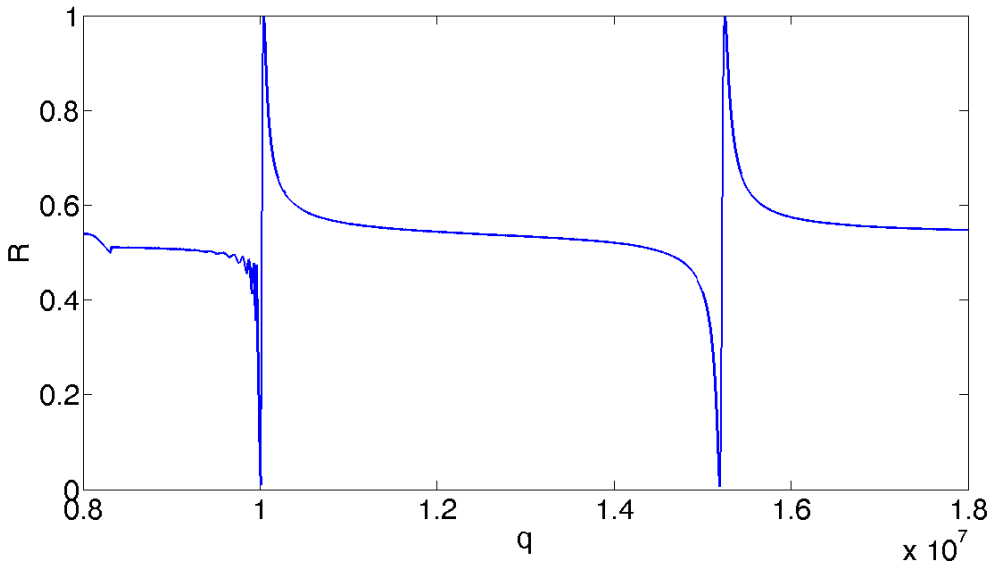

Figure 5.3: Numerical calculation of the reflection coefficient as a function of q, the periodic wave vector of the diffraction grating, for a metal film.

We'd like to compare these results to a different set of parameters that use a higher value of $h_g \cdot \alpha$. The parameters used were $a = 0.0682$ m, $l = 0.02$ m, $\epsilon_p = -35$, $\epsilon_g = 0$. As a first look, setting $\alpha = 2$, Figures 5.6 and 5.7 show visually how closer the numerical calculated resonances are to the analytically calculated resonances for a smaller value of

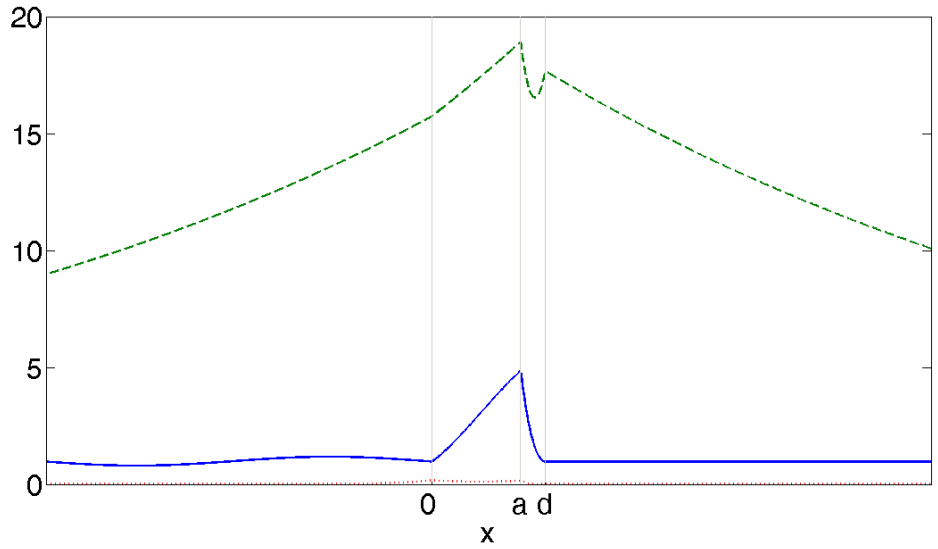

Figure 5.4: Profile of the magnitude of the normalized harmonics $|H_0|^2$ (solid line), $|H_1|^2$ (dashed line), $\sum_{n=2}^{8} |H_n|^2$ (dotted line) for q_1

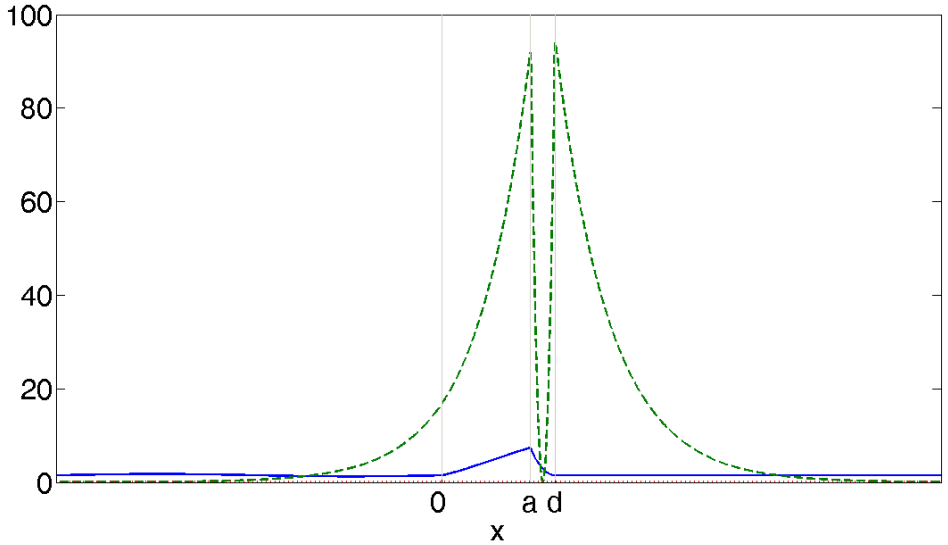

Figure 5.5: Profile of the magnitude of the normalized harmonics $|H_0|^2$ (solid line), $|H_1|^2$ (dashed line), $\sum_{n=2}^{8} |H_n|^2$ (dotted line) for q_2

h_g to confirm the role of the product $h_g \cdot \alpha$.

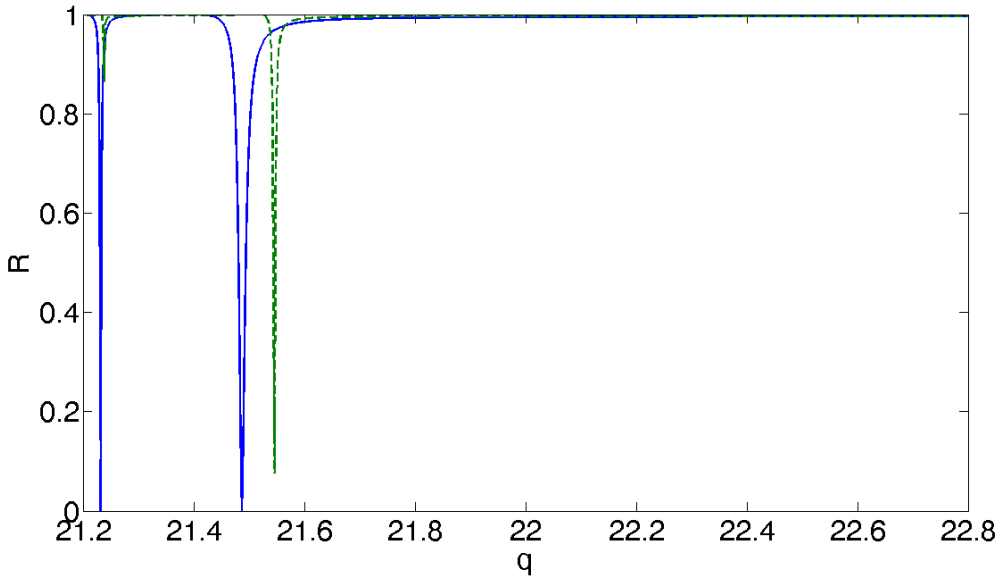

Figure 5.6: Reflection as a function of the modulated wave vector, q for $\alpha = 2$ and $h_g = 0.025$. The solid line shows the analytical solution and the dashed line shows the numerical solution.

Setting $h_g = 0.05$, Figures 5.8, 5.10, and 5.12 show the analytical results for $\alpha = 2$, $\alpha = 4$, and $\alpha = 6$ respectively. Figures 5.9, 5.11, and 5.13 show the numerical results for $\alpha = 2$, $\alpha = 4$, and $\alpha = 6$. The analytical method takes into account only the fundamental and first harmonics generated by the diffraction grating. For the numerical solution that is not the case. There are similarities for the two sets of figures. For each value of α, there are two peaks. The left peak (the peak at a lower value of resonant q), q_1, doesn't change in position much as α changes. In fact, that solution seems to converge to one value of resonant q as α is increased. The other solution, q_2, the right peaks at the higher resonant value of q, are wider than the lower value of q peaks and, rather than converge on a value of q, they seem to diverge faster and faster from each other.

There are also differences between the values of resonant q, which, while showing similar behaviour as α changes, do not actually correspond to each other. As illustrated in Figure 5.20, the q_1 analytical and numerical results agree well but there is a wider and wider divergence between the analytical and numerical calculations of q_2. This can explained by the role played by harmonics higher than the fundamental first. Figures 5.14-5.26 show

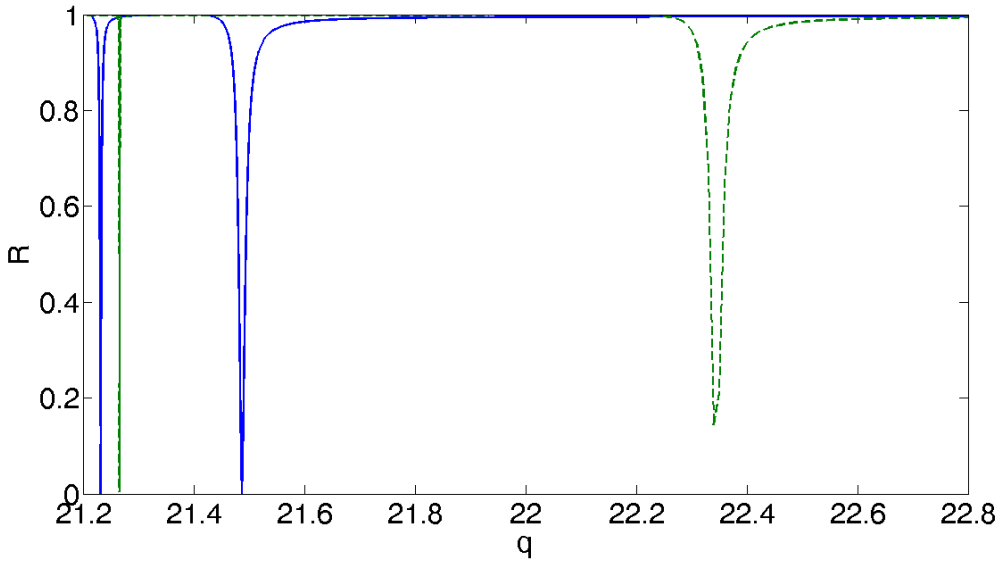

Figure 5.7: Reflection as a function of the modulated wave vector, q for $\alpha = 2$ and $h_g = 0.05$. The solid line shows the analytical solution and the dashed line shows the numerical solution.

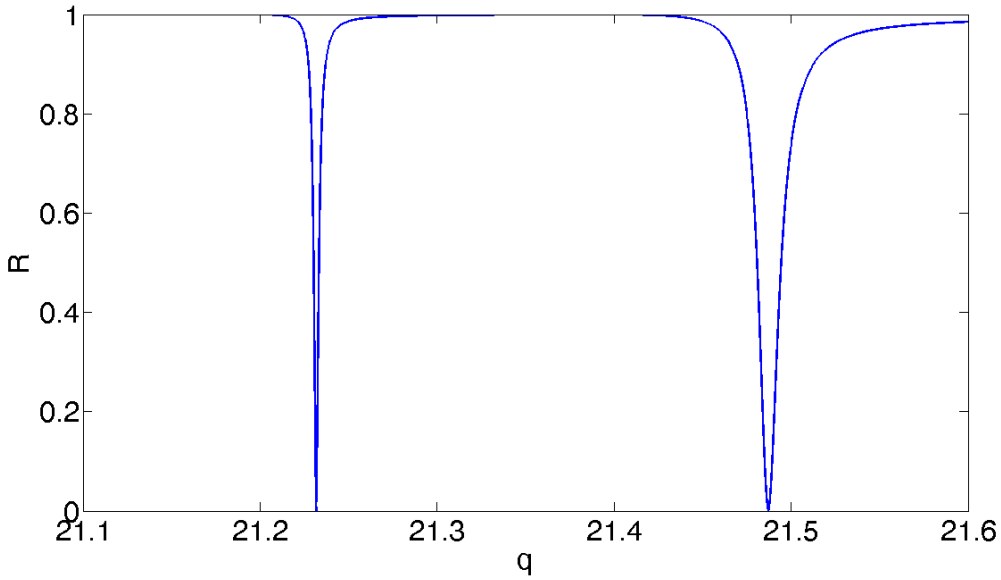

Figure 5.8: Analytical calculation of reflection coefficient as a function of q, the periodic wave vector of the diffraction grating for $\alpha = 2$

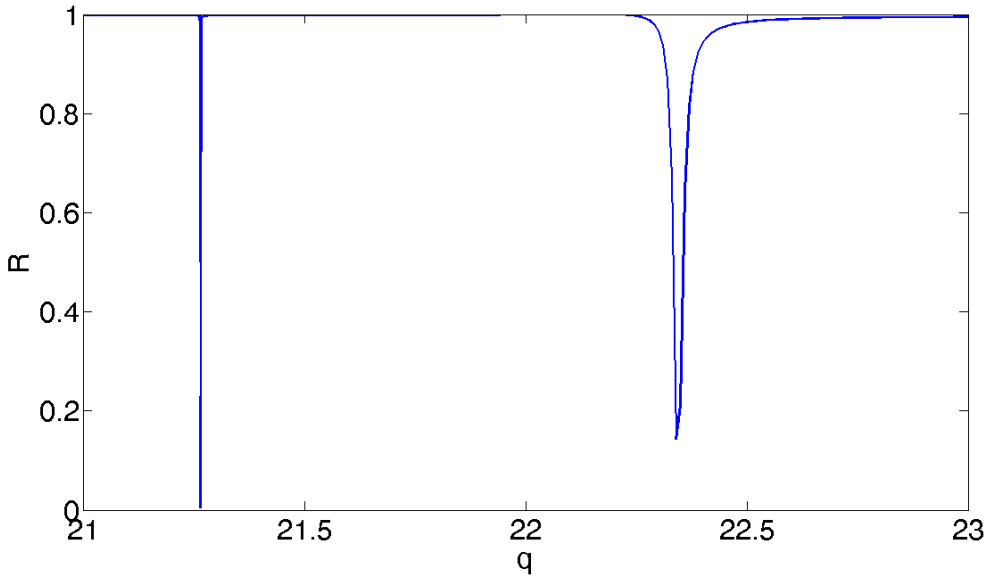

Figure 5.9: Numerical calculation of reflection coefficient as a function of q, the periodic wave vector of the diffraction grating for $\alpha = 2$

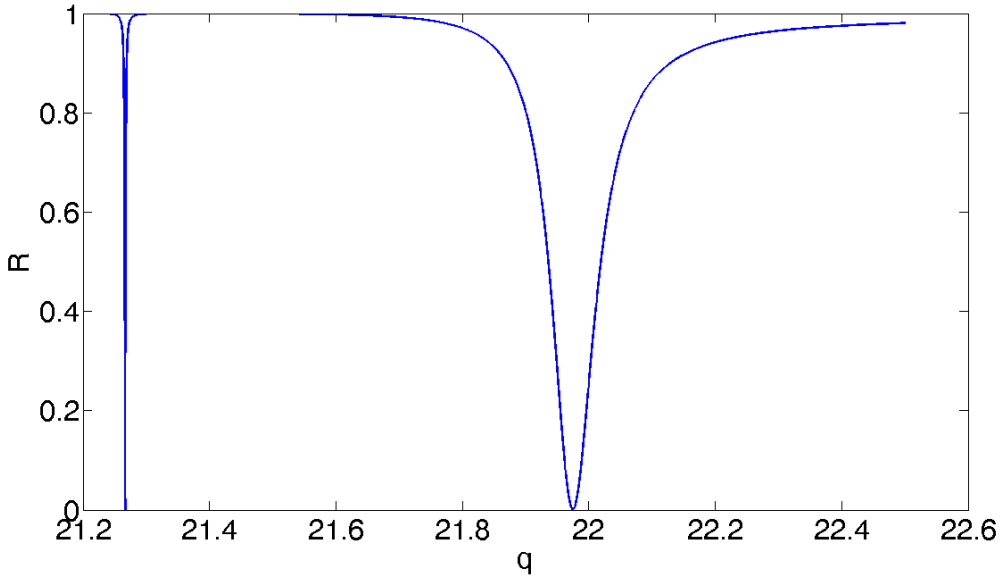

Figure 5.10: Analytical calculation of reflection coefficient as a function of q, the periodic wave vector of the diffraction grating for $\alpha = 4$

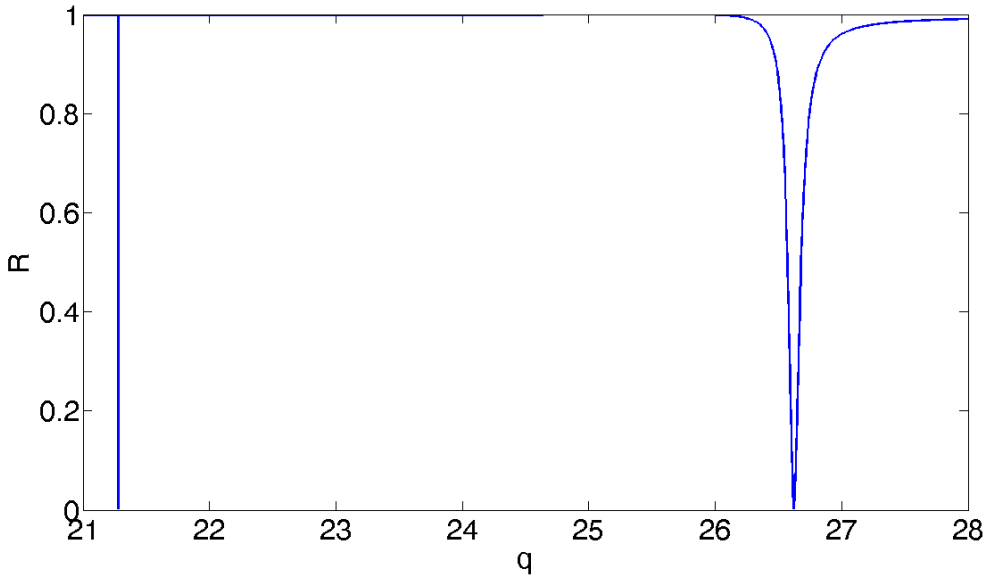

Figure 5.11: Numerical calculation of reflection coefficient as a function of q, the periodic wave vector of the diffraction grating for $\alpha = 4$

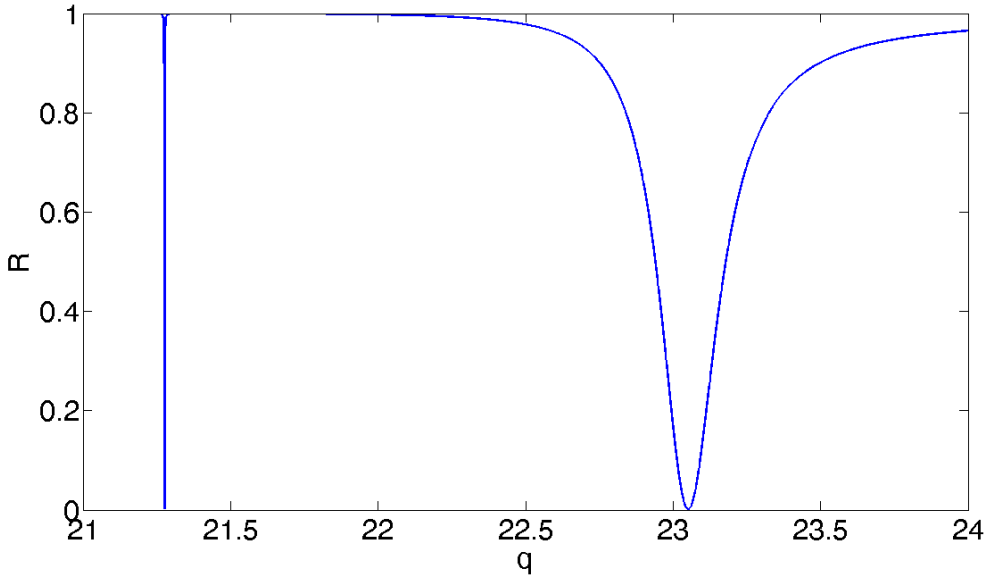

Figure 5.12: Analytical calculation of reflection coefficient as a function of q, the periodic wave vector of the diffraction grating for $\alpha = 6$

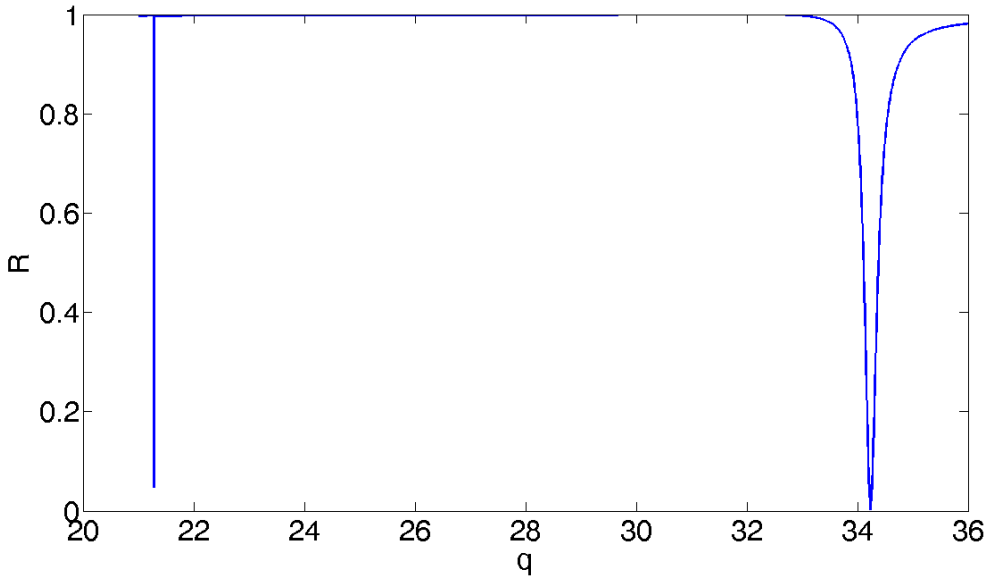

Figure 5.13: Numerical calculation of reflection coefficient as a function of q, the periodic wave vector of the diffraction grating for $\alpha = 6$

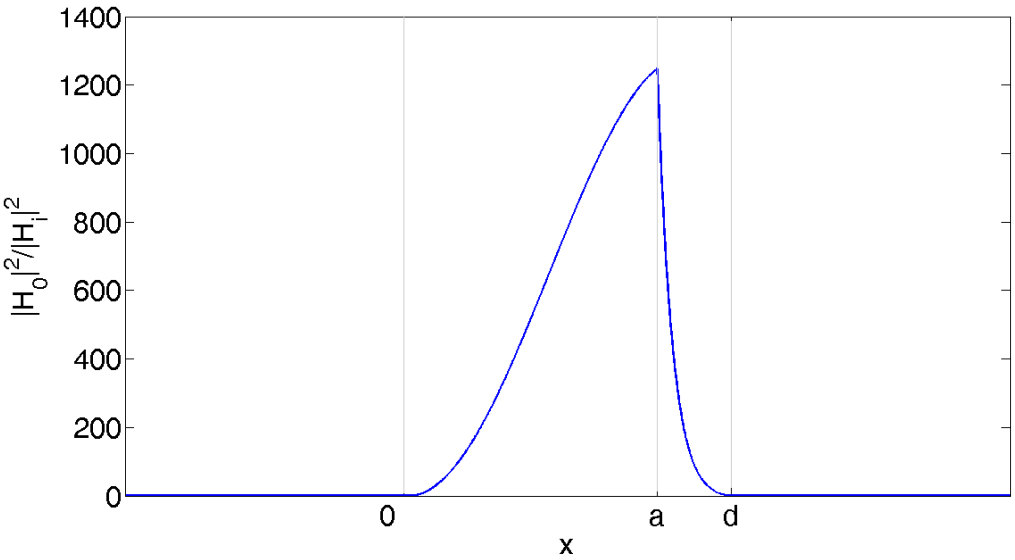

Figure 5.14: The normalized harmonic $|H_0|^2$ for resonance at $q = q_1$ and $\alpha = 2$.

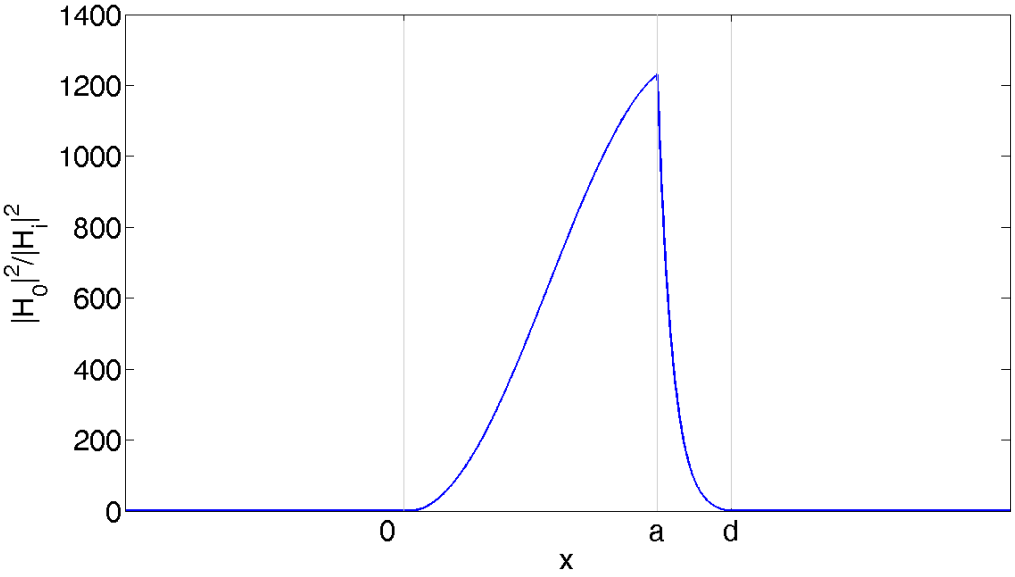

Figure 5.15: The normalized harmonic $|H_0|^2$ for resonance at $q = q_1$ and $\alpha = 4$.

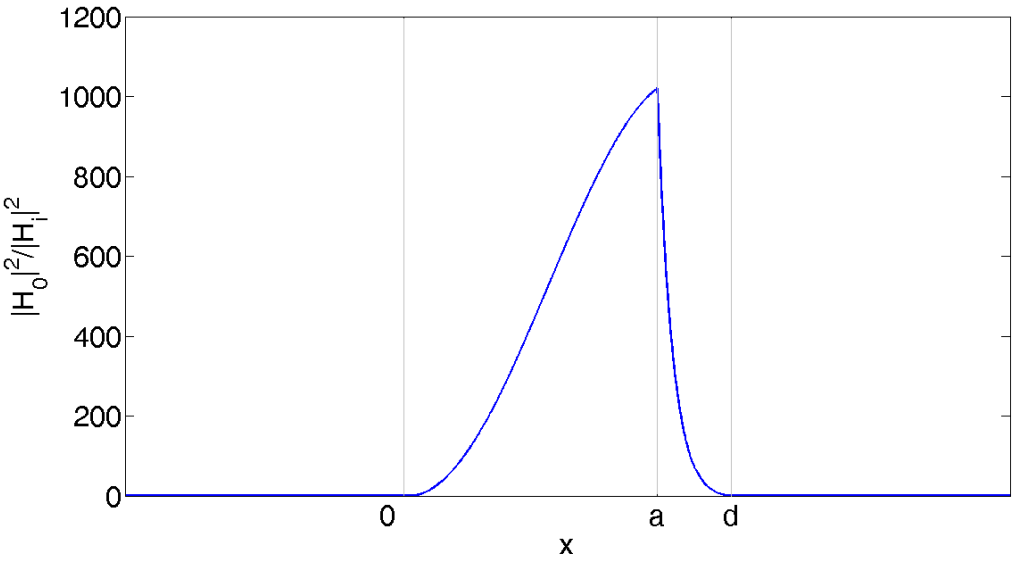

Figure 5.16: The normalized harmonic $|H_0|^2$ for resonance at $q = q_1$ and $\alpha = 6$.

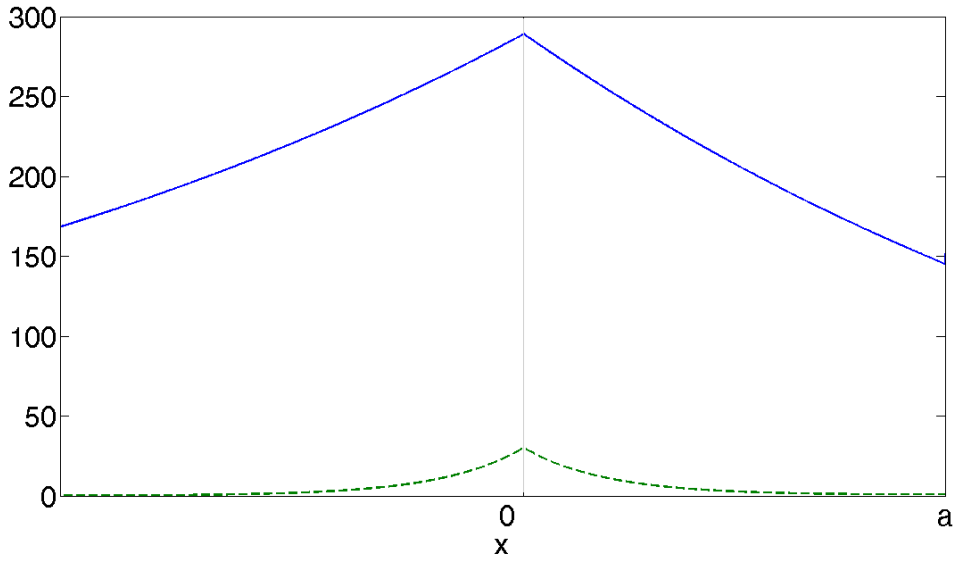

Figure 5.17: The normalized harmonic $|H_1|^2$ (solid line) and the normalized sum $\sum_{n=2}^{8} |H_n|^2$ (dashed line) for resonance $q = q_1$ for $\alpha = 2$

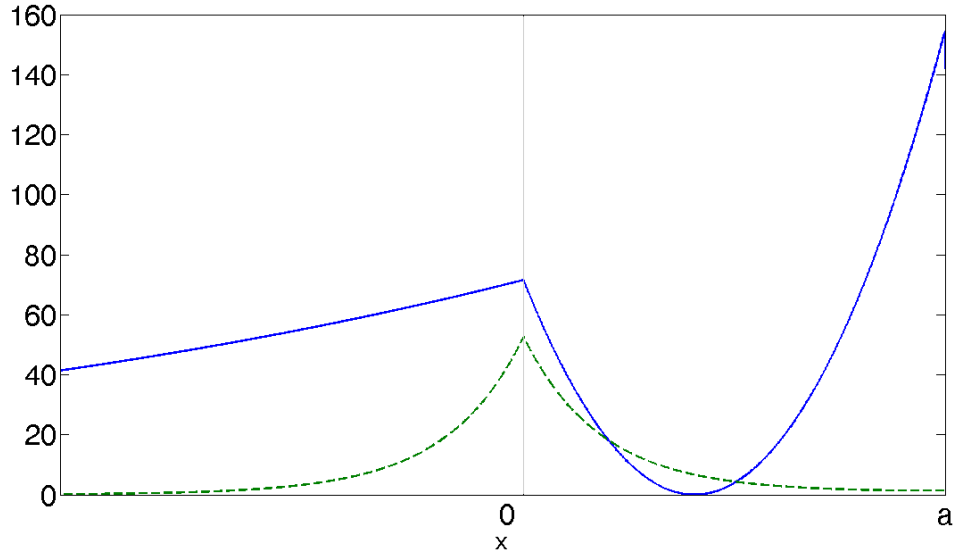

Figure 5.18: The normalized harmonic $|H_1|^2$ (solid line) and the normalized sum $\sum_{n=2}^{8} |H_n|^2$ (dashed line) for resonance $q = q_1$ for $\alpha = 4$

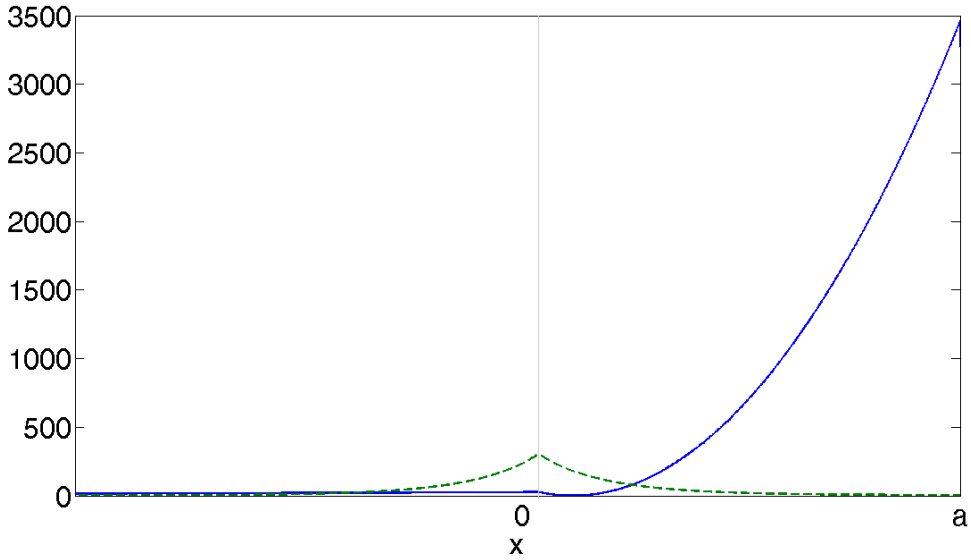

Figure 5.19: The normalized harmonic $|H_1|^2$ (solid line) and the normalized sum $\sum_{n=2}^{8} |H_n|^2$ (dashed line) for resonance $q = q_1$ for $\alpha = 6$

the magnitude of the normalized fundamental harmonic, $|H_0|^2$, the magnitude of the first harmonic, $|H_0|^2$, as well as the total contribution of the 2nd through 8th harmonics, in this case calculated as $\sum_{n=2}^{8} |H_n|^2$.

As α is increased, there is an increasing disconnect between the analytically calculated values of resonant q and the numerically calculated values of resonant q. As Figures 5.17-5.19, for q_1, and 5.24-5.26, for q_2, clearly illustrate, this is because the higher harmonics begin to play a larger and larger role in determining the field in the area around the diffraction grating. Even though the higher harmonics are highly localized at that grating, much more than the first harmonic, they grow in influence as α is increased. Figures 5.27-5.32 display that further. These figures show how the field at the grating is distributed among the first 8 harmonics. Again, as α is increased, the magnitude of the higher harmonics is increased. In the case of the q_1 resonance for $\alpha = 6$, the field's largest components are the 2nd and 3rd harmonics, rather than the fundamental and first.

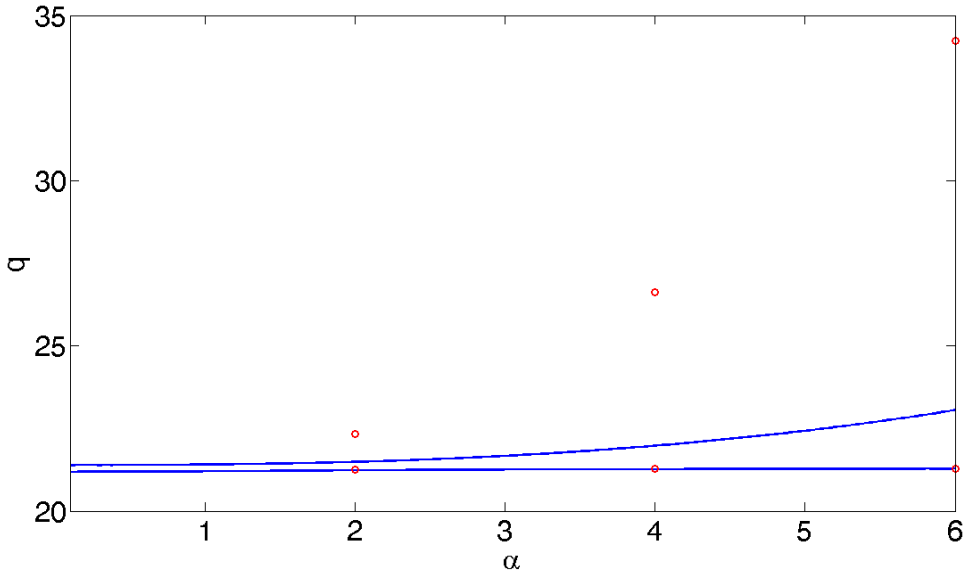

Figure 5.20: Analytical and numerical results for resonant q as a function of the modulation parameter, α. Solid lines show analytical results and circles show numerical results

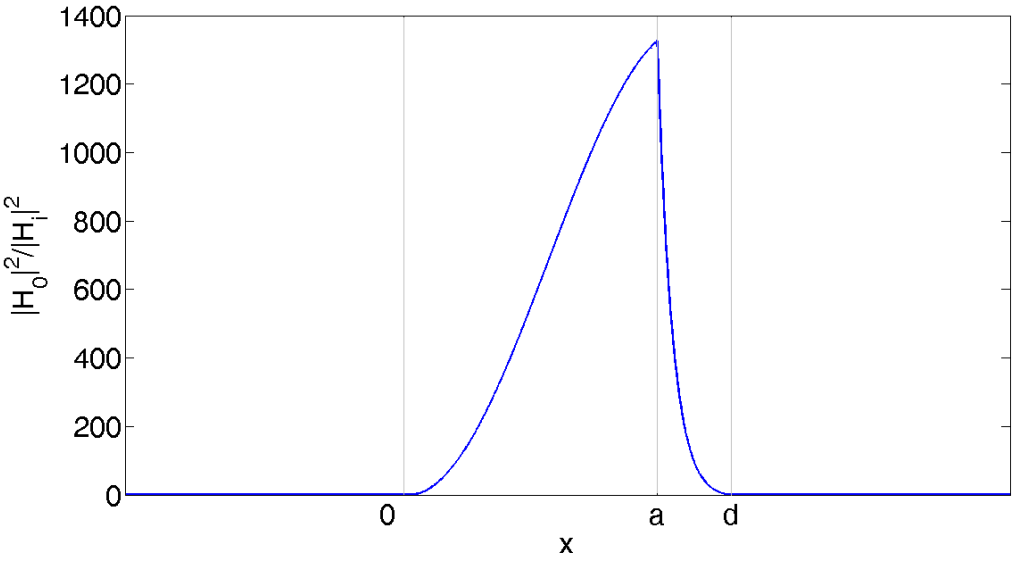

Figure 5.21: The normalized harmonic $|H_0|^2$ for resonance at $q = q_2$ and $\alpha = 2$.

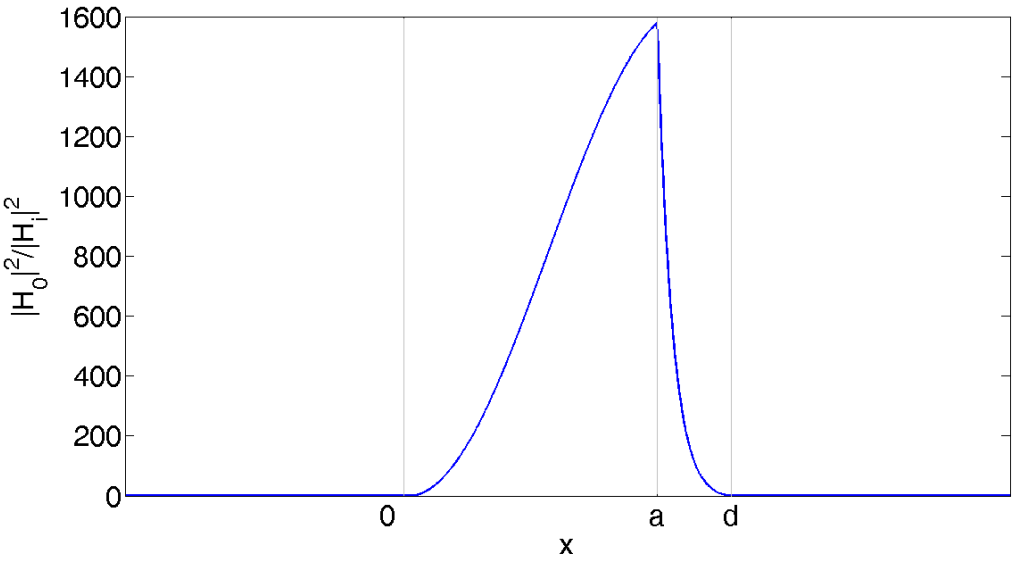

Figure 5.22: The normalized harmonic $|H_0|^2$ for resonance at $q = q_2$ and $\alpha = 4$.

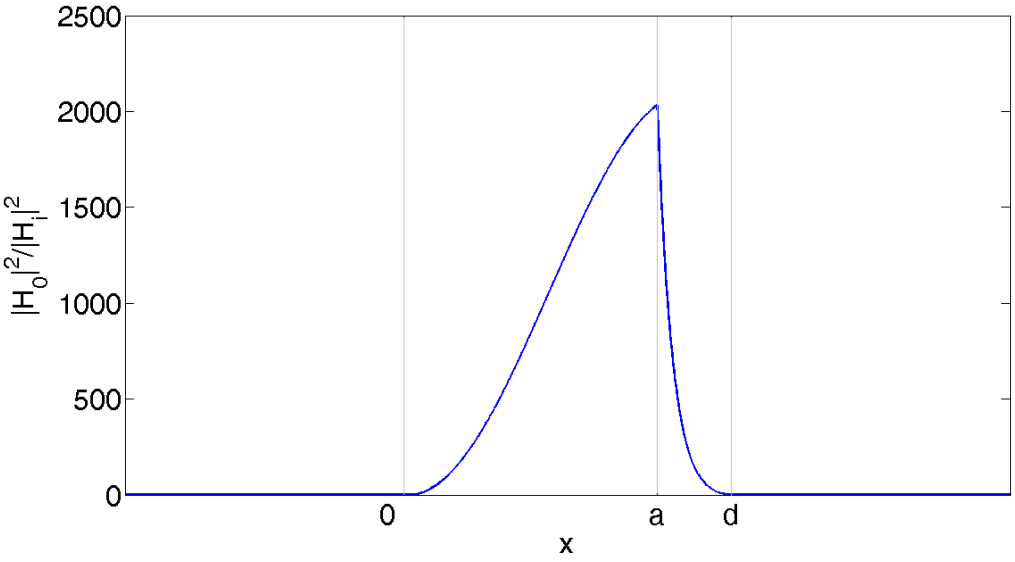

Figure 5.23: The normalized harmonic $|H_0|^2$ for resonance at $q = q_2$ and $\alpha = 6$.

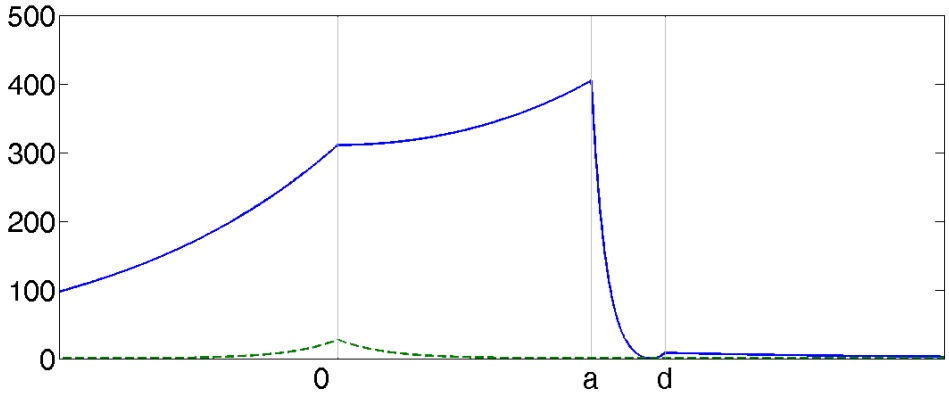

Figure 5.24: The normalized harmonic $|H_1|^2$ (solid line) and the normalized sum $\sum_{n=2}^{8} |H_n|^2$ (dashed line) for resonance $q = q_2$ for $\alpha = 2$

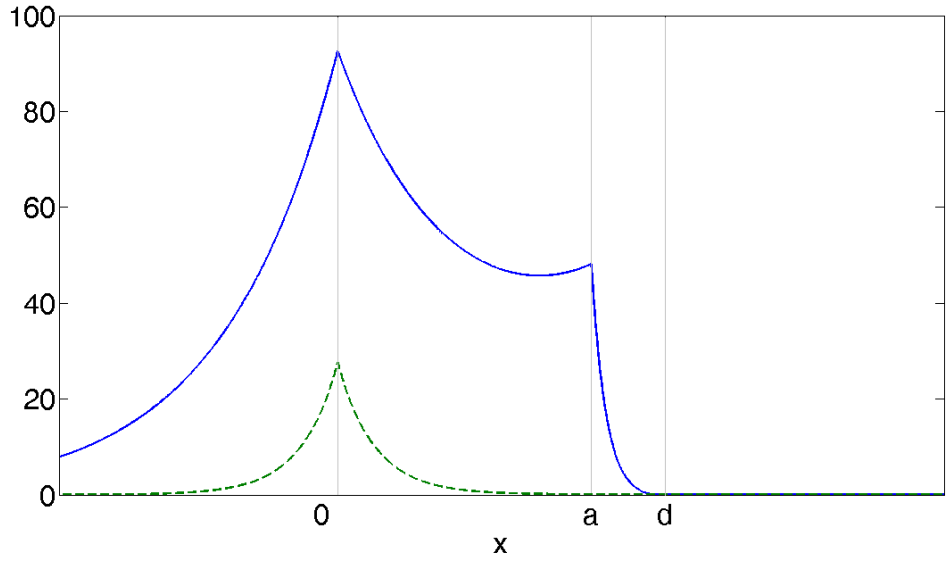

Figure 5.25: The normalized harmonic $|H_1|^2$ (solid line) and the normalized sum $\sum_{n=2}^{8} |H_n|^2$ (dashed line) for resonance $q = q_2$ for $\alpha = 4$

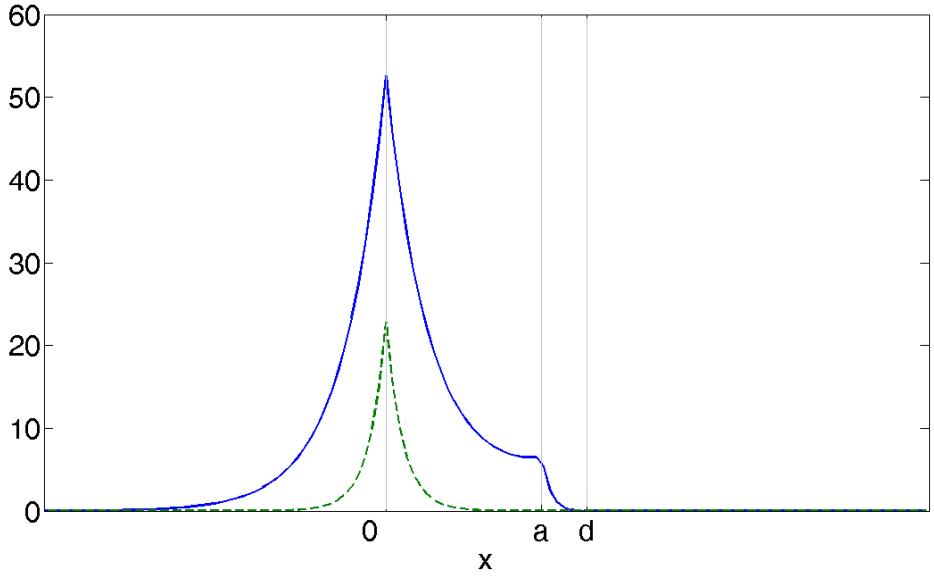

Figure 5.26: The normalized harmonic $|H_1|^2$ (solid line) and the normalized sum $\sum_{n=2}^{8} |H_n|^2$ (dashed line) for resonance $q = q_2$ for $\alpha = 6$

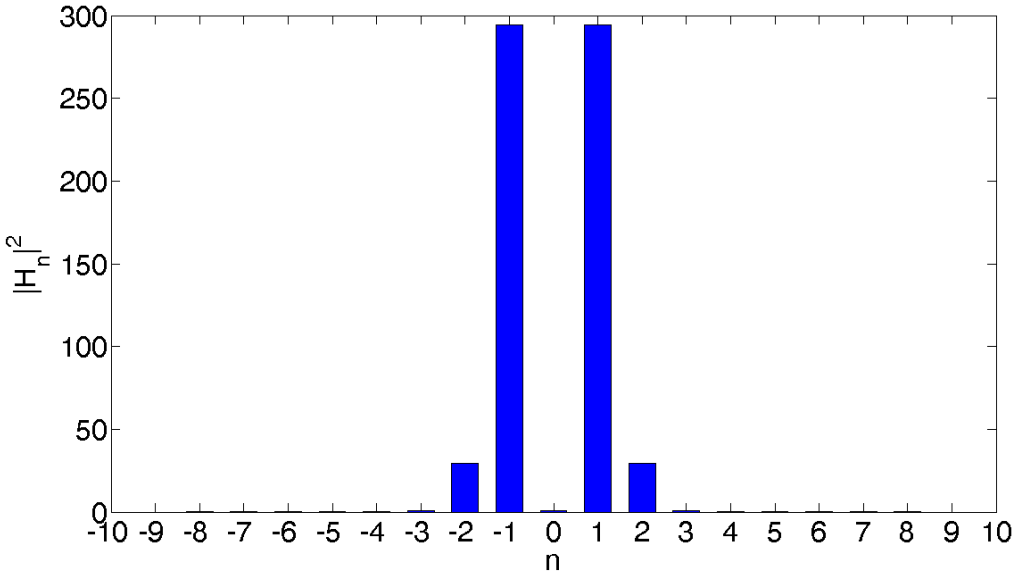

Figure 5.27: The normalized magnitude of the harmonics, $|H_n|^2$ at the diffraction grating at $x = 0$ at $q = q_1$ and $\alpha = 2$.

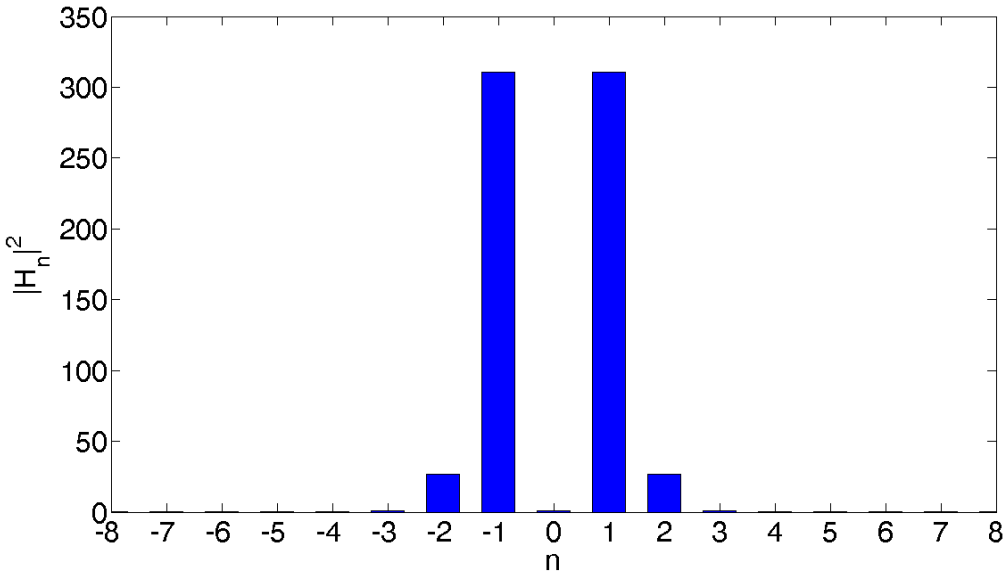

Figure 5.28: The normalized magnitude of the harmonics, $|H_n|^2$ at the diffraction grating at $x = 0$ at $q = q_2$ and $\alpha = 2$.

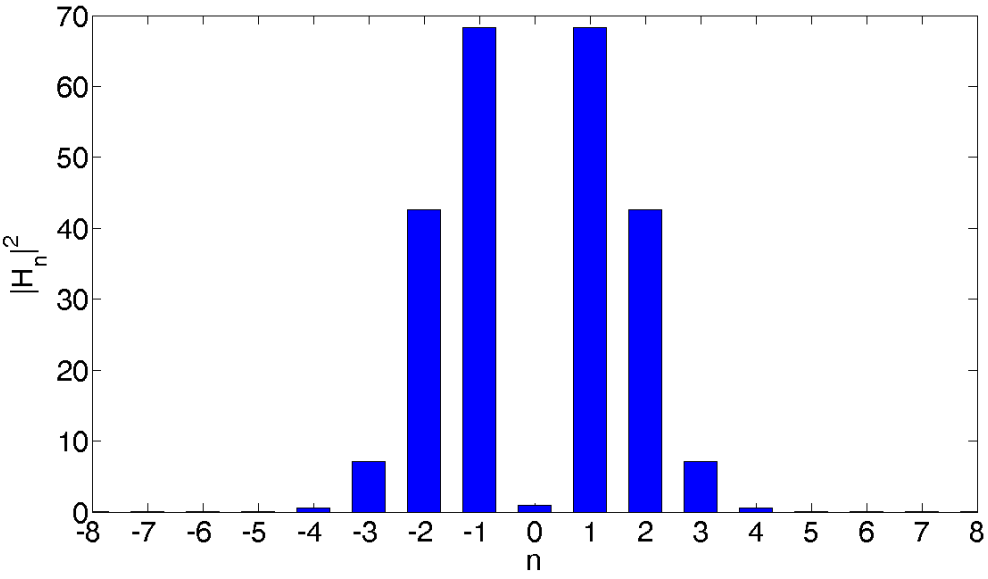

Figure 5.29: The normalized magnitude of the harmonics, $|H_n|^2$ at the diffraction grating at $x = 0$ at $q = q_1$ and $\alpha = 4$.

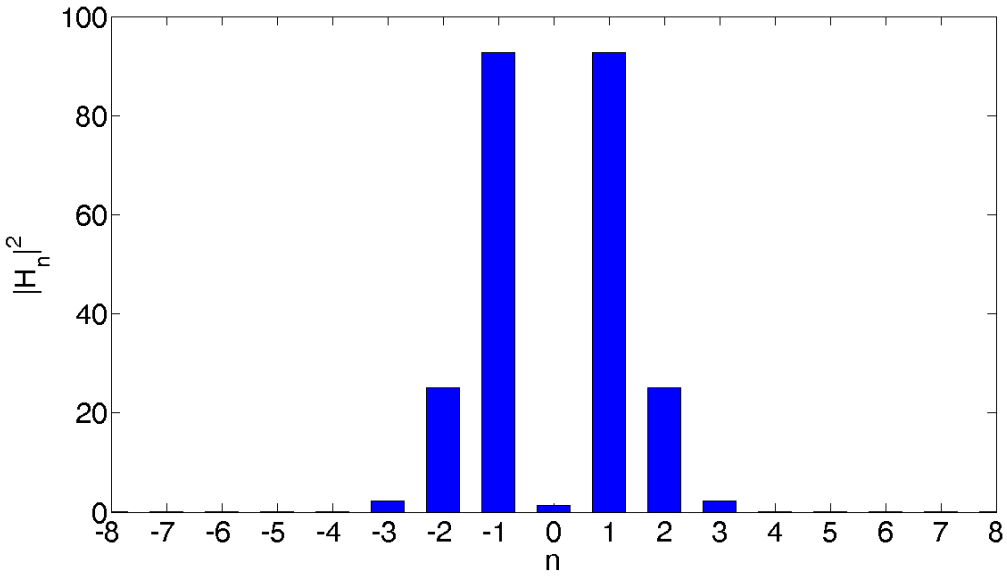

Figure 5.30: The normalized magnitude of the harmonics, $|H_n|^2$ at the diffraction grating at $x = 0$ at $q = q_2$ and $\alpha = 4$.

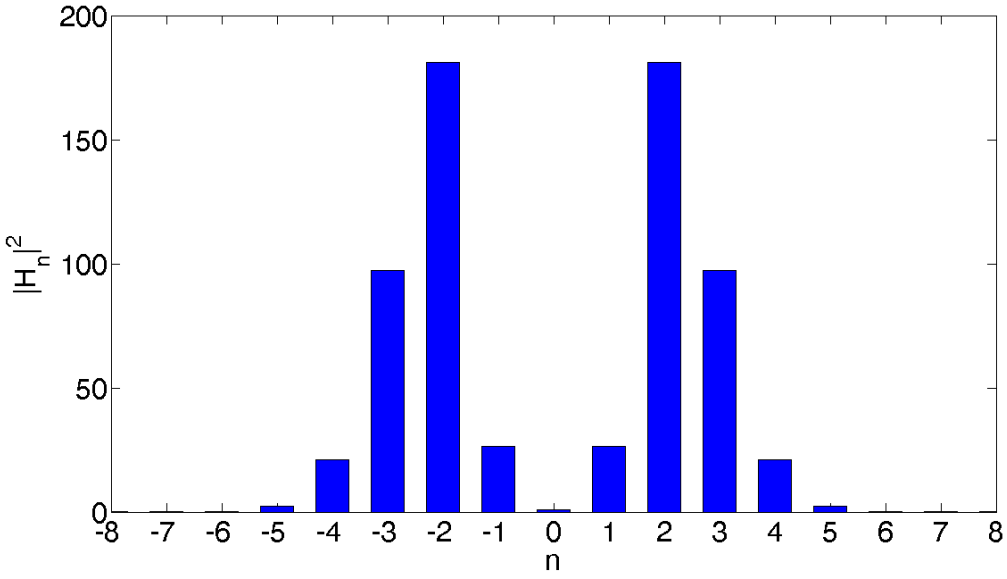

Figure 5.31: The normalized magnitude of the harmonics, $|H_n|^2$ at the diffraction grating at $x = 0$ at $q = q_1$ and $\alpha = 6$.

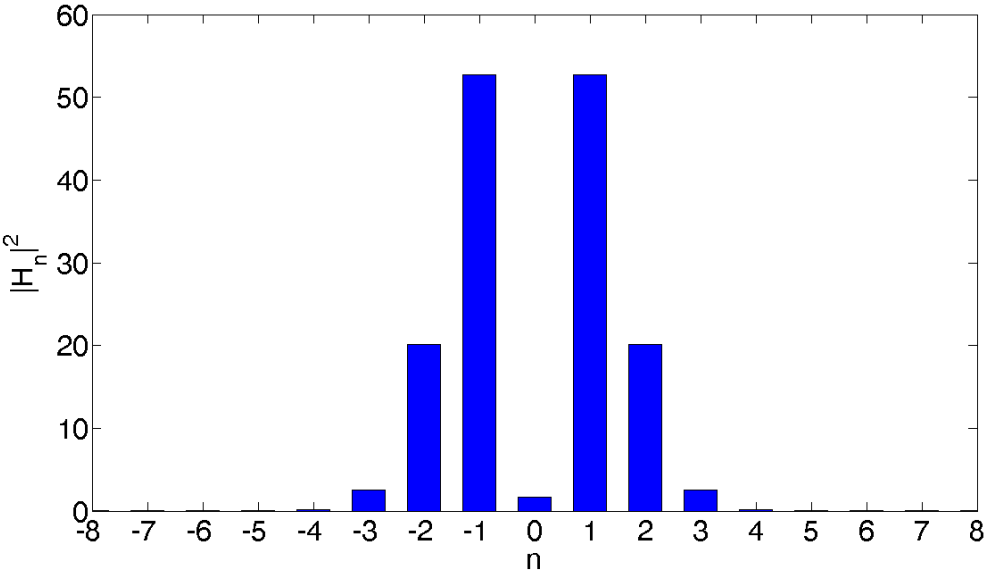

Figure 5.32: The normalized magnitude of the harmonics, $|H_n|^2$ at the diffraction grating at $x = 0$ at $q = q_2$ and $\alpha = 6$.

5.3 Summary

This chapter has examined further the role of higher hamonics in the solution of the fields. Analytical solutions often only account for the fundamental and first harmonics. We have shown that if the coefficient of the nonlinear term in the differential equation, Eq. (5.1), is small enough, then the harmonics are not large and the analytical and numerical solutions agree. If the coefficient of the nonlinear term is made larger, however, the solutions do diverge as the harmonics higher than the first grow in size in comparison to the first and fundamental harmonics.

CHAPTER 6

PLASMA LAYER AS A DIFFRACTION GRATING

It was shown in Chapter 4 that external modulation of the permittivity of an optically opaque layer creates conditions that allow for the excitation of surface waves and the resonant amplification of evanescent modes, resulting in anomalous transparency. In this chapter, we investigate whether partial modulation would allow the same effect. That is we consider a dense plasma slab consisting of two layers: one of uniform density and, next to it, another layer that has periodically modulated density, as illustrated in Figure 6.1. Such a modulation can be achieved by applying a strong electric or magnetic field or perhaps by applying other external forces, e.g. with the launching of ultrasound waves.

We assume that the density modulation causes a modulation of the permittivity in the form $\epsilon_2 = \epsilon_m(1 + g \sin qy)$, $q = 2\pi/a$. The uniform layer has permittivity in the form $\epsilon_1 = 1 - f_{p2}^2/f^2$ with f_{p2} = 2.3 GHz. The spacial period of the modulation is a = 0.15 m. FEM simulations were performed with these parameters. Figure 6.2 shows the effect that adding modulation to part of the plasma has on the transmission. It is interesting to note that there are two resonances, one corresponding to full transmission and the other one to full reflection. As such, not only can the wave be fully transmitted but it can also be fully reflected from the plasma depending on the incident frequency. Figures 6.3 and 6.4 show that the resonant frequencies of these peaks in transmission and reflection can be adjusted by changing some parts of the geometry. Specifically, Figure 6.3 shows the effect that changing the thickness of the second layer has on the transmission. In this case, increasing the thickness of the second layer increases the resonant frequencies. Figure 6.4 shows the effect that changing the permittivity coefficient, ϵ_m, of the modulated layer has on the transmission. As ϵ_m is increased, the resonant frequencies are increased as well.

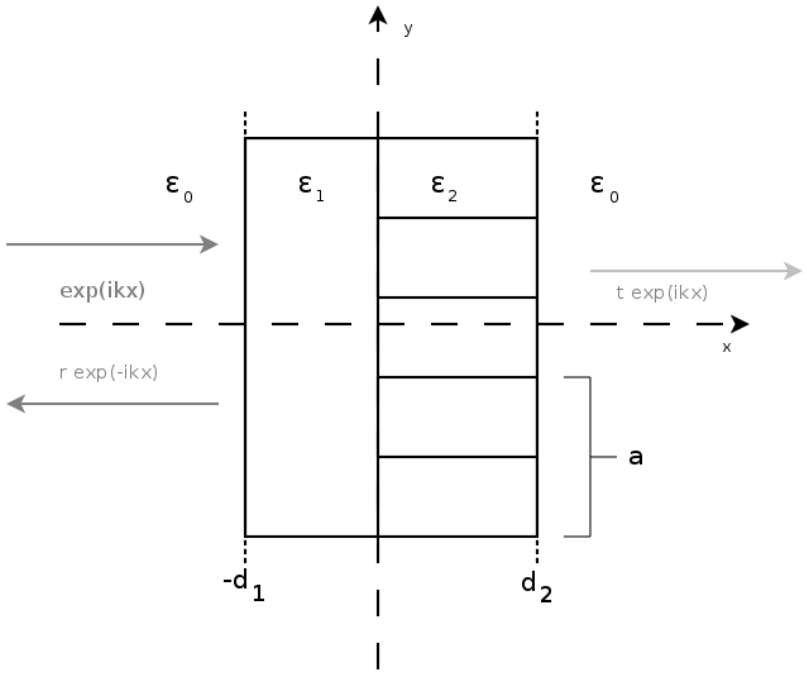

Figure 6.1: Geometry of two layers of plasma, one of which has a periodically modulated permittivity.

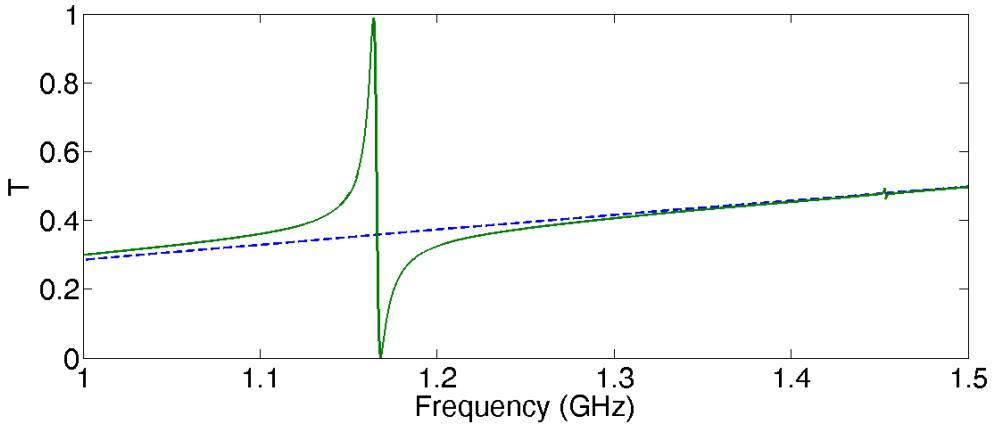

Figure 6.2: Transmission coefficients for two layers of plasma. The dashed line is with $g = 0$ and the solid line is with $g = 0.2$. Other parameters are $f_p = 2.3\,\text{GHz}$, $a = 0.15\,\text{m}$, $\epsilon_m = \epsilon_1$, $d_1 = 0.4\,\text{cm}$, $d_2 = 2\,\text{cm}$

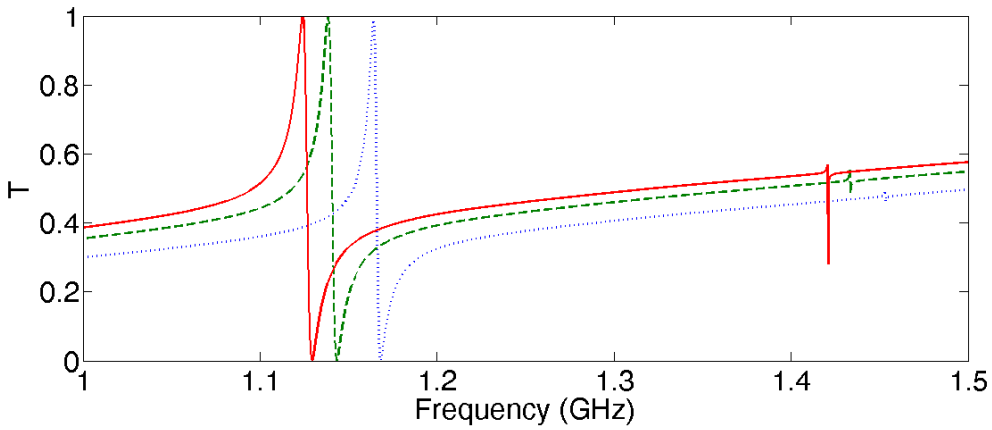

Figure 6.3: Transmission with parameters $f_p = 2.3\,\text{GHz}$, $a = 0.15\,\text{m}$, $\epsilon_m = \epsilon_1$, $d_2 = 2\,\text{cm}$, $d_1 = 0.1$ cm (solid line), 0.2 cm (dashed line), 0.4 cm (dotted line)

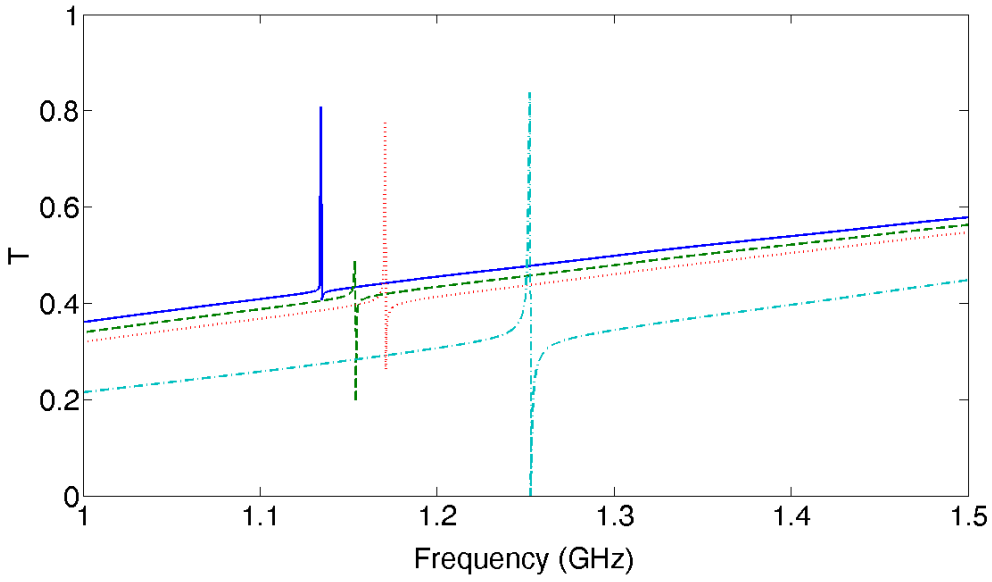

Figure 6.4: Transmission with parameters $f_p = 2.3\,\text{GHz}$, $a = 0.15\,\text{m}$, $d_1 = 2\,\text{cm}$, $d_2 = 0.1\,\text{cm}$, $\epsilon_m = \epsilon_1$ (solid line), $2\epsilon_1$ (dashed line), $3\epsilon_1$ (dotted line), $10\epsilon_1$ (dotted and dashed line)

6.1 Summary

In this chapter, we investigated resonant transmission through a partly modulated plasma layer. As we are not aware of an analytical solution, we use a numerical method to calculate transmission through the system. We found that by modulating the permittivity of even part of the plasma, complete reflection and transmission is realized at resonant angles. We also show that by tweaking the parameters, the resonances can also be tailored to different frequencies.

CHAPTER 7

ENHANCED TRANSMISSION WITH METAL GRID

In Chapter 6, we investigated how transmission could be enabled through a plasma layer by modulating part of the plasma itself. The modulated part of the plasma served to excited the SPPs that would enable resonant transmission. In this chapter, as an alternative, we will consider placing a square diffraction grating made of a metal with finite conductivity and finite thickness beside the plasma which we wish to enhance transmission through. This geometry is illustrated in Figure 7.1.

The metal grating alternates between metal permittivity, ϵ_m, and air permittivity, ϵ_0. ϵ_m is not negative, unlike most materials discussed in this work. At radio frequencies, metals are mostly absorptive and their permittivities are mostly imaginary. Here ϵ_m is modelled as $\epsilon_m = 1 - j\sigma/\omega\epsilon_0$, where $\sigma = 5.998 \cdot 10^7$ S/m. The periodicity of the grating is $a = 15$ cm. The plasma permittivity is modelled as $\epsilon_1 = 1 - f_p^2/f^2$ with $f_p = 2.3$ GHz and has thickness $d_1 = 8$ cm.

A transmission plot for different values of grating thickness, d_2, is shown in Figure 7.2. It seems that for any values of d_2, there is a minimum frequency for resonance. From the figure, it looks like there are one or two main resonances and a handful of smaller ones that either increase transmission or suppress it. While there are a number of peaks that reach $T = 0$, there are none that reach $T = 1$ and transmission seems to be magnified by a factor of two or three at best.

The behaviour over a wider frequency range is illustrated in Figure 7.3. The transmission is shown for $d_2 = 0.5$ cm and is over a wider frequency range, starting from 0 GHz to near the plasma frequency, f_p. Again, there are no resonance peaks below a set frequency. There are some transmission peaks as well as reflection peaks. As the incident frequency, f, approaches the plasma frequency, f_p, the transmission smooths out and acts more like

it would without the plasma or if the plasma was a dielectric.

Figure 7.4 shows the transmission for a thinner plasma, one with only $d_1 = 0.02$ cm with all other parameters same as before. For a thinner plasma, the transmission is of course higher (in this case it ranges from $T = 0.4 - 0.6$ over the frequency range without the diffraction grating). With the diffraction grating, transmission is enhanced over some wider frequency resonances. Still, the transmission does not surpass $T = 0.8$ but complete reflection is still possible at a number of frequencies.

In both cases, very little power is absorbed (less than 0.1 $\%$). The fields are localized to inside the pockets of air between the metal in the grating where there is no absorption, as opposed to the metal areas that have very high absorption.

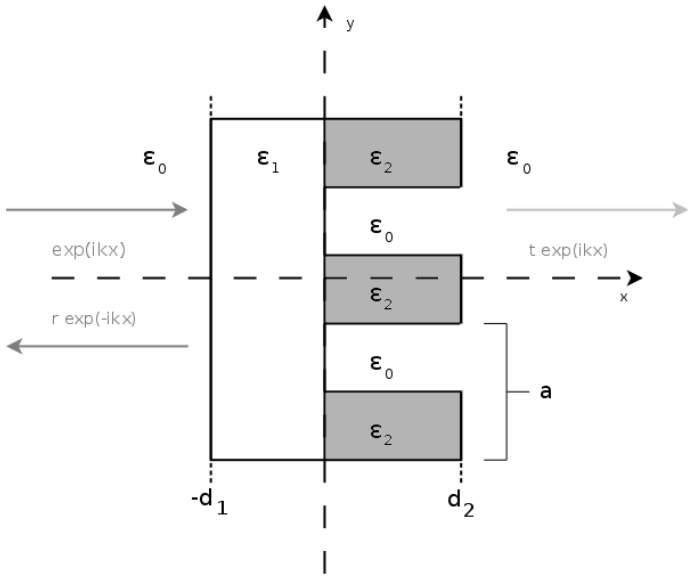

Figure 7.1: Geometry of a plasma layer with permittivity $\epsilon_1 = 1 - f_p^2/f^2$ and thickness d_1. To the right of it is a square diffraction grating that alternates permittivity $\epsilon_m = 1 - i\sigma/\omega\epsilon_0$ and the free space permittivity ϵ_0. The grating has periodicity a and thickness d_2.

We have shown that a metallic square grating of finite width enhances transmission and reflection through a plasma layer. We found many more resonances than in the previous structures that used only sinusoidal modulation. In the system of this chapter, completele tranmission is not attained for any angle. Despite that, no matter the opaqueness of the plasma layer, resonances which completely reflected the incident wave did exist.

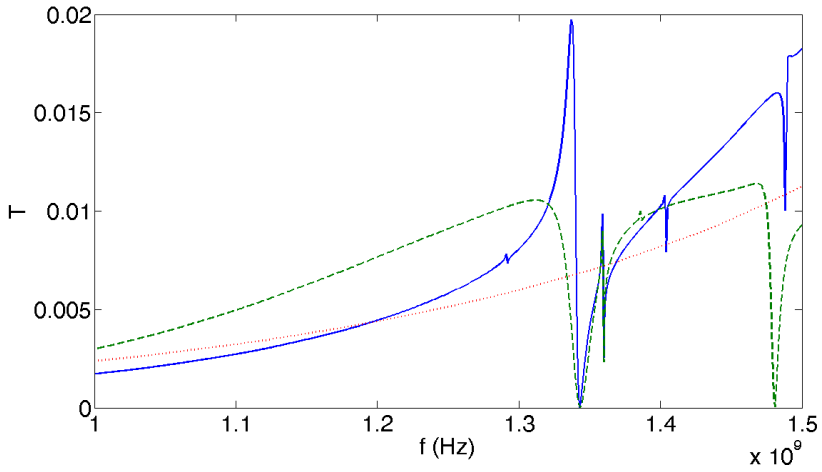

Figure 7.2: Transmission through the plasma and diffraction grating configuration for different thicknesses of the diffraction grating, d_2. The dotted line has $d_2 = 0$ cm, the solid line has $d_2 = 0.5$ cm, and the dashed line has $d_2 = 2$ cm

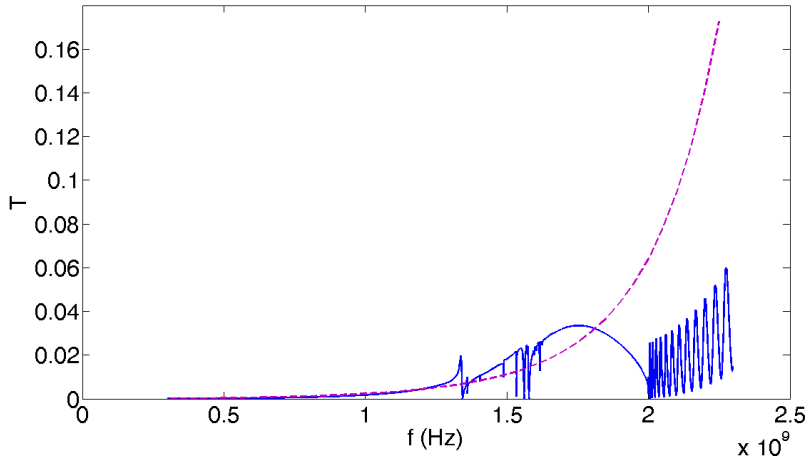

Figure 7.3: Transmission through the plasma and diffraction grating configuration over a wider range of frequencies. Solid line is with the diffraction grating and dashed line is without the diffraction grating.

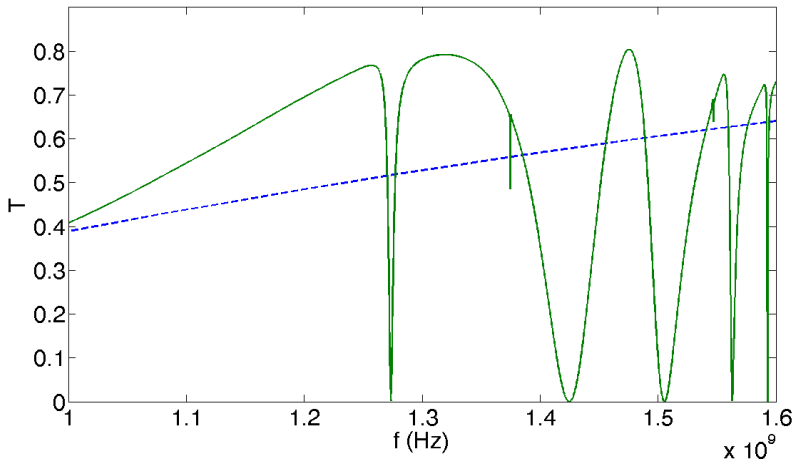

Figure 7.4: Transmission through a thinner plasma and a thinner diffraction grating configuration. Solid line is with the diffraction grating and dashed line is without the diffraction grating.

CHAPTER 8

SUMMARY

This thesis has presented investigations of the phenomena of resonant excitation, amplification of surface modes, and associated resonant transmission for several different geometries. We have analyzed resonant transmission in multi-layer structures which include layers of opaque materials with negative dielectric permittivity, $\varepsilon < 0$ as well as the resonant transmission facilitated by a diffraction grating.

It was shown that resonant tunnelling occurs near the resonant eigenmodes associated with surface modes. In the configuration analyzed in Chapter 2, the surface eigenmodes are excited by the incident wave and required matching is achieved due to the transition layer with $0 < \varepsilon < 1$. This configuration requires a finite incidence angle.

A diffraction grating placed in front of a dense plasma region induces a finite wave vector along the interface so the SPP excitation is possible for normal incidence.

The periodic modulation of plasma density may play a role of the diffraction grating as in Chapter 4. Our numerical simulations have confirmed the resonant transmission that was analytically investigated in earlier work. It was found that numerical and analytical results are in good agreement in this case. The analytical theory presented in Ref. [43] is based on truncation of higher harmonics so that only the first side-band is included. The amplitude of the higher harmonics is proportional to the grating amplitude which is a measure of the effective nonlinearity of the system which can be characterized by the value of the αh_g parameter, where α is modulation parameter. The approximation of weak nonlinearity works well for considered parameters and, as it was shown in Chapter 4, is consistent with the low amplitude of higher harmonics.

In Chapter 5, the excitation of SPP by ideal grating in front of the plasma region, was considered. Earlier work has considered the SPP in the system of two gratings [69]. Re-

cently, an analytical theory was developed that shows that a single grating is sufficient for resonant excitation of SPP and resonant transmission [70]. The elements of this theory are presented in Chapter 5. We have performed numerical simulations of this geometry and confirmed resonant transmission. Further we investigated the role of higher harmonics in this geometry. Our analysis demonstrates that for larger values of the modulation parameter α, the amplitude of higher harmonics increases and that leads to a deviation of numerical results from analytical theory: the location of resonant frequencies shifts for larger α. The development of the analytical theory which includes higher harmonics may be a subject of further studies.

Chapter 6 investigates a hybrid geometry where only a partial depth of plasma layer is modulated. Resonant transmission was shown to occur in this geometry as well.

In Chapter 7, we have attempted the investigation of SPP excitation mediated by the realistic diffraction grating made of copper for radio frequencies. Contrary to the case of high (optical) frequencies where the dense region can be well approximated by negative permittivity (with some dissipation), metal at RF frequencies is a good conductor with a large imaginary permittivity. Our results in Chapter 7 indicate that the transmission may be resonantly enhanced but not as dramatically for thick layers. Multiple resonances are detected in this case.

Control of the dielectric permittivity or, in particular, control of the periodic modulations in the dielectric permittivity can be achieved with an external electric field applied to semiconductor materials and/or with another laser beam utilizing the nonlinear polarization in strong fields. For plasmas in the RF frequency range, control may be possible by an external magnetic field. The resonant properties of the structures studied in this thesis can be of interest for various plasmonic applications. It is worth noting that the leaky mode regimes (or equivalently, the resonant transmission regimes) are characterized by the strong enhancement of the wave amplitude inside the structure. The modes in the evanescent regimes can be realized at dimensions below half a wavelength which possibly can be used as a laser cavity resonator.

BIBLIOGRAPHY

[1] Maier, S.A., Brongersma, M.L.,Kik, P.G., Meltzer, S., Requicha, A.A.G., Atwater, H.A. *Plasmonics - A route to nanoscale optical devices* Advanced Materials **13** 19 1501-1505 (2001)

[2] Sommerfeld, A. *Über die Fortpflanzung electrodynamischer Wellen längs eines Drahtes* Ann. Phys. und Chemie **67** 233-290 (1899)

[3] Zenneck, J. *Über die Fortpflanzung ebener elektromagnetischer Wellen längs einer ebenen Leiterfläche und ihre Beziehung zur drahtlosen Telegraphie* Ann. Phys. **23** 846-866 (1907)

[4] Wood, R.W. *Anomalous diffraction gratings* Physical Review **48** 12 928-936 (1935)

[5] Leonhardt, U. *Optical metamaterials: Invisibility cup* Nature Photonics **1** 4 207-208 (2007)

[6] Mie, G. *Beiträge zur Optik trüber Medien, spaeiell kolloidaler Metallösungen* Ann. Phys. **25** 377 (1908)

[7] Maier, S.A., Atwater, H.A. *Plasmonics: Localization and guiding of electromagnetic energy in metal/dielectric structures* J. Appl. Physics **98** 1 011101 (2005)

[8] Maier. , S.A. *Plasmonics - Towards subwavelength optical devices* Current Nanoscience **1** 1 17-23 (2005)

[9] Atwater, H.A. *The promise of plasmonics* Science American **296** 4 56-63 (2007)

[10] Zia, R., Schuller, J.A., Chandran, A. Brongersma, M.L. *Plasmonics: the chip-scale technology* Materials **9** 7-8 20-27 (2006)

[11] Ozbay, E. *Plasmonics: Merging photonics and electronics at nanoscale dimensions* Science **311** 5758 189-193 (2006)

[12] Zhang, Y., et al. *Surface-enhanced Raman scattering sensor based on D-shaped fiber* Applied Physics Letters **87** 12 123105 (2005)

[13] Kim, Y.C., Peng, W., Banerji, S., Booksh, K.S. *Tapered fiber optic surface plasmon resonance sensor for analyses of vapor and liquid phases* Optics Letters **30** 17 2218-2220 (2005)

[14] Schurig, D., et al. *Metamaterial electromagnetic cloak at microwave frequencies* Science **314** 5801 977-980 (2006)

[15] Ebbesen, T.W., Lezec, H.J., Ghaemi, H.F., Thio, T., Wolff, P.A. *Extraordinary optical transmission through sub-wavelength hole arrays* Nature **931** 6668 667-669 (1998)

[16] Porto, J.A., Martín-Moreno, L., García-Vidal, F.J. *Optical bistability in subwavelength slit apertures containing nonlinear media* Physical Review B **70** 8 081402 (2004)

[17] Lezec, H.J., Degiron, A., Devaux, E., Linke, R.A., Martín-Moreno, L., García-Vidal, F.J., Ebbesson, T.W. *Beaming light from a subwavelength aperture* Science **297** 5582 820-822 (2002)

[18] Pendry, J.B., Smith, D.R. *The quest for the superlens* Scientific American **295** 1 60-67 (2006)

[19] Shelby, R.A., Smith, D.R., Schultz, S. *Experimental verification of a negative index of refraction* Science **292** 5514 77-79 (2001)

[20] Casse, B.D.F., et al. *Towards 3D electromagnetic metamaterials in the THz range* AIP Conference Proceedings **879** 1462-1465 (2007)

[21] Smith, D.R., Pendry, J.B., Wiltshire, M.C.K. *Metamaterials and negative refractive index* Sciences **305** 5685 788-792 (2004)

[22] Blaikie, D., Melville, R. *Experimental comparison of resolution and pattern fidelity in single- and double-layer planar lens lithography* Journal of the Optical Society of America **23** 3 461-467 (2006)

[23] Fang, N., Lee, H., Sun, C., Zhang X. *Sub-diffraction-limited optical imaging with a silver superlens* Science **308** 5721 534-537 (2005)

[24] Stockman, M. *Nanofocusing of optical energy in tapered plasmonic waveguides* Physical Review Letters **93** 93 137404 (2004)

[25] Schuller, J.A., et al. *Plasmonics for extreme light concentration and manipulation* Nature Materials **9** 3 193-204 (2010)

[26] Bergman, D., Stockman, M. *Surface plasmon amplification by stimulated emission of radiation: quantum generation of coherent surface plasmons in nanosystems* Physical Review Letters **90** 2 027402 (2003)

[27] Jackson, J.D. *Classical Electrodynamics* John Wiley & Sons (1999)

[28] Maier, S.A. *Plasmonics: Fundamentals and Applications* Springer (2007)

[29] Agranovich, V.M., Gartstein, Y.N. *Spatial dispersion and negative refraction of light* Physics-Uspekhi **49** 10 1029-1044 (2006)

[30] Sarid, D. *Long-range surface-plasma waves on very thin metal films* Physical Review Letters **47** 26 1927-1930 (1981)

[31] Kretschmann, E., Raether, H. *Radiative decay of non-radiative surface plasmons excited by light* Z. Naturforschung, **23A** 12 2135 (1968)

[32] Otto, A. *Excitation of nonradiative surface plasma waves in silver by the method of frustrated total reflection* Z. Physics **216** 4 398 (1968)

[33] Veronis, G., Fan, S. *Surface Plasmon Nanophotonics* Springer (2007)

[34] Courant, R. *Variational Methods for the Solution of Problems of Equilibrium and Vibrations* Bull Am Math Soc **49** 1 (1943)

[35] Schoenberg, I.J. *Contributions to the Problem of Approximation of Equidistant Data by Analytic Functions. Part A. On the Problem of Smoothing or Graduation. A First Class of Analytic Approximation Formulae* Quart. Appl math **4** 45-99(1946)

[36] Jin, J. *The Finite Element Method in Electromagnetics* John Wiley & Sons, Inc. (2002)

[37] Berenger, J.P. *A perfectly matched layer for the absorption of electromagnetic waves* J. Compu. Phys. **114** 2 185-200 (1994)

[38] Chew, W.C., W.H. Weedon, W.H. *A 3D perfectly matched medium from modified Maxwells equations with stretchedcoordinates* Microwave Opt. Tech. Lett. **7** 13 599-604 (1994)

[39] COMSOL Multiphysics website: www.comsol.com

[40] Fourkal, E.,Velchev, I., Ma,C-M., Smolyakov, A. *Evanescent wave interference and total transparency of a warm high-density plasma slab* Physics of Plasmas **13** 9 092113 (2006)

[41] Rigneault, H., et al. *Enhancement of single-molecule fluorescence detection in sub-wavelength apertures* Physics Review Letters **95** 11 117401 (2005)

[42] Anker, J.N., et al. *Biosensing with plasmonic nanosensors* Nature Materials **7** 6 442-453 (2008)

[43] Dykhne, A.M., Sarychev, A.K., Shalaev, V.M. *Resonant transmittance through metal films with fabricated and light-induced modulation* Physical Review B **67** 19 195402 (2003)

[44] Genchev, Z.D., Dosev, D.G. *Resonant transmittance through periodically modulated films* Journal of Experimental and Theoretical Physics **99** 6 1129-1136 (2004)

[45] Agrawal, G. *Nonlinear Fiber Optics* Academic Press, (2007)

[46] Bozhevolnyi, S., Garcia-Vidal, F. *Focus on plasmonics* New Journal of Physics **10** 105001 (2008)

[47] Smolyaninov, I., Hung, Y.J. *Enhanced transmission of light through a gold film due to excitation of standing surface-plasmon Bloch waves* Physical Review B **75** 3 033411 (2007)

[48] Smolyaninov, I., Hung, Y.J., Davis, C. *Light-induced resonant transmittance through a gold film* Applied Physics Letters **87** 4 041101 (2005)

[49] Alù, A., Engheta, N. *Light squeezing through arbitrarily shaped plasmonic channels and sharp bends* Physical Review B **78** 3 035440 (2008)

[50] Giannattasio, A., Hooper, I., Barnes, W. *Transmission of light through thin silver films via surface plasmon-polaritons* Optics Express **12** 24 5881-5886 (2004)

[51] Lalanne, P., Rodier, J.C., Hugonin, J.P. *Surface plasmons of metallic surfaces perforated by nanohole arrays* Journal of Optics A-Pure and Applied Optics **7** 9 422-426 (2005)

[52] Lalanne, P., Sauvan, C., Hugonin, J.P., et al. *Perturbative approach for surface plasmon effects on flat interfaces periodically corrugated by subwavelength apertures* Physical Review B **68** 12 125404 (2003)

[53] Degiron, A., Ebbesen, T.W. *The role of localized surface plasmon modes in the enhanced transmission of periodic subwavelength apertures* Journal of Optics A: Pure and Applied Optics **7** S90-S96 (2005)

[54] Przybilla, F., Degiron, A., Genet, C., et al. *Efficiency and finite size effects in enhanced transmission through subwavelength apertures* Optics Express **16** 13 9571-9579 (2008)

[55] Martin-Moreno, L., Garcia-Vidal, F.J. *Minimal model for optical transmission through holey metal films* Journal of Physics-Condensed Matter **20** 30 304214 (2008)

[56] Martin-Moreno, L., et al. *Theory of extraordinary optical transmission through subwavelength hole arrays* Physical Review Letters **86** 6 1114-1117 (2001)

[57] Bravo-Abad, J., Martin-Moreno, L., Garcia-Vidal, F.J. *Resonant transmission of light through subwavelength holes in thick metal films* IEEE Journal of Selected Topics in Quantum Electronics **12** 6 1221-1227 (2006)

[58] Barbara, A., Quemerais, P., Bustarret, E., Lopez-Rios, T. *Optical transmission through subwavelength metallic gratings* Physical Review B **66** 16 161403 (2002)

[59] Sarychev, A.K., Podolskiy, V.A., Dykhne, A.M. *Resonance transmittance through a metal film with subwavelength holes* IEEE Journal of Quantum Electronics **38** 7 956-963 (2002)

[60] Raether, H. *Surface Plasmons, volume 111 of Springer-Verlags Tracts in Modern Physics* Springer-Verlag New York (1988)

[61] Zayats, A.V., Smolyaninov, I.I., Maradudin, A.A. *Nano-optics of surface plasmon polaritons* Physics Reports **408** 3-4 131-314 (2005)

[62] Darmanyah, S.A., Neviere, M., Zayats, A.V. *Analytical theory of optical transmission through periodically structured metal films via tunnel-coupled surface polariton modes* Physical Review B **70** 7 075103 (2004)

[63] Darmanyah, S.A., Zayats, A.V. *Light tunneling via resonant surface plasmon polariton states and the enhanced transmission of periodically nanostructured metal films. An analytical study* Physical Review B **67** 3 035424 (2003)

[64] Kats, A.V., Nikitin, A.Y. *Analytical treatment of anomalous transparency of a modulated metal film due to surface plasmon-polariton excitation* Physical Review B **70** 23 235412 (2004)

[65] Krishnan, A., Thio, T., Kima, T.J., et al. *Evanescently coupled resonance in surface plasmon enhanced transmission* Optics Communications **200** 1-7 (2001)

[66] Treacy, M.M.J. *Dynamical diffraction explanation of the anomalous transmission of light through metallic gratings* Physical Review B **66** 19 195105 (2002)

[67] Smolyaninov I.I., Hung, Y.J. *Reply to "Comment on 'Enhanced transmission of light through a gold film due to excitation of standing surface-plasmon Bloch waves'"* Physical Review B **77** 3 036402 (2008)

[68] Weiner, J. *Comment on "Enhanced transmission of light through a gold film due to excitation of standing surface-plasmon Bloch waves"* Physical Review B **77** 3 036401 (2008)

[69] Bliokh, Y.P. *Plasmon mechanism of light transmission through a metal film or a plasma layer* Optics Communication **259** 2 436-444 (2006)

[70] N. Sternberg, AI Smolyakov *Resonant transmission through dense plasmas via amplification of evanescent mode* Piers Online **5** 8 781-785 (2009)

[71] Pochi Yeh *Optical Waves in Layered Media* Wiley (1988)

APPENDIX A

TRANSMISSION MATRICES

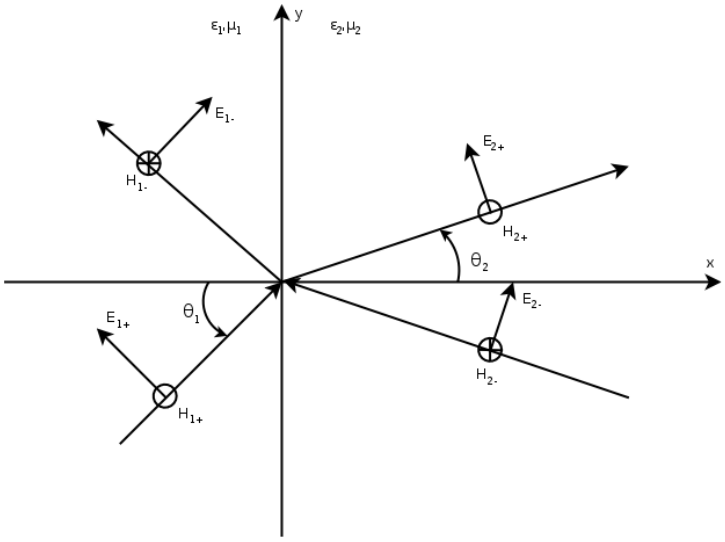

Figure A.1: Reflection and refraction of a TM wave (p wave)

For transmission and reflection problems through layered media, transmission matrices provide a systematic way of calculating reflection and transmission coefficients. As layers repeat themselves, so do the boundary conditions and a matrix formulation seems natural. In Fig. A.1, we consider a transverse magnetic (TM) wave at an interface. The boundary conditions impose the continuity of E_y and H_z:

$$(E_{1+} + E_{1-}) \cos\theta_1 = (E_{2+} + E_{2-}) \cos\theta_2 \tag{A.1a}$$

$$\sqrt{\frac{\epsilon_1}{\mu_1}}(E_{1+} - E_{1-}) = \sqrt{\frac{\epsilon_2}{\mu_2}}(E_{2+} - E_{2-}) \tag{A.1b}$$

These equations can be rewritten, in concise matrix form, as:

$$D_1 \begin{pmatrix} E_{1+} \\ E_{1-} \end{pmatrix} = D_2 \begin{pmatrix} E_{2+} \\ E_{2-} \end{pmatrix} \tag{A.2}$$

where

$$D_i = \begin{pmatrix} \cos\theta_i & \cos\theta_i \\ \sqrt{\frac{\epsilon_i}{\mu_i}} & -\sqrt{\frac{\epsilon_i}{\mu_i}} \end{pmatrix} \tag{A.3}$$

and are called the dynamical matrices of the p wave for medium i (i = 1,2). The transmission matrix M, the matrix that links the amplitudes of the waves on the two sides of the interface, comes about as,

$$\begin{pmatrix} E_{1+} \\ E_{1-} \end{pmatrix} = D_1^{-1} D_2 \begin{pmatrix} E_{2+} \\ E_{2-} \end{pmatrix} = M \begin{pmatrix} E_{2+} \\ E_{2-} \end{pmatrix}. \tag{A.4}$$

The propagation matrix is written as,

$$P_l = \begin{pmatrix} e^{ik_{lx}d} & 0 \\ 0 & e^{-ik_{lx}d} \end{pmatrix} \tag{A.5}$$

where $k_{lx} = kn_l \sin\theta_l$ ($k = \omega/c$) and d is the thickness of layer l. P_l accounts for the phase shift acquired while the wave propagates through the layer. The general expression for a transmission matrix for a system with s layers is,

$$\begin{pmatrix} E_{1+} \\ E_{1-} \end{pmatrix} = \begin{pmatrix} M_{11} & M_{12} \\ M_{21} & M_{22} \end{pmatrix} \begin{pmatrix} E'_{s+} \\ E'_{s-} \end{pmatrix} \begin{pmatrix} M_{11} & M_{12} \\ M_{21} & M_{22} \end{pmatrix} = D_0^{-1} (\prod_{l=1}^{s} D_l P_l D_l^{-1}) D_s \tag{A.6}$$

It is the matrix M that gives the relation between the incident, reflected, and transmitted waves. Knowing that, we can calculate the reflection and transmission coefficients from the elements of the matrix M [71],

$$r = \frac{M_{21}}{M_{11}} \tag{A.7a}$$

$$t = \frac{1}{M_{11}}. \tag{A.7b}$$